DEVELOPING A NOVEL DEDICATED OUTDOOR AIR SYSTEM (DOAS) FOR ENERGY EFFICIENCY AND ENVIRONMENTAL HEALTH

BAO YANI

PhD

The Hong Kong Polytechnic University

2018

The Hong Kong Polytechnic University

Department of Building Services Engineering

Developing a Novel Dedicated Outdoor Air System (DOAS) for Energy Efficiency and Environmental Health

Bao Yani

A thesis submitted in partial fulfilment of the requirements for the degree of Doctor of Philosophy

June 2018

CERTIFICATE OF ORIGINALITY

I hereby declare that this thesis is my own work and that, to the best of my knowledge and belief, it reproduces no material previously published or written, nor material that has been accepted for the award of any other degree or diploma, except where due acknowledgement has been made in the text.

_____ (Signed)

Bao Yani (Name of Student)

ABSTRACT

A novel dedicated outdoor air system (DOAS) for better energy efficiency and environmental health objectives is proposed in this study. It consists of a multi-stage variable speed direct expansion (DX) air-conditioner as the central system to generate extra-low temperature (XT) outdoor air (OA) to handle the entire space cooling load and a mixing chamber as the terminal system to mix XT OA and return air (RA) to become supply air (SA). For the successful application of the proposed system (XT-DOAS), the major concern is how the multi-stage DX air-conditioner must be designed to achieve the desired air conditions and better energy efficiency under highly variable indoor and outdoor operating conditions.

As a performance evaluation of the XT-DOAS as compared to a conventional system, simulation studies were conducted based on actual equipment performance models and realistic building and system characteristics. The results showed that XT-DOAS as compared to conventional system, was superior for achieving the desired relative humidities; could better achieve the desired thermal comfort conditions; saved 22.6% annual energy use for air-conditioning; and reduced the annual cumulative number of non-comfortable hours by 31%.

To further enhance the performance of XT-DOAS, the optimum number of cooling stages and treated OA temperature need to be determined. As the thermodynamic states of moist air entering and leaving individual cooling stages will affect the performance of XT-DOAS, the optimization process requires the development and validation of a coil performance model that takes into account the extra-high and extra-

low entering air temperature at the first and the last cooling stages. Factory test data and field measurement data were collected for the model development. Based on the developed model, energy and exergy analyses confirmed that the optimum configuration for XT-DOAS is two cooling stage with a treated OA temperature of 7 °C.

As the terminal system of XT-DOAS is of VAV control, the drawback is the risk of overcooling due to the minimum air flow fraction requirement of VAV system. To maintain space air temperature and to avoid overcooling, conventional VAV (Con_VAV) systems are provided with reheating coil because of the uncertainties in the possible variations in indoor and outdoor conditions thus the fluctuations of cooling demand. To confirm the effective use of the optimized XT-DOAS (without reheat provision) operating under a highly variable indoor and outdoor conditions, a probabilistic approach based on Monte Carlo simulations with 10,000 iterations was adopted to investigate the overcooling risk of XT-DOAS as compared to Con_VAV. The results showed that the potential annual overcooling hours using XT-DOAS were 29 hours, which is equivalent to 0.31% long-term percentage of dissatisfied (LPD). These results, as compared to 426 overcooling hours and 1.69% LPD achieved by the typical Con_VAV system, confirmed the excellent performance of XT-DOAS.

From the above, the investigation of XT-DOAS in this thesis can be summarized into four major aspects: the effective use for achieving the desired air conditions and better energy efficiency; the development of a realistic coil performance model; the determination of the optimum configuration; and the assessment of overcooling risk.

Keyword: extra-low temperature outdoor air system; humidity control; thermal comfort; coil performance model; energy and exergy performance analyses; Monte Carlo simulation; uncertainty analysis; overcooling risk; VAV system; subtropical office buildings.

PUBLICATIONS ARISING FROM THE THESIS

Journal papers:

Bao, Y., Lee, W. L. and Jia, J. (2017) Applying a novel extra-low temperature dedicated outdoor air system for humidity control and energy efficiency, *Science and Technology for the Built Environment*, 23(1): 16–29. (Based on Chapter 5)

Bao, Y., Lee, W. L. and Jia, J. (2018) Exergy analyses and modelling of a novel extra-low temperature dedicated outdoor air system, *Energies*, 11: 1165. (Based on Chapter 6)

Bao, Y., Lee, W. L. and Jia, J. (2018) Probabilistic risk assessment of overcooling for a novel extra-low temperature dedicated outdoor air system (XT-DOAS) for Hong Kong office buildings, to be submitted. (Based on Chapter 7)

Conference paper:

Bao, Y. and Lee, W. L. (2017) Using Monte Carlo simulation for sensitivity analysis of supply air temperature for a novel extra-low temperature dedicated outdoor air system (XT-DOAS), in *Shanxi (Taiyuan) - HK Joint Symposium 2017: Smart City, the way to a better tomorrow*. Taiyuan, China.

Other journal paper:

Bao, Y., Liu, T. and Lee, W. L. (2018) The influence of sleeping habits on cooling energy use in residential sector in Hong Kong, *Building and Environment*, 132: 205–213.

ACKNOWLEDGEMENTS

This thesis represents my hard work in the last three years of PhD study. It would not have been possible without the encouragement, support and guidance from many people.

I am deeply grateful for the supervision, guidance and support from Dr. Lee Wai Ling, who is not only my supervisor but also my good friend. Her strong professional knowledge and reasonable arguments facilitated the successful completion of my PhD study in a timely manner. Her patience and encouragement also enabled me to face every challenge positively during my tough study life.

Besides my supervisor, I would like to thank other mentors and staffs in the Department of Building Services Engineering for their academic support, especially Dr. Chau Chi Kwan, Dr. Jia Jie, Li Han and Fan Man. Their constructive advices were helpful for the commencement of my PhD study. I also gratefully acknowledge the financial support from The Hong Kong Research Grants Council and The Hong Kong Polytechnic University (PolyU).

I would also like to thank Dr. Lee Pan, Dong Jishuai (my team-mate) and Yang Wenjing (my classmate), for sharing views on my research. For other friends and colleagues in PolyU, it is with pleasure that I have had your company all the time and you created many wonderful memories for me.

I greatly appreciate the meticulous care and attention given by my family members: my husband Tsang Hing Leung, my parents and my parents-in-law. I feel so lucky and grateful that I have met my soul mate, Mr Tsang, during my PhD life in Hong Kong. His understanding and constant encouragement were essential for my success.

TABLE OF CONTENTS

LIST OF FIGURES

LIST OF TABLES

NOMENCLATURE

a_i	*i*-th empirical coefficient
A	heat transfer area for air side
AC	air-conditioning
AHU	air handling unit
ALD	ASHRAE likelihood of dissatisfied
b_i	*i*-th empirical coefficient
c_i	*i*-th empirical coefficient
CAP	total cooling capacity (kW)
CAV	constant air volume
C_{da}	specific heat of dry air(kJ/kg·°C)
CLC	cooling load based control
CoAD	cold air distribution system
ConH	condensation hour
Con_VAV	conventional variable air volume system
COP	coefficient of performance
C_{pa}	specific heat of moist air (kJ/kg·°C)
C_{pw}	specific heat capacity of water (kJ/(kg·°C)
CV	coefficient of variation
C_{wv}	specific heat of water vapour (kJ/kg·°C)
d_i	*i*-th empirical coefficient
dbt	new hourly dry bulb temperature of weather file (°C)
dbt_o	existing hourly temperature of typical metrological year weather (°C)

$\langle dbt_{o\max} \rangle_m$	monthly maximum temperatures for the month '*m*' of typical metrological year weather (°C)
$\langle dbt_o \rangle_m$	monthly mean temperatures for the month '*m*' of typical metrological year weather (°C)
$\langle dbt_{o\min} \rangle_m$	monthly minimum temperatures for the month '*m*' of typical metrological year weather (°C)
dpt	new hourly dew point temperature of weather file (°C)
DB	dry bulb
DDC	direct digital controller
DOAS	dedicated outdoor air system
DP	dew point
DPT	dew point temperature
$\Delta DSWF_m$	absolute change in the monthly mean global solar radiation for the month '*m*' of Hong Kong Observatory weather (Wh/m^2)
DX	direct expansion
e	residual
ex	exergy of moist air per unit mass dry air (kJ/kg dry air)
E	electricity consumptions (kWh)
EIR	energy input ratio
En	energy use (MWh)
Ex,cd,in	exergy of moist air entering in the condenser (MWh)
Ex,cd,out	exergy of moist air out of the condenser (MWh)
Ex,desired	exergy desired for a system (MWh)
Ex,ep,in	exergy of moist air entering in the evaporator (MWh)
Ex,ep,out	exergy of moist air out of the evaporator (MWh)
Ex,loss	exergy loss of DX unit (MWh)
Ex,needed	exergy needed for the desired effect of the system (MWh)

$Ex,tot,loss$	total exergy loss of multi-stage DX system (MWh)
FF	function of air flow fraction
FPMB	fan-powered mixing box
FT	function of temperature
g	correction performance coefficient
gsr	new hourly global solar radiation of weather file (Wh/m^2)
gsr_o	existing hourly global solar radiation of typical metrological year weather (Wh/m^2)
$\langle gsr_o \rangle_m$	existing monthly mean global solar radiation for the month 'm' of typical metrological year weather (Wh/m^2)
h	specific enthalpy (kJ/kg)
H_{fg}	latent heat of evaporation of water (kJ/kg)
HKO	Hong Kong Observatory
HR	hour
IA	index of agreement
IAQ	indoor air quality
k	last progressive time step of the calculation period
LHS	latin hypercube sampling
$LMTD$	log mean temperature difference between air and refrigerant
LPD	long-term percentage of dissatisfied
m	air mass flow rate (kg/s)
MAE	mean absolute error
$MAFF$	minimum air flow fraction
$MAPE$	mean absolute percentage error
MCS	Monte Carlo simulation
MIMO	multi-input multi-output

N	cooling stage number of multi-stage DX unit
NCH	number of non-comfortable hours
O	observed value
$\overline{O}$	mean observed value
OA	outdoor air
OCC	occupant
p	Pressure (kPa)
P	predicted value
PAU	primary air-handing unit
PDF	probability distribution function
PLF	part load fraction
PLR	part load ratio
Q	cooling output (kW)
ΔQ	surplus cooling of VAV system at MAFF
R^2	coefficient of determination
RA	return air
R_{da}	the ideal gas constant of dry air (kJ/kg·K)
RH	relative humidity
$RMSE$	root-mean-square error
RTF	run time fraction
s	new hourly specific humidity of weather file (g/kg)
s_o	existing hourly specific humidity of typical metrological year (g/kg)
SA	supply air
SAT	supply air temperature (°C)

SD	standard deviation
SHR	sensible heat ratio
$SPHU_m$	monthly percentage changes of specific humidity the temperature between Hong Kong Observatory and typical metrological year weather
t	time (hour)
T	temperature (°C)
T'	temperature (K)
TMY	typical metrological year
ΔT	temperature difference between air in and out of DX coil (°C)
$\Delta TMAX_m$	monthly absolute change in the maximum temperature for the month 'm' of Hong Kong Observatory weather (°C)
$\Delta TEMP_m$	monthly absolute change in the mean temperature for the month 'm' of Hong Kong Observatory weather (°C)
$\Delta TMIN_m$	monthly absolute change in the minimum temperature for the month 'm' of Hong Kong Observatory weather (°C)
U	overall heat transfer coefficient between air and evaporator surface (W/(m^2·°C))
V	volume flow rate (m^3/s)
VAV	variable air volume
VS	variable speed
W	power (kW)
WB	wet bulb
x	new hourly weather variable
x_o	hourly baseline weather variable
$\langle x_o \rangle_m$	monthly mean value of the weather variable x_o for the month 'm'
Δx_m	absolute change in the monthly mean value of the variable for the month 'm'

XT	extra-low temperature
XHT	extra-high entering air temperature
XLT	extra-low entering air temperature
ZRE	standard residual

Greek symbol

ρ	density (kg/m^3)
ω	humidity ratio (kg/kg)
η_{Ex}	exergy efficiency
α_m	fractional change in the monthly mean value of the variable for the month '*m*'
αdbt_m	fractional change of the temperature between Hong Kong Observatory and typical metrological year weather for the month '*m*'
αgsr_m	scaling factor for global solar radiation for the month '*m*'
αs_m	scaling factor for specific humidity for the month '*m*'

Subscript

0	reference environmental state
0*s*	dead state
a	air
c	critical state
comf	comfortable
ci	condenser inlet
ch	chemical
com	compressor
design	design condition

e	evaporating
ei	evaporator (DX coil) inlet
eo	DX coil outlet
Fan	fan
in	indoor
j	*j*-th stage DX coil
lat	latent
m	month
me	mechanical
o	baseline state
oc	overcooling
op	operative
ra	return air
rated	rated condition
rw	return chilled water
sa	supply air
sen	sensible
spx	conditioned spaces
sys	multi-stage DX system
sw	supply chilled water
t	time
th	thermal
w	water
ws	saturated state of water vapour
y	annual value

CHAPTER 1

INTRODUCTION

1.1 Background

The enormous energy usage in buildings becomes a serious issue in the world. IPCC (2014) pointed out that efficient energy usage in buildings can make contribution to reducing greenhouse effect and relieving global warming. A report (Pérez-Lombard *et al.*, 2008) pointed out that there had been a steady increase in building energy consumptions in developed countries and regions and the amount had reached 20% to 40% of their total consumptions. Hong Kong, owing to the large number of high-rise residential and commercial buildings, the energy usage in buildings accounts for almost 90% of its total energy consumption (Luo *et al.*, 2015).

Hong Kong is of subtropical climate where summers are hot and humid. The substantial increase in building energy consumption is mainly due to the wide adoption of air-conditioning (AC) system for cooling and dehumidification (Tso and Yau, 2003).

To remove moisture in air, a conventional AC system in commercial buildings often uses cold-coils to process outdoor air (OA) and return air (RA) to a low temperature close to saturation which is 90-95% relative humidity (RH). The desired RH is achieved by matching the sensible heat ratio (SHR) of the AC equipment with the space SHRs, but a perfect match is rarely achieved. This divergence between equipment and space SHRs leads to poor humidity control, which can degrade occupant comfort, health and productivity, and cause damage from mould growth and

condensation (Ge *et al.*, 2011). Generally, reheating process is needed to reheat the cooled air for matching the two SHRs and improving thermal comfort, but it is energy inefficient (Hickey, 2001; Li and Deng, 2007c; Wan *et al.*, 2007). Besides, conventional AC system has the risk of crossed bacterial contamination due to the internal air circulation between different zones (Liu *et al.*, 2007).

Therefore, the energy efficiency and environmental health associated with use of AC system in Hong Kong, especially for office environments where air-conditioning is used almost year-round, are critical issues.

1.2 Objectives of This Study

Considering the critical issues mentioned above in Section 1.1 and based on the research gaps in later literature review (Chapter 2), a novel extra-low temperature dedicated outdoor air system (XT-DOAS) is proposed in this study and aims to achieve better energy efficiency and environmental health. The proposed XT-DOAS is applied to office building in Hong Kong and the objectives of this study are described in brief as follows:

1) To evaluate XT-DOAS's performance in achieving the desired air conditions (with focus on humidity control and thermal comfort) and better energy efficiency (Chapter 5).

2) To optimize the system configuration of XT-DOAS for achieving the desired air conditions and better energy and exergy efficiency based performance curves built upon realistic data sets (Chapter 6).

3) To investigate the overcooling risk of XT-DOAS, which is a common issue for VAV system (Chapter 7).

1.3 Organization of This Thesis

This thesis comprises eight chapters, which include an introduction of this study; a review of relevant research works; a description of the proposed XT-DOAS; an outline of the methodologies used; an investigation of the humidity control, energy efficiency and overcooling risk of XT-DOAS; and a conclusion and recommendation drawn from this study. Energy efficiency analysis will include exergy analyses leading to the optimization of the proposed XT-DOAS.

Chapter 1 introduces the backgrounds, objectives and organization of this study.

Chapter 2 provides a review of relevant research works and identifies the research gaps in previous studies.

Chapter 3 gives a detail description of the system configuration of proposed XT-DOAS.

Chapter 4 explains the main research methodology adopted in this study.

Chapter 5 investigates the humidity control and energy efficiency of XT-DOAS when compared to a conventional system.

Chapter 6 optimizes the system configuration of XT-DOAS based on energy and exergy analyses.

Chapter 7 assesses the overcooling risk of XT-DOAS using a probabilistic approach (Monte Carlo Simulation).

Chapter 8 presents the conclusions drawn from this study and provides several recommendations for future research.

CHAPTER 2

LITERATURE REVIEW

This chapter reviews relevant research works on the key components of the proposed XT-DOAS, aiming to identify the research gaps.

2.1 Dedicated Outdoor Air System (DOAS)

The idea of utilizing dedicated outdoor air systems (DOAS) appeared in the 1980s but its application was restricted to some very unique situations in the early years (Mumma, 2001). The recent occurrence of severe acute respiratory syndrome (SARS), avian flu and anthracnose in some countries made environmental health quality one of the most important elements needed for an AC system (Liu *et al.*, 2007). To achieve better environmental health, the techniques of using dedicated outdoor air systems (DOAS) have widely been applied as it can avoid moisture-related air quality problems and microbial contamination (Yu *et al.*, 2009).

DOAS is an alternative technology to handle latent load and part of sensible load by providing 100% OA into conditioned spaces. It can also satisfy ventilation requirement for human health. Generally, a conventional DOAS comprises two parallel systems (see Figure 2.1); an OA system as the central system to produce high quantities of OA that handles the entire latent loads and part of the space sensible loads; and a terminal system to handle the remaining space sensible loads. As such, OA flow rate is higher and RA does not need to be circulated across different zones to enhance the indoor air quality (IAQ). The OA system often uses active-desiccant technology; whilst the

terminal system can be chilled beams/ceilings (Niu *et al.*, 2002). Energy savings can be derived from reheating and dehumidification energy reductions. In addition, some other advantages of DOAS are obvious such as less noise, lower air draft and better thermal comfort (Yu *et al.*, 2009).

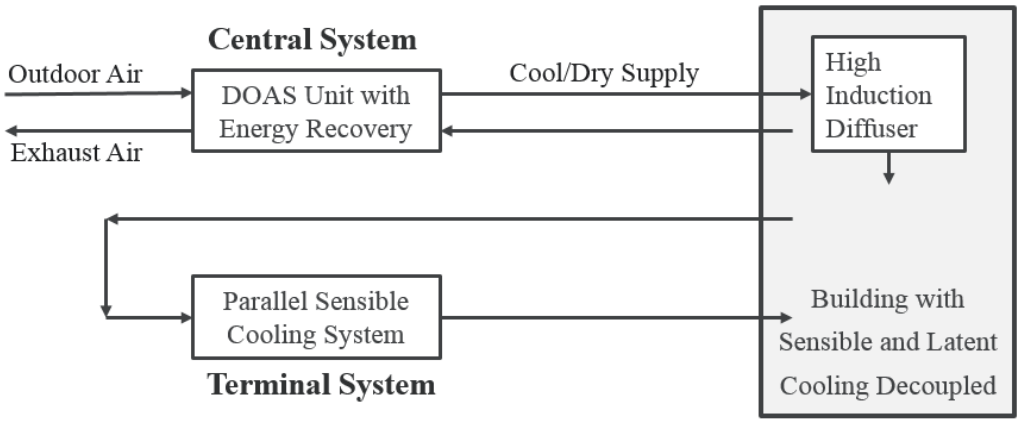

Figure 2.1 Schematic of a dedicated outdoor air system (Dieckmann et al., 2003)

However, there are concerns with such a system configuration. The use of active-desiccant technology to produce OA, despite it is energy effective (Fong *et al.*, 2011), is space intensive to hinder its popular use in land scarcity cities like Hong Kong (Lee and Lee, 2013). The use of chilled beams/ceilings as a terminal system will cause condensation problem, especially in subtropical regions where summers are long, hot and humid (Niu *et al.*, 2002).

Many research efforts have been made to eliminate condensation with different control methods and system configurations. Yin et al. (Yin *et al.*, 2014) proposed to set the beam/ceiling surface temperature higher than the indoor dew point temperature (DPT). Mumma (Mumma, 2002) proposed a control system to regulate the operations of

DOAS and chilled ceiling based on the indoor RH to avoid condensation. A study by Chen et al. (Chen *et al.*, 2014) on active beams indicated that by the use of a dynamic tracking system to control the off coil temperature of the secondary air above DPT, condensation-free environment could be achieved even in hot and humid climate like Singapore. The actual use of an active chilled beam system in a Singapore office building (Kosonen and Tan, 2005) also confirmed that by limiting the indoor humidity gain through minimizing infiltration and by supplying sufficient conditioned air, condensation-free indoor environment could be achieved. However, these proposed methods will unavoidably introduce constraints on the cooling capacity (Mumma, 2002) and the operation of the terminal system (Chen *et al.*, 2015).

To address the concerns, research studies have been done to investigate into using other system configurations associated with DOAS. A series of studies have been done to investigate the use of chilled water system to treat OA and the use of dry fan-coil unit as the terminal system. However, it was found that the potential energy benefit is not significant and the condensation problem still exists (Lee *et al.*, 2012; Jia and Lee, 2013; Jia *et al.*, 2013). Another study investigated the use of fan-coil unit as the OA system and chilled ceiling as the terminal system. It was found that condensate-free can only be achieved on the provision of a surface temperature control (Nutprasert and Chaiwiwatworakul, 2014).

2.2 Cold Air Distribution System (CoAD)

Cold air distribution (CoAD) systems, also known as low-temperature air distribution systems, adopt supply air (SA) at a lower temperature (typically between 4 °C and

10 °C) than conventional air distribution systems (typically between 10 °C and 15 °C) for space cooling (Kirkpatrick and Elleson, 1996). CoAD system is not a new technology, and has long been used in industrial applications for humidity control with SA at 4 °C or even lower. In 1950s, its application was extended to residential and small commercial buildings using SA at 9 °C. It was later applied in hospitals with SA at 2 °C to 4 °C. However, there is no clear definition for CoAD. It was suggested that the actual supply air temperature (SAT) should be determined by operational needs (Bauman *et al.*, 1992).

CoAD system developed quickly in recent decades for its better energy efficiency, lower costs, better humidity control and IAQ. Compared to conventional system, the lower SAT leads to reduction in SA volume flow rate, thus decreases fan energy usage, and ducts size. Together with the omission of air handling units, the use of CoAD results in an obvious cut in initial and operating costs (Kirkpatrick and Elleson, 1996). Furthermore, the cooling of SA below its dew point (DT) will result in deep dehumidification of moist air to produce cold and dry air. The cold and dry air delivered to the conditioned space results in lower indoor humidity level (Murphy, 2011), and thus the threat of mould and mildew growth will be decreased and the IAQ can be enhanced (Yu *et al.*, 2009).

Further advantages of a lower indoor humidity level is to help reduce skin moisture and perspiration and thus increase thermal comfort (Berglund, 1991). The friction between skin and clothing will also decrease to make fabrics feel smoother and clothing less sticky. The indoor dry bulb (DB) temperature can also be set higher to derive additional energy savings (Berglund, 1991, 1994). Figure 2.2 shows the

equivalent thermal comfort line which indicates that it is possible to increase the DB temperature from 23.9 °C to 24.4 °C by decreasing the RH from 50% to 35% (Kirkpatrick and Elleson, 1996). However, a further drop in space RH (below about 30%) is not recommended because of the associated discomfort (dry nose, throat, eyes and skin) and health concerns (drying of skin and mucous surfaces) (Kirkpatrick and Elleson, 1996).

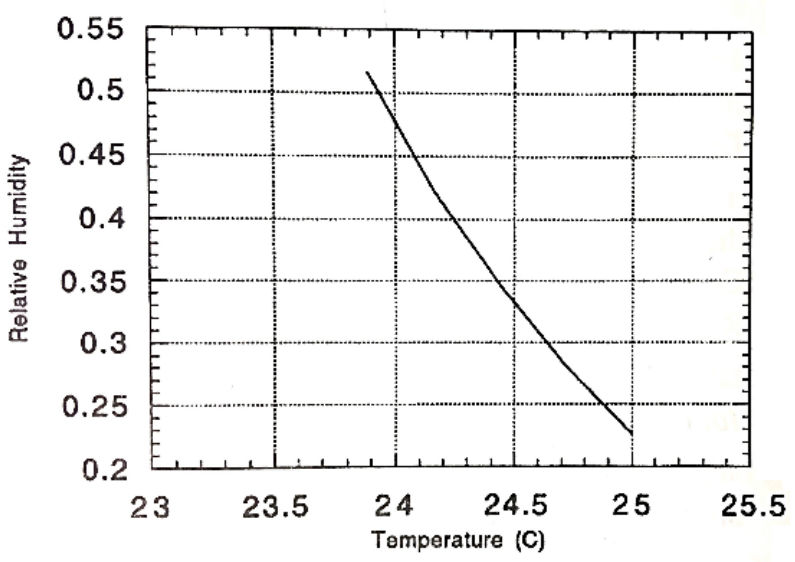

Figure 2.2 Equivalent thermal comfort (Kirkpatrick and Elleson, 1996)

CoAD system generally adopts ice storage system, chilled-water system and direct expansion (DX) system as the cooling plant to generate SA. Ice storage system stores cold energy during off-peak periods (with cheaper electricity) which can later be used to save energy cost (Dincer and Rosen, 2002). Because of its high economic efficiency (Rismanchi *et al.*, 2012), it has been deployed in many countries (Chan *et al.*, 2006a) (Vetterli and Benz, 2012; Sanaye and Hekmatian, 2016). However, as different control strategies and configurations are available, sizing of different components of an storage system is still a challenge (Song *et al.*, 2018). The SAT will also be increased

with a drop in heat transfer effectiveness during the complicated ice melting process (Kirkpatrick and Elleson, 1996). As for conventional chilled-water system, chilled water generation temperature is typically between 4 °C and 8 °C. This temperature range can only produce SA at 8 °C or even higher. If a lower SAT is required, anti-freeze agents like ethylene or propylene glycol have to be added to the chilled water system (Bauman *et al.*, 1992; Kirkpatrick and Elleson, 1996). The associated problems are reduced heat transfer and corrosion. The cost implication is also a concern. DX system can also be used in CoAD as introduced by Kirkpatrick and Elleson (1996) but relevant research is little. Compared to chilled-water system, the SAT is less stable because of the use of compressor with simple on-off control. However, with DX systems equipped with variable speed compressors and supply fans have become popular, a better control of SAT can be achieved. Thus, the use of DX system for CoAD can be a good option.

A concern of the use of CoAD for living and working environments is the thermal discomfort associated with cold air dumpling when cold air is supplied directly to the air-conditioned spaces. However, this can be solved by mixing cold air with warm room return air to become a warmer SA (Youssef *et al.*, 2017). The cold air mixing process can be achieved by installing a fan-powered mixing box (FPMB) in the terminal system. To suit ducting arrangement, FPMB can be series or parallel connected (see Figure 2.3).

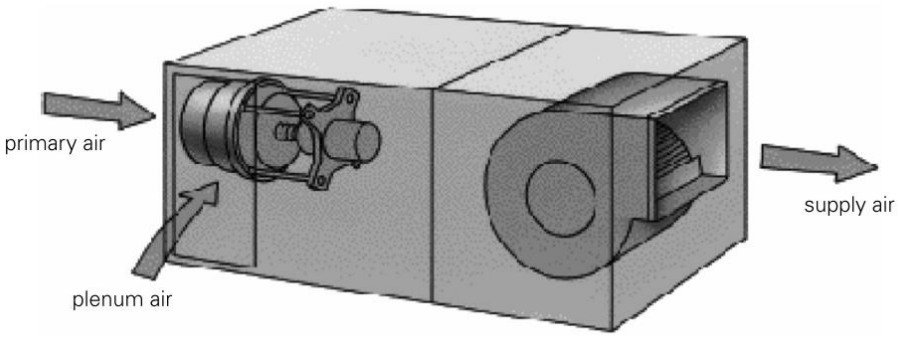

(a) Series FPMB

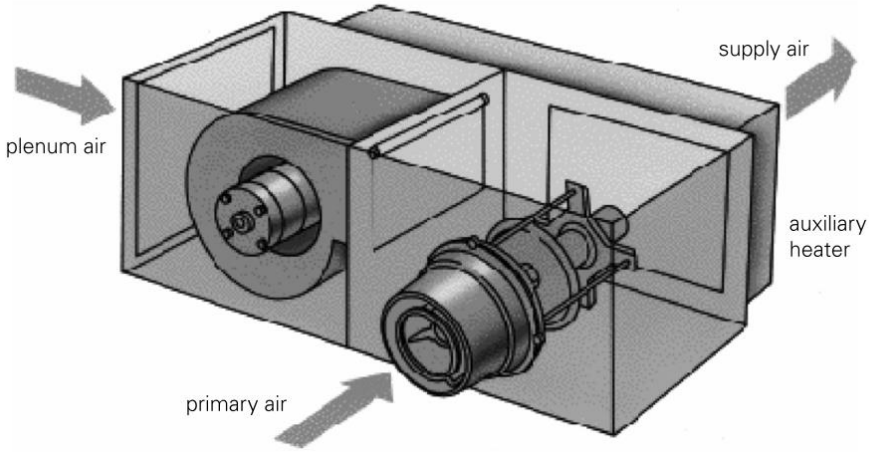

(b) Parallel FPMB

Figure 2.3 Fan-powered mixing boxes (FPMB) (TRANE, 2000)

2.3 Direct Expansion (DX) Air-conditioning (AC) System

Direct expansion (DX) air-conditioning (AC) system (see Figure 2.4) uses a refrigerant vapour expansion/compression cycle to cool the SA directly. The refrigerant at the evaporator (DX coil) absorbs heat from the air when changed from liquid to vapour. The vapour then flows to the compressor as a low-pressure vapour and moves out of the compressor as a high-pressure vapour. The high-pressure vapour then flows to the

condenser which gives out heat when changed from vapour to liquid. Finally, the refrigerant moves to the evaporator where the entire cycle is repeated.

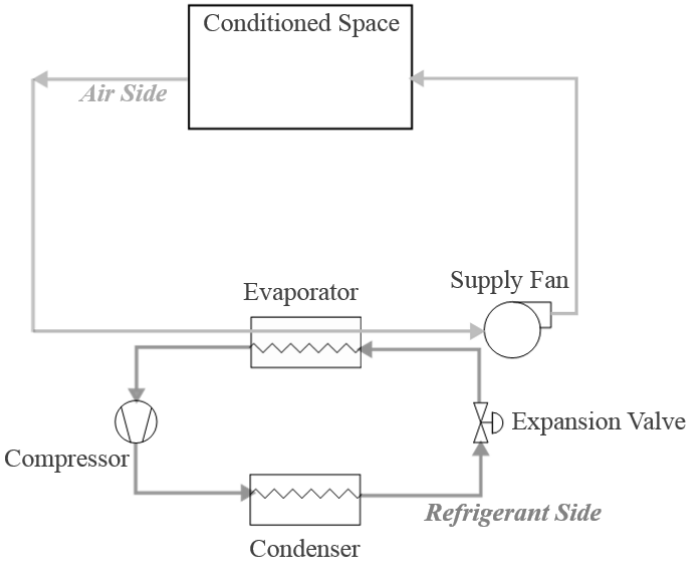

Figure 2.4 Schematic diagram of a typical DX AC system

Compared to conventional chilled water-based system, DX AC has better dehumidification performance (Li *et al.*, 2015a) and energy efficiency (Li and Deng, 2007c), and is widely used in small to medium-scaled buildings as it is less expensive, less complex, flexible in installation and in operation (Li *et al.*, 2015a).

Conventional DX AC systems are equipped with single speed compressors and fans. Capacity control relies on on-off cycling of compressor to maintain indoor DB temperature but indoor RH is often sacrificed to cause thermal discomfort and poor IAQ (Li *et al.*, 2015a). In order to enhance control of both the indoor air temperature and RH when using DX AC, new generation DX ACs are often equipped with variable

speed (VS) compressors and supply fans (Andrade and Bullard, 2002; Li and Deng, 2007a).

However, the indoor air temperature and humidity are strongly coupled (Krakow, KI *et al.*, 1995; Li and Deng, 2007c; Li, Zhao *et al.*, 2015). Conventional proportional-integral-derivative (PID) control strategy is difficult to control indoor air temperature and humidity simultaneously (Krakow *et al.*, 1995a). Thus for DX AC using VS compressor and fan (VS-DX AC system), the variations in the speeds of compressor and fan will lead to a wide fluctuations in evaporating temperature and thus the SA condition (Li and Deng, 2007c; Liang *et al.*, 2008).

To achieve simultaneous control of indoor temperature and humidity with acceptable control accuracy and sensitivity, Li and Deng (Li and Deng, 2007a, 2007b) proposed and investigated the use of a direct digital controller (DDC) for VS-DX AC system by an experimental study. The results showed that through DDC control to vary the compressor and supply fan speeds, the equipment SHR could match with the conditioned space SHR under fixed inlet air conditions (24 °C DB/ 50% RH). Xu et al. (Xu *et al.*, 2010), in another study on VS-DX AC, has established a correlation between cooling output and equipment SHR to enable further enhancement of the control algorithm of VS-DX AC.

To further improve the operating and energy performance of VS-DX AC, the use of a multi-input multi-output (MIMO) controller has been proposed (Qi and Deng, 2009). Based on a linearized dynamic model, the MIMO controller was designed and developed in an experimental study (Qi and Deng, 2008). Unlike conventional on-off

control method or single-input single-output (SISO) control strategy, MIMO controller can simultaneously control the indoor air temperature and humidity with adequate control sensitivity and accuracy. Same conclusion was drawn in a similar study by Huh and Brandemuehl (2008).

2.4 Multiple Units

Multiple units are commonly applied in central chilled water system to meet various cooling load demand. In such a system, every chiller is independent of each other to provide standby capacity, operational flexibility, and less disruption maintenance (Beghi *et al.*, 2011). Compared to a single-chiller system, use of multi-chiller system can take advantage of chillers optimization to achieve a higher coefficient of performance (*COP*) under part load conditions (Chang *et al.*, 2005).

On chiller optimization, research works have been focused on evaluating the use of different control strategies for achieving a higher *COP* for the entire system (Sun *et al.*, 2010; Fan *et al.*, 2011a; Huang *et al.*, 2016) Despite multiple chillers are typically connected in parallel, sequential control is often suggested (ASHRAE, 2011). As such, many chiller sequencing control strategies are proposed based on part load performance, such as return chilled water temperature based control, bypass flow based control, direct power based control, and cooling load based control (CLC) (Honeywell, 1997). Among them, CLC is the most effective method as it can directly calculate and predict the cooling load by measuring the flow rate, supply and return temperature of chilled water (Huang and Li, 2014).

Other than chiller optimization, a lot of studies have been done to investigate the influence of different designs on the system's overall performance including heat rejection mediums (Fan *et al.*, 2011b), ambient conditions (Thangavelu *et al.*, 2017), compressor efficiencies (Beghi *et al.*, 2011), unit capacities (Yu and Chan, 2006; Coelho *et al.*, 2014) and part load performances (Chang and Chen, 2009).

Multiple units connected together are rarely used in DX AC systems. However, considering that the *COP* of an air-conditioner is closely related to the temperature lift between the condenser and evaporator (Wyssen *et al.*, 2010), considerable energy savings can be achieved if DX units are connected in series to take advantage of the small temperature lifts. Some studies have found that the *COP* of a heat pump unit could be improved up to as high as 10 with the small temperature lifts (Meggers *et al.*, 2010; Wyssen *et al.*, 2011).

2.5 Research Gaps

As discussed above, recent studies advocated the use of DOAS to avoid moisture-related and cross contamination problems for better environmental health and energy efficiency. However, for conventional DOAS, the active-desiccant technology used in OA system is space intensive, and chilled beams/ceilings used in terminal systems have condensation problem, thus their popular use in Hong Kong has been limited. Therefore, a novel DOAS is proposed for better energy efficiency and environmental health.

Compared to a chilled water-based system, DX AC system is less expensive, less complex and the dehumidification performance is better. Furthermore, DX AC system is flexible in installation and in operation, and is considered more energy efficient than conventional chilled water-based system. Adding the wide adoption of VS compressor and fan, the energy efficiency and humidity control of DX AC can further be enhanced.

The use of parallel connected multiple chillers in chilled water-based system has been widely investigated and has proofed effective. However, the use of series connected multi-stage DX system is virtually none.

CoAD has many advantages such as energy efficient, lower costs, better humidity control and indoor air quality. However, little has been done on the use of multi-stage DX AC for generation of extra-low temperature air for CoAD.

Combined the concept of DOAS and CoAD, and given the advantages of multi-stage DX with VS compressor and supply fan, a novel extra-low temperature dedicated outdoor air system (XT-DOAS) is proposed in this study and its detailed configuration is described in Chapter 3. Li et al. (2016) have done a preliminary inquiry to the feasible use of extra-low temperature system in office environments. However, in this study, the better humidity control characteristics of CoAD and the multi-stage energy benefits, which are crucial for the successful use of XT-DOAS, have not been considered.

To fill the research gaps, the focus of this study is on how the XT-DOAS must be designed and matched to achieve the desired cooling and dehumidification

performance under varying cooling load conditions. The proposed work includes performance evaluations in achieving the desired air conditions and better energy efficiency; an identification of the optimal system configuration and operating parameters; and the quantification of the environmental health benefits based upon the condensation and overcooling risks.

CHAPTER 3

SYSTEM DESCRIPTION OF XT-DOAS

This chapter describes and explains the configuration of XT-DOAS with a central OA system (Multi-stage DX unit) and a terminal system (Mixing box). Its preliminary design conditions are also introduced.

3.1 Configuration of XT-DOAS

The proposed XT-DOAS consists of a multi-stage DX unit as the central OA system and a mixing box as the terminal system. They both are assumed provided with variable air volume (VAV) control because Hong Kong office buildings typically adopt VAV systems (Mui, 2006). Figures 3.1 and 3.2 show the schematic diagram and the psychrometric process of the XT-DOAS. The central system uses a multi-stage DX unit to treat a variable volume of OA (State 0) with minimum flow setting to a saturated and extra-low temperature (XT) state (State 2) and subsequently delivers to the mixing box of individual zones to mix with the space RA (State 1) to become SA (State 3). A variable volume of SA successively delivers to the space to offset the instantaneous cooling demand to maintain the desired space conditions (State 1). The minimum OA flow setting is to satisfy the minimum ventilation requirement of the occupied spaces (ASHRAE, 2016).

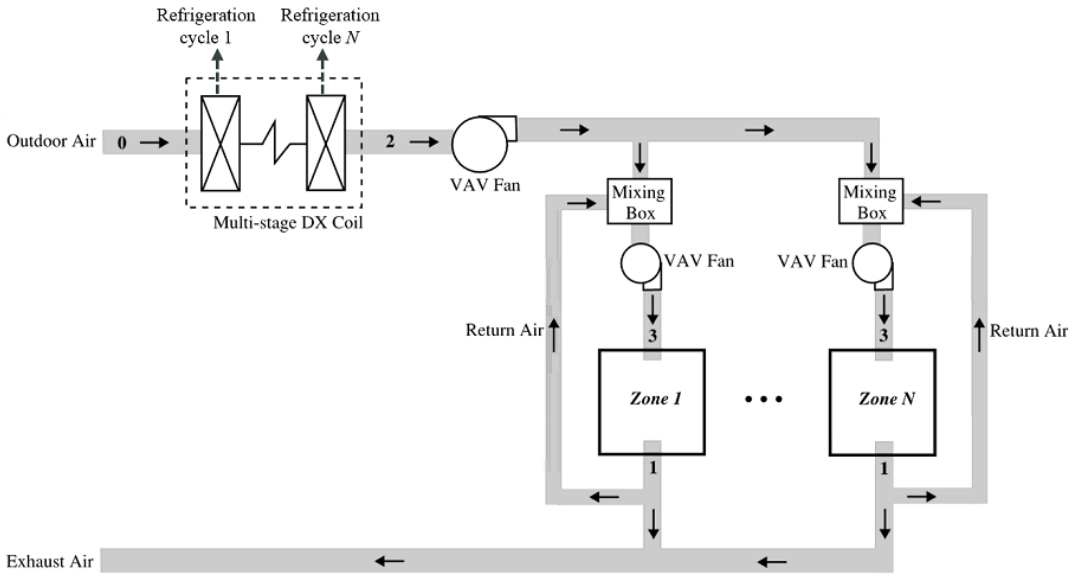

Figure 3.1 Schematic diagram of XT-DOAS

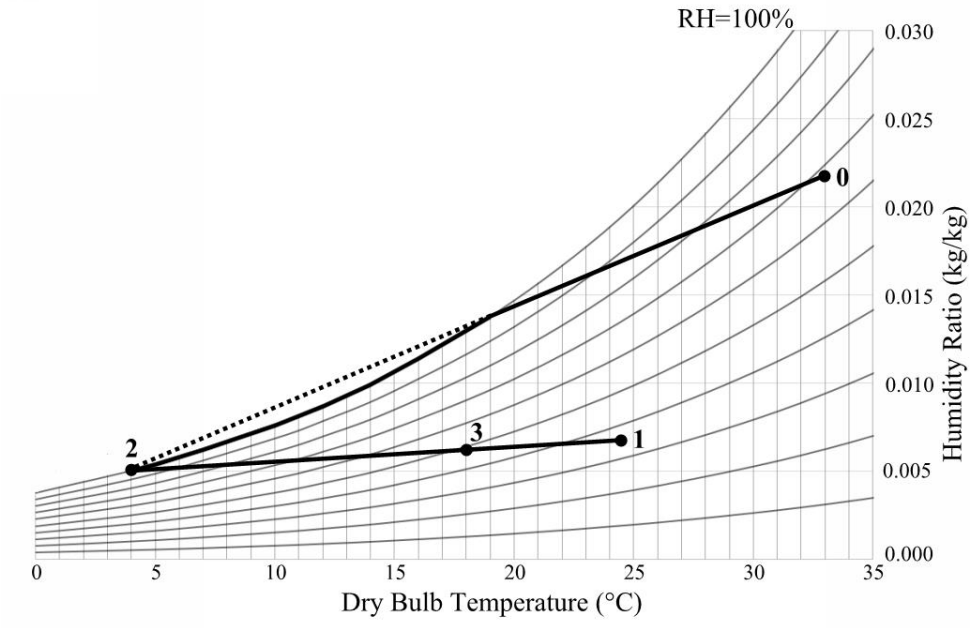

(Dotted line is to show the apparatus dew point)

Figure 3.2 Psychrometric process of XT-DOAS

The major components of XT-DOAS are described in detail as follows.

3.1.1 Multi-stage DX Unit

The central OA system is a variable speed multi-stage DX coil. DX unit is considered because of its ability to operate at low evaporating temperatures to achieve the intended cooling and dehumidification objectives (Kirkpatrick and Elleson, 1996). Variable-speed system capable of regulating its motor speed to modulate output is considered more energy efficient (Li and Deng, 2007c) and has better humidity control (Krakow *et al.*, 1995a). The novel concept of multiple DX units connected in series to become multi-stage DX unit is considered in this study. Each DX coil belongs to a separate refrigeration circuit with its own compressor thus can help meet variable load and produce T_2 as low as 4 °C with little difficulty (Kirkpatrick and Elleson, 1996). This configuration enables improved equipment performance associated with working under higher evaporating temperatures (1st stage) and smaller temperature lifts (between evaporator and condenser) (Meggers and Leibundgut, 2011). It also enables the use of different control strategies to have further energy benefits (Beghi *et al.*, 2011).

3.1.2 Mixing Box

A series connected mixing box is provided for each air-conditioned space to mix the XT OA with the space RA to become SA. SA at a higher temperature is delivered directly to the air-conditioned spaces to avoid condensation on the diffusers. However, condensation in the mixing box is still a concern.

Condensation often occurs when a vapour mixed with a non-condensation gas. These situations can be divided into three types: 1) cooling at the boundaries when the gas flows over a cold surface; 2) adiabatic or nearly adiabatic expansion; and 3) mixing with another cooler gas. In the mixing box of XT-DOAS, the RA (hot condensable vapour) is mixed with XT OA (cool gas). As such, both the vapour concentration and temperature will drop to cause condensation.

Generally, the condensation can be avoided by controlling the relative rates of heat and mass transfer in the mixing process. Under a slowing mixing, condensation can occur easily on dust particles and other suspended matter in the gas. On the contrary, fast mixing will produce high values of the supersaturation, and self-nucleation will dominate. Therefore, under a sufficient fast mixing, is also possible for the system to by-pass the two-phase region to avoid condensation (Levine and Friedlander, 1960).

With the use of SA at a relatively higher temperature, the cold air dumpling problem associated with CoAD system is not a concern. In accordance, no special consideration is needed in selecting diffusers for XT-DOAS, except the use of slot diffuser as always recommended for VAV system (Trane, 2012).

3.2 Design Conditions

Based on Figures 3.1 and 3.2, the design conditions of each state are summarized in Table 3.1.

Table 3.1 Design state conditions of XT-DOAS

State	Condition (T °C [DB]/RH%)
0	33/68
1	24.5/35
2	4/100
3	18/48

It can be seen that the desired indoor conditions of XT-DOAS (State 1) were set at 24.5 °C DB and 35% RH, which has the equivalent thermal comfort level as the common desired indoor condition for Hong Kong office environment (24 °C DB/50% RH) (Macfarlane, 1978). It is required to be established because the SA condition of XT-DOAS is much colder and drier than the conventional system, and thus their achievable space air conditions will be different. The said equivalent condition was determined based on same thermal comfort level as the conventional system and a space RH not lower 30% for comfort and health considerations (Kirkpatrick and Elleson, 1996). Details are shown in Appendix A. In addition, the slightly higher indoor temperature helps reduce sensible cooling energy use to offset the additional latent cooling energy use (Berglund, 1991).

Moreover, to avoid thermal discomfort caused by dumpling XT OA directly into the air-conditioned space, the XT OA is designed to mix with RA to become SA at 18 °C (State 3) for better thermal comfort (Li *et al.*, 2015). The outdoor air conditions (State 0) used in this study were referred to the hourly data of the Typical Meteorological Year (TMY) file of Hong Kong.

The number of cooling stages (N) of the multi-stage DX unit was initially assumed as three with equal sharing of load. This is taking consideration that the temperature differential across a DX coil is typically 10 °C. The treated OA temperature (T_2, the

leaving air temperature at the multi-stage DX unit, State 2) was assumed at 4 °C, being the lowest SAT for CoAD. However, based subsequent configuration optimization of XT-DOAS, the number of cooling stages, the treated OA temperature and the associated airflow rates were adjusted. Details are discussed in Chapter 5, 6 and 7.

CHAPTER 4

METHODOLOGY

This chapter presents the research methodology in this study, for investigating the performance characteristic of XT-DOAS when adopted in an office environment in Hong Kong. The investigations were done based on a case study building and *EnergyPlus* simulations. In the *EnergyPlus* simulations, co-simulation tools and field measurement results were used to facilitate the modelling. They are described below.

4.1 Case Study Building

Table 4.1 Building and design characteristics

Description	Parameter			Value
Internal loads	Occupant density (m^2/person)			9
	Lighting power density (W/m^2)			25
	Appliances power density (W/m^2)			25
Physical details	No. of storey			40
	Floor dimension (L × W) (m)			36×36
	Area per floor (m^2)			1296
	Air-conditioned area per floor (m^2)			1071
	Floor to floor height (m)			3.2
Envelope details	Wall	Resistance (m^2·°C/W) (thickness (m)/conductivity (W/m·°C))	Granite panel	0.009 (0.025/2.9)
			Cavity	0.157
			Concrete	0.046 (0.1/2.16)
			Plaster	0.053 (0.02/0.38)
		Heat transfer coefficient (W/m^2·°C)		3.8
	Single glazing window	Shading coefficient (SC)		0.55
		Window to wall ratio (WWR)		0.5
		Heat transfer coefficient (W/m^2·°C)		5.5
	Roof	Heat transfer coefficient (W/m^2·°C)		0.8

A typical office building was chosen as the case study building. This building's construction characterises were established by reference to finding of extensive surveys conducted in Hong Kong (Jia and Lee, 2013; Jia *et al.*, 2013). The operating hours were assumed 8:00 to 22:00 for weekdays, and 8:00 to 13:00 for Saturdays. The daily patterns of the AC system, occupant, lighting and appliances load, etc. were by referenced to the defaults given in BEAM Plus (BEAM, 2012). The load-related design parameters were determined according to local building energy codes (EMSD, 2012). The building's construction and load-related design parameters are summarized in Table 4.1.

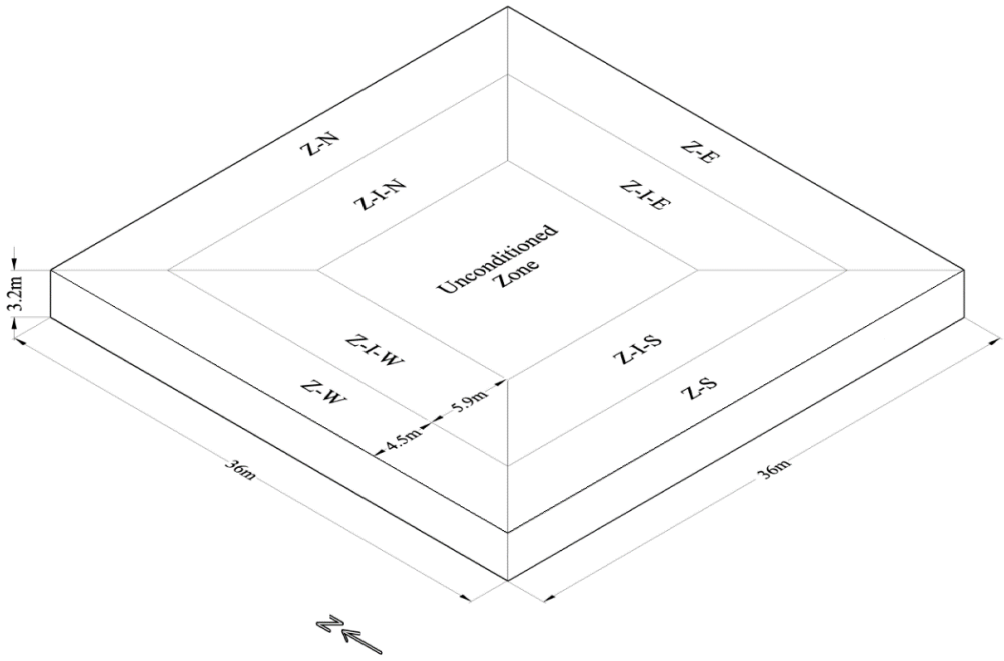

Z-W: Perimeter West Zone; Z-I-W: Interior West Zone;
Z-S: Perimeter South Zone; Z-I-S: Interior South Zone;
Z-N: Perimeter North Zone; Z-I-N: Interior North Zone;
Z-E: Perimeter East Zone; Z-I-E: Interior East Zone.

Figure 4.1 Typical floor layout of the case building

Figure 4.1 shows the typical floor layout. Only one floor is shown because all floors in the building are identical. The floor is divided into perimeter and interior zones and the two zones are further divided into nine zones by orientations. The central zone is not air-conditioned while the other zones are air-conditioned.

4.2 Modelling and Simulation

For evaluating the performance of the proposed XT-DOAS when adopted in the case study building (Section 4.1), a series of simulations were performed using *"EnergyPlus"*. Two co-simulation tools, *MLE+* and *jEPlus*, were employed to facilitate modelling of different control strategy and to accelerate *EnergyPlus* simulations.

4.2.1 *EnergyPlus*

EnergyPlus can simulate the heat transfer through the building envelope, heat gains within the buildings and all the HVAC components. It combines the best capabilities and features of two building performance simulation programs (Building Loads Analysis and System Thermodynamics (BLAST) and DOE-2) along with new capabilities, such as the more accurate prediction of space temperature (Strand *et al.*, 2000).

As a component based system simulation program, *EnergyPlus* can independently model the cooling, defrosting and the dehumidification processes, and thus can model the use XT-DOAS in the case study building. In it, the multi-stage DX unit, being the

most important component of XT-DOAS, can be modelled by user-defined mathematical models. In *EnergyPlus*, DX coil performance model is represented by the following five performance curves (EnergyPlus, 2015):

a) $PLF = f(PLR)$

b) $CAP\text{-}FT = f(WB_{ei}, DB_{ci})$

c) $EIR\text{-}FT = f(WB_{ei}, DB_{ci})$

d) $CAP\text{-}FF = f(m/m_{rated})$

e) $EIR\text{-}FF = f(m/m_{rated})$

where *PLF* is the part load fraction (*PLF*) correlation curve as a function of part load ratio (*PLR*); *CAP-FT* is the total cooling capacity (*CAP*) modifier curve as a function of temperature (*FT*); *EIR-FT* is the energy input ratio (*EIR*) modifier curve as a function of temperature; WB_{ei} is the entering air wet bulb temperature at the DX coil (evaporator), °C; DB_{ci} is the entering air DB temperature at the condenser, °C; *CAP-FF* is the *CAP* modifier curve as a function of air flow fraction (*FF*); *EIR-FF* is a *EIR* modifier curve as a function of air flow fraction; *m* is the actual air mass flow rate, kg/s; m_{rated} is the rated air mass flow rate, kg/s.

Generally, *PLF* curve is set as default in *EnergyPlus*:

$$PLF = 0.85 + 0.15 \times PLR \tag{4.1}$$

Other four performance curves are mathematically shown below (EnergyPlus, 2015):

$$\begin{aligned} CAP\text{-}FT &= CAP/CAP_{rated} \\ &= a_1 + a_2 \cdot WB_{ei} + a_3 \cdot WB_{ei}^2 + a_4 \cdot DB_{ci} + a_5 \cdot DB_{ci}^2 + a_6 \cdot WB_{ei} \cdot DB_{ci} \end{aligned} \quad (4.2)$$

$$\begin{aligned} EIR\text{-}FT &= EIR/EIR_{rated} \\ &= b_1 + b_2 \cdot WB_{ei} + b_3 \cdot WB_{ei}^2 + b_4 \cdot DB_{ci} + b_5 \cdot DB_{ci}^2 + b_6 \cdot WB_{ei} \cdot DB_{ci} \end{aligned} \quad (4.3)$$

$$CAP\text{-}FF = c_1 + c_2 \cdot \left(m/m_{rated}\right) + c_3 \cdot \left(m/m_{rated}\right)^2 + c_4 \cdot \left(m/m_{rated}\right)^3 \quad (4.4)$$

$$EIR\text{-}FF = d_1 + d_2 \cdot \left(m/m_{rated}\right) + d_3 \cdot \left(m/m_{rated}\right)^2 + d_4 \cdot \left(m/m_{rated}\right)^3 \quad (4.5)$$

Amongst the five performance curves, *CAP-FF* and *EIR-FF* relating *CAP* and *EIR* with the ratio of *m* across the cooling coil to m_{rated}, is of no difference to a conventional system. However, the performance curves of *CAP-FT* and *EIR-FT* need to be corrected/developed because XT-DOAS will receive high entering air temperature and generate extra-low leaving air temperature to affect the DX coil performance (EnergyPlus, 2015). The correction/development of the *CAP-FT* and *EIR-FT* curves are described in Chapter 5 and Chapter 6.

Based upon the developed performance curves for the DX multi-stage unit, the use of XT-DOAS for the case study building can be modelled for *EnergyPlus* simulations. The outputs from *EnergyPlus* include the hourly air temperatures, humidity ratios, mass flow rates, coil's loads, thermal comfort and the energy consumption of the equipments etc. They will be used for performance analyses of XT-DOAS.

4.2.2 *MLE+*

An advanced control strategy has been assumed for the multi-stage DX unit. Details are presented in Chapter 5. However, as *EnergyPlus* is a stand-alone simulation engine processing text-based input files to run simulations, it cannot be used to model advanced control feedback strategies such as Model Predictive Control (Camacho and Bordons, 2007). *MLE+* was therefore adopted as a co-simulation tool.

MLE+ is introduced by Bernal et al. (2012) and is a new tool for energy-efficient building automation design, co-simulation and analysis. Its excellent capabilities are introduced as follows:

a) Support high fidelity building simulation software (eg. *EnergyPlus*) and standard scientific computation software (eg. *Matlab/Simulink*).
b) Compare and rapidly simulate scenarios of different control algorithm implementations across a range of building model parameters.
c) Identify and validate simplified models from high order physical models.
d) Optimize parameters of a building model.
e) Design advanced controllers and their quantitative analysis for a building.

In this study, *MLE+* served as a co-simulation tool to combine *Matlab/Simulink* with *EnergyPlus* to enable simulation of optimization control (Zhao *et al.*, 2013). *MLE+* takes full advantage of the *Matlab/Simulink* environment, including interactive simulation, code debugging, code generation and all available toolboxes; making the application of *Matlab* programming easier.

4.2.3 *jEPlus*

jEPlus was used also as a co-simulation tool to investigate the overcooling risk of XT-DOAS based on Monte Carlo simulation (to be introduced in Chapter 7). It is an open-source research tool and was developed in 2009 (Zhang, 2009). It has been developed specifically for performing complex parametric analysis with *EnergyPlus* (eg. Monte Carlo simulation). *jEPlus* have also been used by other researchers for the same purpose (Zhang, 2009; Zhang and Korolija, 2010; Naboni *et al.*, 2013).

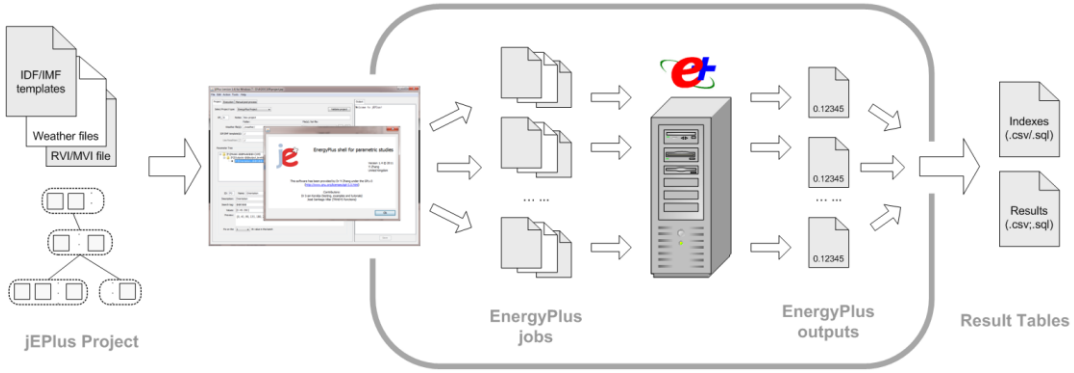

Figure 4.2 The concept of *jEPlus* (jeplus, 2015)

jEPlus allows users to load user-defined weather files and input parameters in a graphical interface to automatically create and carry out *EnergyPlus* simulation jobs (Zhang and Korolija, 2010). The principle of this co-simulation is that *jEPlus* can work with EP-Macro program which is part of the *EnergyPlus* package. It treats *EnergyPlus* model as a single parameter for synchronous change of values at different places in the model and replaces large chunks of model definition. Figure 4.2 shows the concept of *jEPlus*. By using *jEPlus*, complex parametric investigations are replaced by a unique parameter tree and the values of the parameters can be specified with flexible syntax.

With parallel simulations by the controller in *jEPlus*, *EnergyPlus* results can output as Excel (.csv) and database (.sql) which can easily be recognized.

4.3 Field Measurement

A filed measurement was conducted at a pilot installation (Lee, 2010) to collect performance data for DX units operating at extra-low temperature conditions for correction and development of *CAP-FT* and *EIR-FT* curves (Section 5.3.2 and Section 6.3.1). The pilot installation comprised two DX air-conditioners each with a cooling capacity of 22.7 kW together with a total enthalpy heat exchanger. They were connected in series to generate SA at 6 °C DB to maintain a 56 m^2 store room at 10 °C DB. The store room is for dangerous goods. It requires to be maintained at around 10 °C DB year round. To reduce the explosion risk, no air recirculation is allowed, which resembles a DOAS configuration. Given the two DX units were with different operating conditions and thus efficiencies, a sufficiently wide range of data were collected to correct/develop the extra-low temperature part of *CAP-FT* and *EIR-FT* curves. Specifications of the DX air-conditioners and the configuration of the pilot installation are shown in Table 4.2 and Figure 4.3, respectively.

In the pilot installation, a remote monitoring system is deployed to monitor the air-side operating conditions and the power consumption of the two DX air-conditioners and the condenser fans. The air-side operating conditions include the outdoor air temperature, and the entering and leaving air DB and WB temperatures at each of the two air-conditioners. They were measured by a psychrometer inserted into the air circuit. The OA and RA flow rates were measured by flow nozzles. The accuracy of

the major instruments are summarized in Table 4.3. The data recorded between 2011 and 2012 at sampling intervals of 30 minutes were retrieved from the remote monitoring system for analysis. To remove the transient variations in the data series, the moving average values were computed based on a fixed moving time window of 60 minutes. The computed data and their applications are introduced in Chapter 5 and Chapter 6.

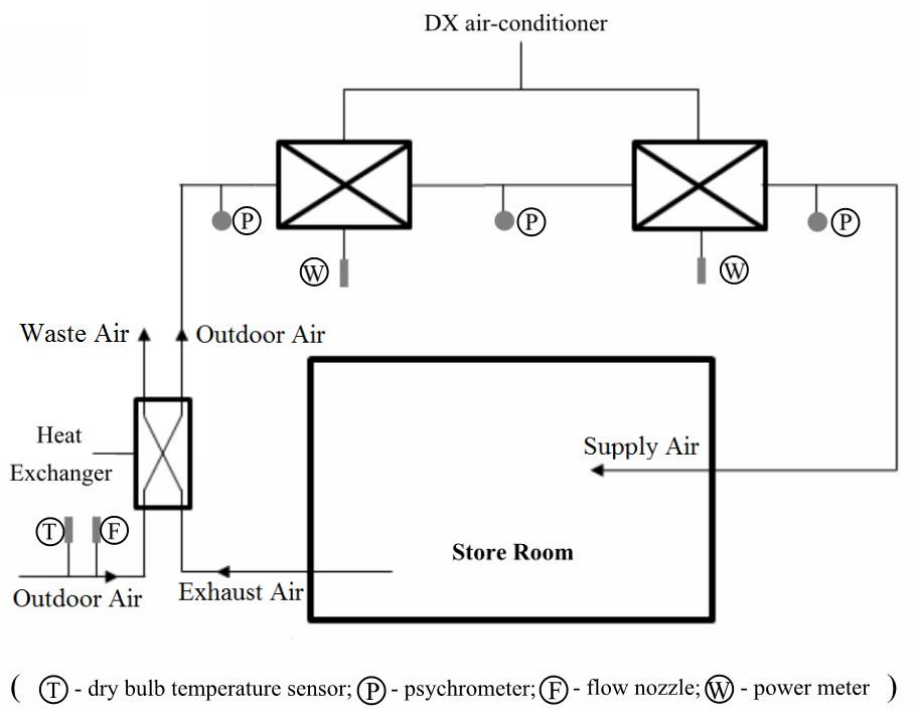

Figure 4.3 Configuration of the pilot installation

Table 4.2 Specifications of the DX air-conditioners

Name	Parameter	Specification
DX Air Handler	Type of refrigerant	R134a
	Type/drive of supply air fan	Centrifugal fan/direct
	Supply air volume flow rate (m^3/s)	0.21
	Outdoor air volume flow rate (m^3/s)	0.21
	Power consumption (kW)	2.20
Condensing Unit	Cooling capacity (kW)	22.70
	Compressor capacity control	Variable speed
	Power consumption (kW)	9.63

Table 4.3 Accuracy and performance standard of major instruments

Instrument	**Measured parameter**	**Range**	**Accuracy**
Psychrometer	Dry bulb temperature Wet bulb temperature	-50 to 100 °C	±0.1 °C
Flow nozzle	Air flow rate	15.3 to 2230 L/min	±2%
Power meter 7330	Power consumption	0-1×10^{6} A	± (0.25% rdg +0.05% F.S.)

CHAPTER 5

HUMIDITY CONTROL AND ENERGY EFFICIENCY OF XT-DOAS IN HONG KONG

This chapter presents evaluations on the effective use of XT-DOAS in Hong Kong office environments. The focus is on evaluating its performance in achieving better humidity control and energy efficiency objectives by conducting *EnergyPlus* simulations. Through hour-by-hour simulations, using actual performance data of a pilot installation and realistic building and system characteristics, the annual AC energy consumption, indoor discomfort hours and condensation risk of XT-DOAS, as compared to a conventional system, were investigated.

5.1 Introduction

To evaluate the performance of XT-DOAS in hot and humid office environments as compared to a conventional system, the concerns are whether the humidity control, and energy efficiency of XT-DOAS are better than conventional AC systems.

As introduced in Chapter 3, VAV control is provided for both the central OA system and the terminal system of XT-DOAS. VAV system has a better humidity control than constant air volume (CAV) system (Murphy, 2010) because of its constant supply air condition to maintain better matching between the equipment and space SHRs even at part load conditions.

To demonstrate the strong humidity control ability of XT-DOAS, the comparison study with the conventional system was based on the worst scenario. This is by assuming the use of the less favourable CAV control for the central OA system instead of VAV control.

To address the concerns of humidity control and energy efficiency, the resultant space relative humidities, thermal comfort level, energy performance and the condensation risk achieved by the XT-DOAS, as compared to a conventional system, were performed.

5.2 Systems Comparison

Figure 5.1 shows the configuration and the psychrometric process of the XT-DOAS with CAV OA system. A constant volume of XT OA is mixed with a variable volume of RA to satisfy the instantaneous space cooling demand. The constant volume of OA (State 0) is treated by the three-stage DX coil to a saturated state with extra-low temperature (State 2) (designed to offset the latent and sensible loads coming from the OA and the indoor heat sources). It is then mixed with the space RA (State 1) to become SA (State 3). The variable speed fan is used to vary the SA volume flow rate and thus the RA flow rate and SA condition for achieving the desired indoor condition (State 1). Use of a three-stage DX coil is the preliminary design of XT-DOAS. State N1 and N2 represent the air state leaving out of the first stage and second stage DX coil respectively.

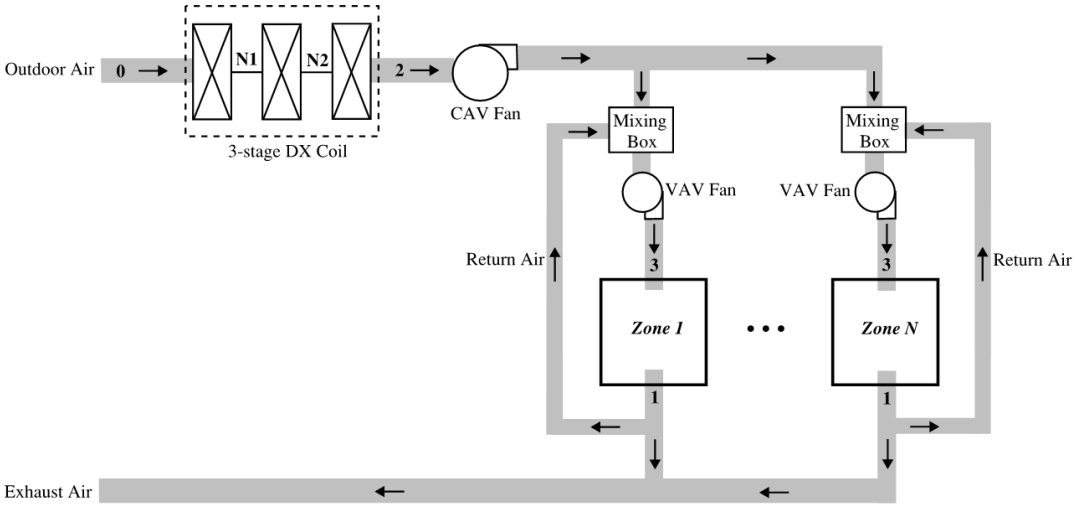

(a) Schematic diagram

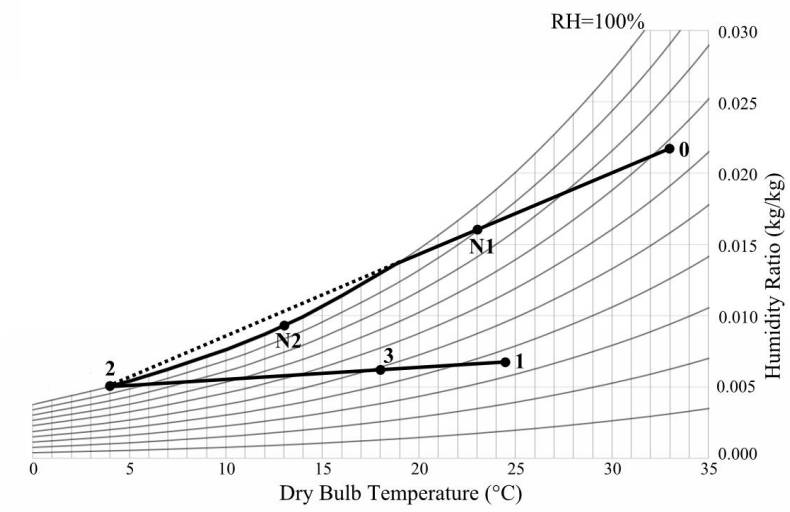

(b) Pyschrometric process

Figure 5.1 XT-DOAS with CAV OA system

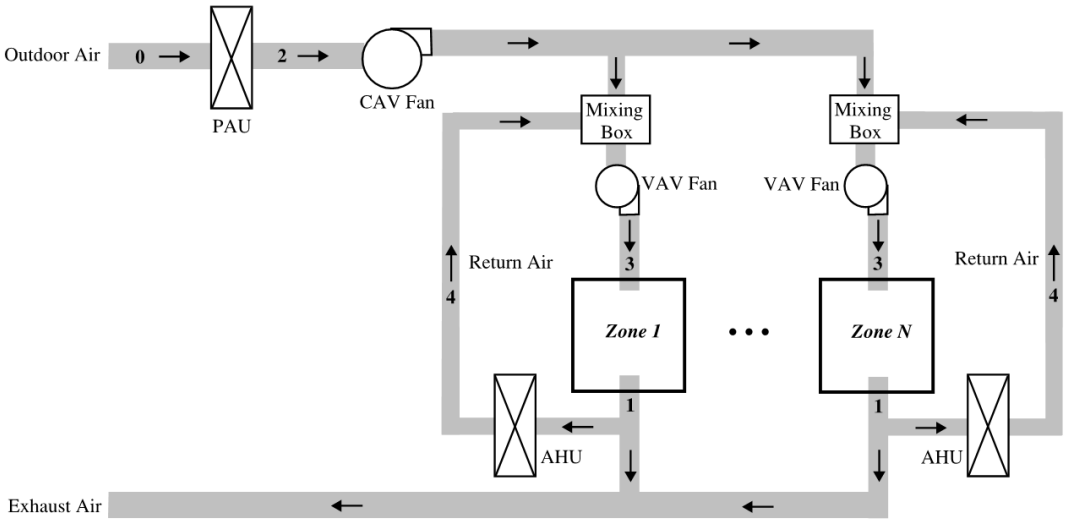

(a) Schematic diagram

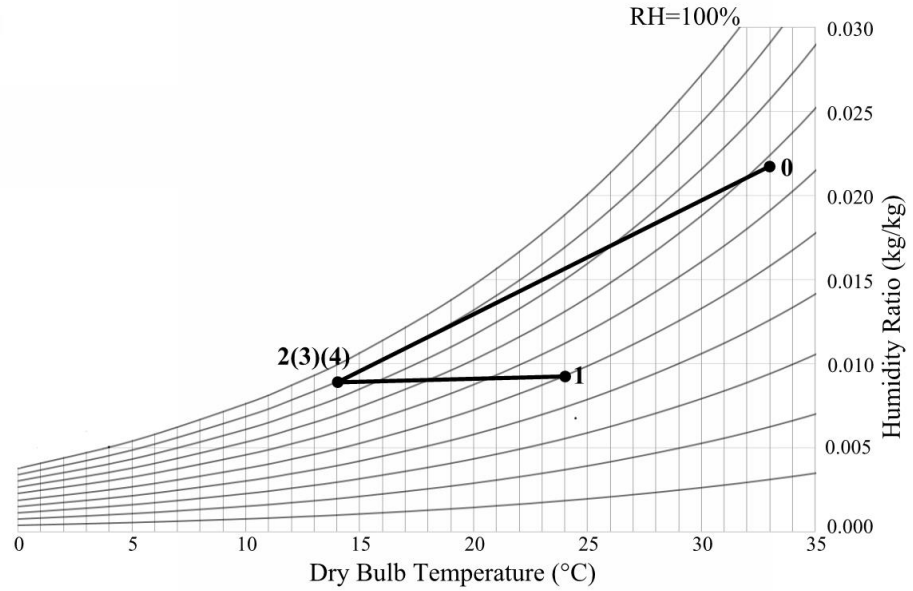

(b) Pyschrometric process

Figure 5.2 Conventional system with CAV OA system

For a fair comparison, the conventional system in this chapter was also assumed to have CAV control for central OA system and its configuration and psychrometric process are shown in Figure 5.2. The primary air-handing unit (PAU) and air handling

unit (AHU) are using DX coil. The PAU is used to cool and dehumidify a constant volume of OA from State 0 to State 2. The AHU is used to cool the RA from State 1 to State 4 which is the same condition as State 2 for better matching of equipment and space SHRs (ASHRAE, 2009). The two streams of air are subsequently mixed and supplied as SA (State 3). The variable speed fan is used to vary the SA volume flow for achieving the desired indoor conditions (State 1).

The design conditions of the two systems when applied in the case study building (see Section 4.1) are summarized in Table 5.1. They were sized by common design practice. The following are the assumptions:

1. The outdoor air conditions (State 0) refer to the hourly weather conditions in Hong Kong in 1995, which is the typical meteorological year for Hong Kong (Chan *et al.*, 2006b).

2. The design space condition is 24 °C DB temperature and 50% RH, which is commonly used for Hong Kong office environments, and is also within the thermal comfort zone (Macfarlane, 1978).

3. The design thermodynamic states and air flow rates of the conventional system were determined by psychrometric analysis based on the peak sensible and latent loads simulated by *EnergyPlus* (EnergyPlus, 2015).

4. The design SAT of the XT-DOAS was determined based on a previous study for optimizing energy usage and thermal comfort (Li *et al.*, 2015). The associated

thermodynamic states and air flow rates were determined by psychrometric analysis based on the peak sensible and latent loads simulated by *EnergyPlus* (EnergyPlus, 2015).

5. The equivalent design space condition for XT-DOAS is 24.5 °C DB temperature and 35% RH which has the equivalent thermal comfort level with conventional system (24 °C DB /50% RH). It was mentioned in Section 3.1 and the details of the determination are show in Appendix A.

6. The coefficient of performance of the DX coil system at Air Conditioning, Heating and Refrigeration Institute (AHRI) rated conditions (AHRI, 2001) is 3.5, which is the most found equipment performance in the market.

7. The temperature lifts of XT-DOAS were determined based on the sensible and latent loads of the conditioned zones under design condition for meeting the coincident cooling and dehumidification demands. Equal sharing of load amongst the three cooling stages was assumed.

8. The SAT T_3 (State 3 for both XT-DOAS and conventional system) remains constant but the SA volume flow rate (V_3) varies with the instantaneous cooling demand.

9. The OA flow rate (V_0) is maintained constant. The amount for the conventional system was determined by the people- and area-related factors for satisfying the ventilation requirement in the breathing zone of the occupied spaces (ASHRAE,

2016). Meanwhile, the amount for XT-DOAS was determined by the peak cooling load which is higher than the value determined for the conventional system.

Table 5.1 Design conditions

Design Conditions		System	
		XT-DOAS	**Convention**
Internal loads	Sensible load (kW)	63.82	64.82
	Latent load (kW)	6.13	5.83
	Sensible heat ratio	0.912	0.917
State Point (T°C(DB)/RH%)	0	33/68	
	1	24.5/35	24/50
	N1	23/90	-
	N2	13/100	-
	2	4/100	14/90
	3	24.5/35	14/90
	4	-	14/90
Air flow rate (m^3/s)	Outdoor air	2.40	1.20
	Maximum return air	5.17	4.11
DX air-conditioner performance	Rated *COP*	3.5	

5.3 Control Strategy and Performance Correction

EnergyPlus was adopted to investigate the humidity control and energy efficiency for both XT-DOAS and conventional system. Due to the multi-stage and extra-low temperature characteristics of XT-DOAS, before analysing its performance, the optimized control strategy and DX coil performance correction need to be introduced.

5.3.1 Optimized Control Strategy

The coefficient of performance (*COP*) of a DX coil is often affected by its part load ratio (*PLR*). In *EnergyPlus* (EnergyPlus, 2015), they are related as shown in Equations (5.1) to (5.5).

$$COP = \frac{Q}{W} \tag{5.1}$$

$$PLR = \frac{Q}{Q_{rated}} \tag{5.2}$$

$$W = Q_{rated} \cdot RTF \cdot EIR\text{-}FT \tag{5.3}$$

$$RTF = \frac{PLR}{PLF} = \frac{PLR}{0.85 + 0.15PLR} \tag{5.4}$$

$$COP = \frac{0.85 + 0.15PLR}{EIR\text{-}FT} \tag{5.5}$$

where Q is the cooling output, kW; W is the operating chiller power, kW; and Q_{rated} is the rated cooling output, kW; RTF is the run time fraction.

It can be seen that the *COP* is often affected by its *PLR*. *COP* increases with *PLR* at a given environmental condition. To achieve a higher *COP*, an optimized control strategy was proposed.

As mentioned in Section 5.2, for the three-stage DX coil of XT-DOAS, equal sharing of load amongst the three cooling stages was assumed. Thus, an optimization control could be introduced to stage-off one of the cooling stages for each one-third drop in rated cooling capacity. As such, the *PLR* of the active coil could be maximized to improve the overall *COP*. However, the same does not apply to the conventional system because it is a single stage DX unit.

Unfortunately, *EnergyPlus* has limited capability for algorithm development and optimal control synthesis and cannot be directly interfaced with scientific computation and simulation software like *Matlab*/*Simulink* (Bernal *et al.*, 2012). Thus to model the

proposed control strategy for the XT-DOAS, *MLE+* (Zhao *et al.*, 2013) was used as a co-simulation tool to combine *Matlab*/*Simulink* with *EnergyPlus* for optimization control.

Figure 5.3 shows the control implementation schematic diagram. The hour-by-hour cooling demand is simulated by *EnergyPlus* and output to *Matlab*/*Simulink* through *MLE+*. The control code in *Matlab*/*Simulink* continuously compares $Q(t)$ with Q_{rated} of the three-stage DX unit. On every one-third drop in cooling demand, *Matlab*/Simulink resets the availability schedule to stage-off one of the cooling stages. Otherwise, *Matlab*/*Simulink* does not output any control signal and the number of cooling stages stays at the last position and no further change to the status of on and off stages happens.

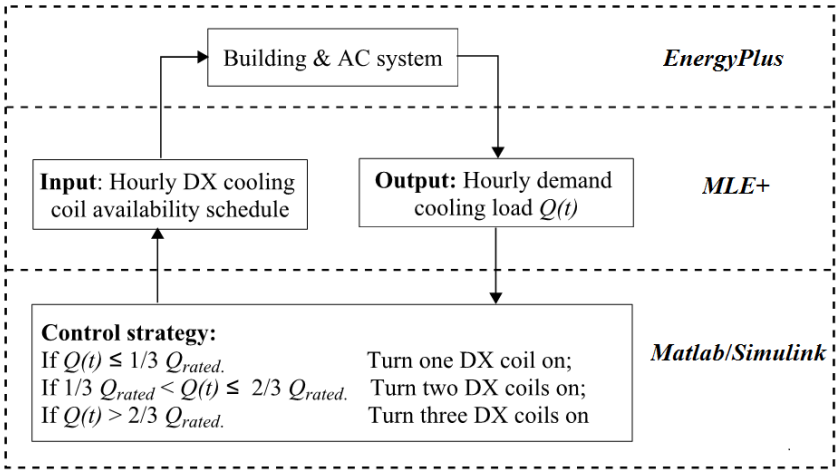

Figure 5.3 Co-simulation schematic diagram with *MLE+*

5.3.2 DX Coil Performance Correction

Compared to the conventional system, XT-DOAS has the extra-low temperature operating characteristic that will affect the multi-stage DX unit's energy performance. In this comparison study, energy performance is one of the assessment criteria to confirm the effective use of XT-DOAS. Thus, the energy performance of the DX coil needs to be corrected for operating at less favourable extra-low temperatures.

As mentioned in Section 4.2.1, in *EnergyPlus*, the energy performance curve that needs to be corrected is the *EIR-FT* curve:

$$\begin{aligned} EIR\text{-}FT &= EIR / EIR_{rated} \\ &= b_1 + b_2 \cdot WB_{ei} + b_3 \cdot WB_{ei}^2 + b_4 \cdot DB_{ci} + b_5 \cdot DB_{ci}^2 + b_6 \cdot WB_{ei} \cdot DB_{ci} \end{aligned} \quad (5.6)$$

Performance data for DX unit operating at extra-low temperature are not available in public domain. The field measurement data as described in Section 4.3 was employed to correct the DX coil performance curve. Based also on the corresponding OA and RA flow rates measured by the flow nozzles, the *EIR* of the DX coil operating at a range of WB_{ei} and DB_{ci} in Equation (5.7) and the performance correction coefficient *g* in Equation (5.8) can be determined.

$$EIR = \frac{W_{com} + W_{Fan}}{Q} = \frac{W_{com} + W_{Fan}}{\rho_a \cdot V_{sa} \cdot \left(h_{ei} - h_{eo} \right)} \quad (5.7)$$

$$g\left(WB_{ei}, DB_{ci}\right) = b_1 + b_2 \cdot WB_{ei} + b_3 \cdot WB_{ei}^2 + b_4 \cdot DB_{ci} + b_5 \cdot DB_{ci}^2 + b_6 \cdot WB_{ei} \cdot DB_{ci} \quad (5.8)$$

At a given time, W_{com} is the measured compressor power, kW; W_{Fan} is the measured condenser fan power, kW; ρ_a is the air density, kg/m^3; V_{sa} is the measured SA volume flow rate, m^3/s; h_{ei} is the evaporator inlet air enthalpy, kJ/kg; h_{eo} is the evaporator outlet air enthalpy, kJ/kg. h_{ei} and h_{eo} are calculated based on the instantaneous *DB* and *WB* temperatures.

Based on the averaged data computed as explained in Section 4.3, the average correction coefficient g for each coincident WB_{ei} and DB_{ci} was obtained. Combining the actual operating data for extra-low temperatures with the manufacturer's standard performance data, a total of 132 data sets were obtained. Table 5.2 summarizes the g values for a range of WB_{ei} and DB_{ci}.

Based on the results in Table 5.2, a multiple regression analysis was conducted to determine the coefficients for Equation (5.8). SPSS was employed for the analysis (Hayes and Matthes, 2009).

Table 5.2 Correction coefficient (g) at various WB_{ei} and DB_{ci} conditions

WB_{ei}	DB_{ci} (°C)										
(°C)	**25**	**26**	**27**	**28**	**29**	**30**	**31**	**32**	**33**	**34**	**35**
6	3.711	3.669	3.626	3.584	3.543	3.502	3.461	3.420	3.380	3.340	3.300
8	3.321	3.271	3.222	3.173	3.125	3.076	3.028	2.981	2.933	2.886	2.839
10	2.973	2.916	2.859	2.803	2.748	2.692	2.637	2.582	2.528	2.474	2.420
12	2.665	2.602	2.538	2.475	2.412	2.350	2.288	2.226	2.164	2.103	2.042
14	2.400	2.329	2.258	2.188	2.118	2.049	1.980	1.911	1.842	1.774	1.706
16	2.176	2.098	2.020	1.943	1.866	1.789	1.713	1.637	1.561	1.486	1.411
18	1.993	1.908	1.823	1.739	1.655	1.571	1.488	1.405	1.322	1.239	1.157
20	0.819	0.835	0.851	0.868	0.885	1.395	0.920	0.938	0.956	0.975	0.994
22	0.807	0.822	0.837	0.852	0.868	1.259	0.900	0.917	0.934	0.951	0.969
24	0.793	0.806	0.820	0.834	1.202	1.166	0.877	0.893	0.908	0.924	0.940
26	0.774	0.786	0.799	0.811	1.195	1.241	0.851	0.865	0.879	0.894	0.909
28	0.753	0.764	0.775	0.786	0.798	0.809	0.822	0.834	0.847	0.860	0.874

The coefficients for Equation (5.8) determined based on the ordinary least square method is shown in Table 5.3. The accuracy of resultant model was checked based on the coefficient of variation (*CV*) of the root-mean-square error (*RMSE*) and the coefficient of determination (R^2), which are defined mathematically as follows:

$$CV = \frac{RMSE}{\left|\sum_{i=1}^{n} \frac{y_i}{n}\right|} \tag{5.9}$$

$$RMSE = \sqrt{\frac{1}{n} \cdot \sum_{i=1}^{n} \left(y_i - \hat{y}_i\right)^2} \tag{5.10}$$

$$R^2 = 1 - \frac{\sum_{i=1}^{n} \left(y_i - \hat{y}_i\right)^2}{\sum_{i=1}^{n} \left(y_i - \bar{y}\right)^2} \tag{5.11}$$

where y_i is the *i*-th actual value of *EIR* based on different WB_{ei} and DB_{ci} in Equations (5.7); $\bar{y}$ is the mean of actual values; $\hat{y}_i$ is the *i*-th fitted value which can be calculated from the different WB_{ei} , DB_{ci} and regressed coefficients in Equations (5.8); *n* is total number of data pairs.

Table 5.3 Coefficients of the regression equation

Coefficient	**Value**
b_1	6.331
b_2	-0.4128
b_3	0.00502
b_4	0.0189
b_5	-0.00192
b_6	0.00387
R^2	0.97

The results show that *CV* value is 1.199%, which is much smaller than the recommended value of 3-5% in previous studies (Reddy and Claridge, 2000), and the R^2 is 0.97. They confirmed the accuracy of the regression model. Figure 5.4 shows the difference between actual values and fitted values of the performance correction coefficient *g*. The resultant model was used for performance analysis of XT-DOAS.

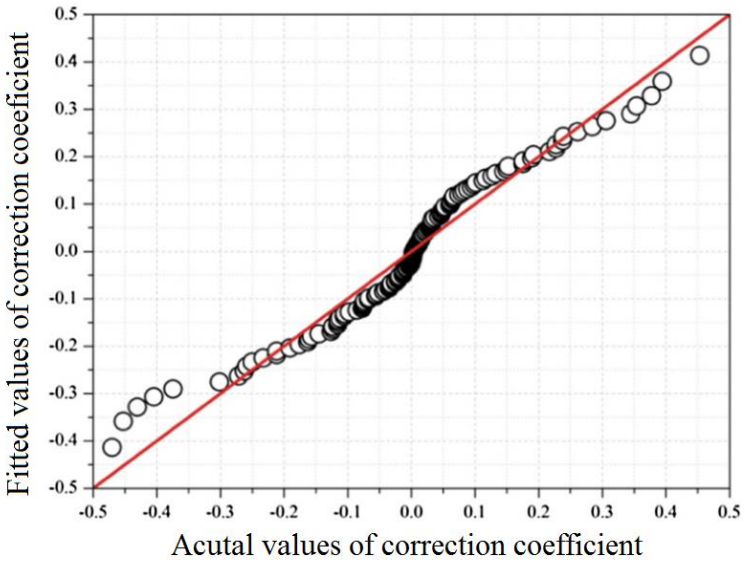

Figure 5.4 Actual and fitted values of the performance correction coefficient

5.3.3 Performance Analysis

For a comprehensive analysis of the performance of XT-DOAS as compared to the conventional system in achieving the intended energy efficiency, humidity control and better environmental health objectives, the comparative evaluation will consist analyses of: a) energy use; b) resultant space RHs; and c) condensation risk.

Based on the resultant air conditions extracted from *EnergyPlus* results, the humidity control performance, the number of non-comfortable hours (NCH) and the condensation risk of the two systems can be compared.

Whether the resultant air conditions are comfortable is determined by comparing against the requirements in ASHARE 55-2013 (2013). The comfort zone in ASHRAE is set based on the operative temperature and humidity ratio.

Based on the resultant air conditions, condensation risk on the SA terminal devices can be revealed by a comparison of the SAT and the zone DPT. If the SAT is lower than zone DPT, condensation occurs and the operational hours concerned are counted towards the annualised cumulative condensation hours ($ConH_{total}$).

5.4 Results and Discussion

The results from simulation and calculation including energy use, resultant space RHs, non-comfortable hours (NCH) and condensation risk are discussed as follows.

5.4.1 Energy Use

Breakdowns of annual energy use of XT-DOAS and the conventional system are compared in Table 5.4. For XT-DOAS, because of its higher maximum SA and OA flow rates (7.57 Vs 5.31 m^3/s for SA and 2.40 Vs 1.20 m^3/s for OA), energy consumption of the fans is 80.9% higher than the conventional system. But the higher fan energy consumption is offset by the better performance of the three-stage DX coils, leading to a cooling energy use reduction by 28.3% and an overall saving in energy use of the order of 22.6%. The results confirm that the proposed XT-DOAS is more energy efficient than the conventional system.

Table 5.4 Breakdown of annual energy use

End use	Annual energy use (kWh/m^2)		Energy Saving
	XT-DOAS	Conventional	
Cooling	208.3	290.4	28.30%
Fans	28.7	15.9	-80.90%
Total Air-conditioning	237	306.3	22.60%

To explain the reduction in cooling energy use of XT-DOAS, its annual mean coefficient of performance (abbreviated as) $\overline{COP}$ as defined in Equation (5.12), as compared with that of the conventional system, is as shown in Figure 5.5. Their rated *COP* were both assumed 3.5 (see Table 5.1).

$$\overline{COP} = \frac{\sum Q(t)}{\sum W(t)} \tag{5.12}$$

where Q(t) is the operating cooling output, kW; W(t) is the operating chiller power, kW.

It can be seen from Figure 5.5 that the $\overline{COP}$ for XT-DOAS is 52.2% higher than that of the conventional system, which is 2.07 as compared to 1.36. A higher $\overline{COP}$ is attributed to combinations of a smaller temperature lift and the better control strategy for XT-DOAS.

The improvement in $\overline{COP}$ associated with a smaller temperature lift has been reported in an earlier study (Li *et al.*, 2015). Contribution of the control strategy can be revealed from Figure 5.6 showing that the annual mean *PLR* ($\overline{PLR}$) for XT-DOAS is 67.6% higher than that of the conventional system, which is 0.57 as compared to 0.34.

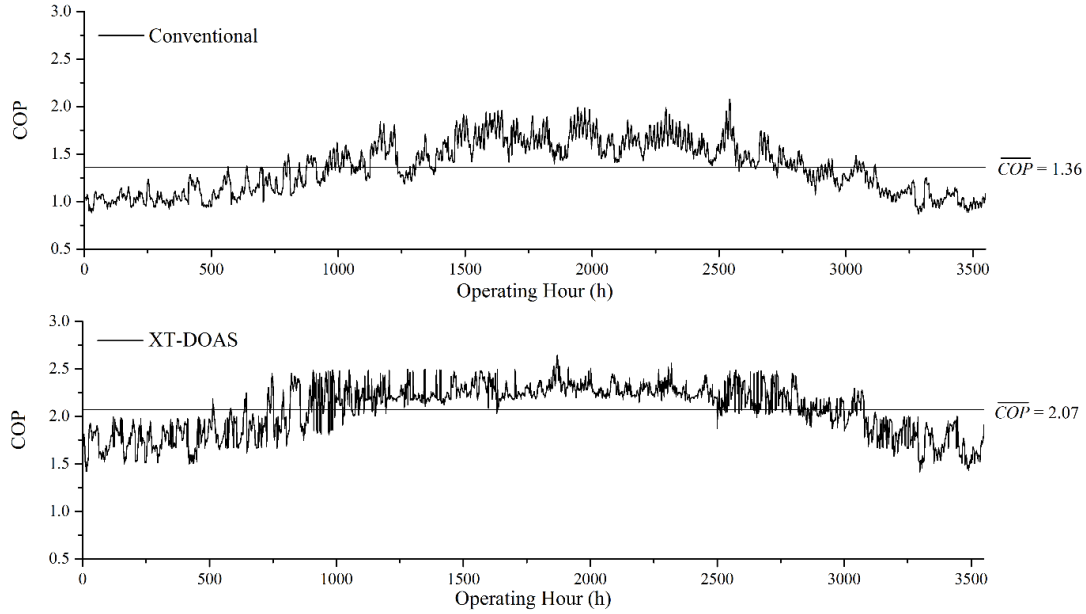

Figure 5.5 *COP* comparison

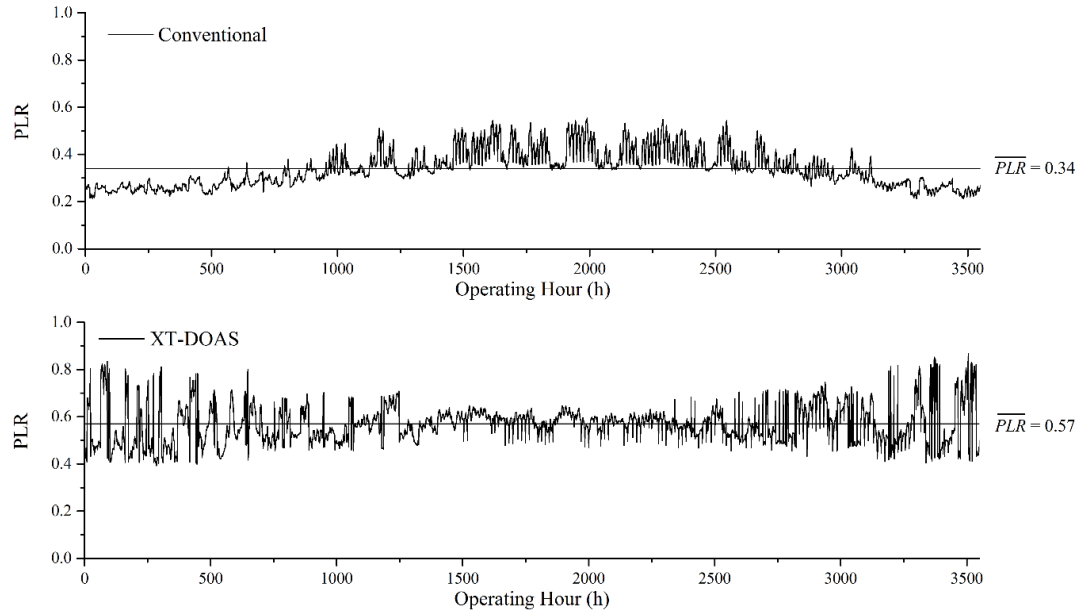

Figure 5.6 *PLR* comparison

5.4.2 Resultant Relative Humidities

The different desired space temperatures (24 °C for conventional and 24.5 °C for XT-DOAS) can basically be achieved by the two studied systems, the average DB temperatures are 24.2 °C and 24.7 °C, respectively; the focus in this analysis is thus on the resultant RHs since the achieving the desired RH is an essential characteristic of XT-DOAS.

The *RMSE* was again used to quantify the deviation of the resultant space RHs from the different desired value (50% for conventional and 35% for XT-DOAS). A higher level of deviation is reflected by a larger *RMSE*, calculated by the following equation:

$$RMSE_{RH} = \sqrt{\frac{1}{n} \cdot \sum_{i=1}^{n} \left(RH_{spx} - RH_{design} \right)^2} \tag{5.13}$$

where RH_{spx} is the resultant space RH and RH_{design} is the design RH; n is the annual operating hour.

In addition, Standard Deviation (*SD*) was calculated to measure the amount of variation of the resultant space RHs. A higher *SD* indicates the data points are spread out over a wider range of values and deviated further from the mean value. The equation can be seen as follows:

$$SD_{RH} = \sqrt{\frac{1}{n} \cdot \sum_{i=1}^{n} \left(RH_{spx} - \overline{RH} \right)^2} \tag{5.14}$$

where $\overline{RH}$ is the mean value of the resultant space RH.

The calculated *RMSE, SD,* together with the resultant maximum, minimum and mean RHs are presented in Table 5.5, illustrating that both *RMSE* and *SD* of XT-DOAS are smaller than the conventional system.

Table 5.5 Summary of *RMSE, SD* and space RHs

Description		**XT-DOAS**	**Conventional System**
RMSE		4.78	6.51
SD		4.06	4.93
RH (%)	Maximum	61.1	53.6
	Minimum	20.0	21.9
	Mean	32.5	45.7

For SA conditions (T_3 and ω_3) of the two systems, as mentioned in Section 5.2, T_3 is maintained constant but not ω_3. For the conventional system, T_3 is at 14 °C and the range of ω_3 is between 0.00468 kg/kg and 0.00964 kg/kg with a *SD* of 0.00107 kg/kg, while T_3 of XT-DOAS is at 18 °C, and the range of ω_3 is between 0.00343 kg/kg and 0.01047 kg/kg with a *SD* of 0.00066 kg/kg.

A higher *SD* for ω_3 of the conventional system is due to a variation in air flow rate entering the AHU. Whilst a smaller *SD* for ω_3 of XT-DOAS can be explained by a relatively constant treated OA and RA humidity ratios (ω_2 and ω_1, respectively) as derived by Equation (5.15):

$$\frac{V_1 \cdot \omega_1 + V_2 \cdot \omega_2}{V_2 + V_1} = \omega_3 \tag{5.15}$$

where V_1 is the RA volume flow rate, m^3/s; V_2 is the OA volume flow rate, m^3/s; ω_2 is the OA humidity ratio, kg/kg; ω_3 is the SA humidity ratio, kg/kg; ω_1 is the RA humidity ratio, kg/kg.

To explain the difference in the resultant RH of the two systems (Table 5.5), reference is made to the following equations:

$$Q_{sen} = \rho \cdot V_3 \cdot C_{pa} \cdot \left(T_1 - T_3\right) \tag{5.16}$$

$$Q_{lat} = \rho \cdot V_3 \cdot H_{fg} \cdot \left(\omega_1 - \omega_3\right) \tag{5.17}$$

where Q_{sen} is the sensible load, kW; Q_{lat} is the latent load, kW; C_{pa} is the specific heat capacity, kJ/kg·°C; H_{fg} is the heat of evaporation of water, kJ/kg; T_3 is the SAT, °C; T_1 is the RA temperature, °C.

Thus,

$$\omega_1 - \omega_3 = \frac{Q_{lat}}{Q_{sen} \cdot H_{fg}} \cdot C_{pa} \cdot \left(T_1 - T_3\right) \tag{5.18}$$

Based on Equation (5.18), for a rather constant Q_{lat}/Q_{sen}, T_1, and T_3 for the two systems, a smaller change in ω_3 for XT-DOAS (Table 5.5) results in a relatively stable ω_1.

The results confirm that XT-DOAS is better than the conventional system in achieving the desired RH.

5.4.3 Non-comfortable Hours

In this chapter, the indoor thermal comfort level is represented by the number of NCHs. In *EnergyPlus*, the number of NCHs is determined by an hour-by-hour comparison of the resultant air conditions with ASHRAE Standard 55-2013's recommended comfort conditions whereby a comfort zone for a range of humidity ratios, operative temperatures, and air speeds for different activity levels and clothing values are defined (Crawley *et al.*, 2000). For summer when the occupants are seated for office works and the clothing value is 0.5 clo, peripheral conditions for the comfort zone are shown in Figure 5.7 and the air speeds should not be greater than 0.20 m/s.

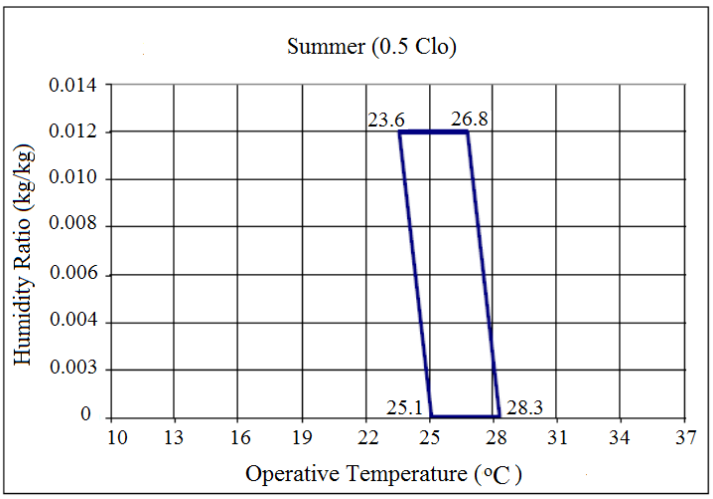

Figure 5.7 Summer comfort range in ASHRAE 55-2013

Figure 5.8 and Table 5.6 compare the NCH for the two systems. It can be seen in Figure 5.8 that the comfort level achieved by the use of XT-DOAS is constantly higher than that of the conventional system. The summary in Table 5.6 shows that the annualized NCH for the conventional system is 929.2 hours while that of XT-DOAS is 641.2 hours. This corresponds to 31.0% improvement in thermal comfort.

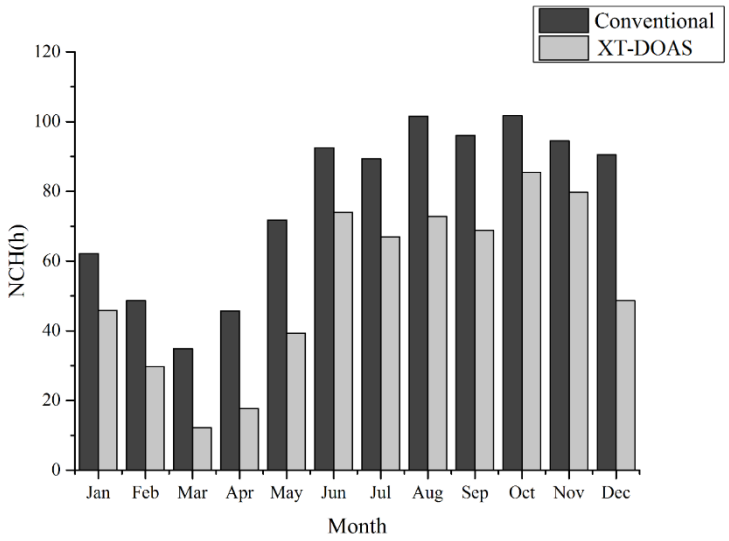

Figure 5.8 NCH of XT-DOAS and Conventional systems

Table 5.6 Annual NCH of the two systems

Month	Annual NCH		Improvement in NCH
	XT-DOAS	Conventional	
Jan.	45.8	62.2	26.4%
Feb.	29.7	48.7	39.0%
Mar.	12.2	34.8	64.9%
Apr.	17.7	45.7	61.3%
May	39.3	71.8	45.3%
Jun.	74.0	92.5	20.0%
Jul.	67.0	89.3	25.0%
Aug.	72.8	101.5	28.3%
Sep.	68.8	96.0	28.3%
Oct.	85.5	101.7	15.9%
Nov.	79.7	94.5	15.7%
Dec.	48.7	90.5	46.2%
Total	641.2	929.2	31.0%

To further confirm that the results are reasonable, the resultant air conditions at the perimeter and interior zones for the two systems are shown in Figures 5.9, and compared in Table 5.7. Due to the absence of solar radiation, the operative temperatures in interior zones are lower than the perimeter zones. Humidity ratios in interior zones are higher than in the perimeter zones, which is closer to the upper

boundary of the recommended comfort zone. This is reasonable because the annual average SHR of the interior zones (0.8899 for conventional system; and 0.8764 for XT-DOAS) is smaller than that of the perimeter zones (0.9159 for conventional system; and 0.8992 for XT-DOAS).

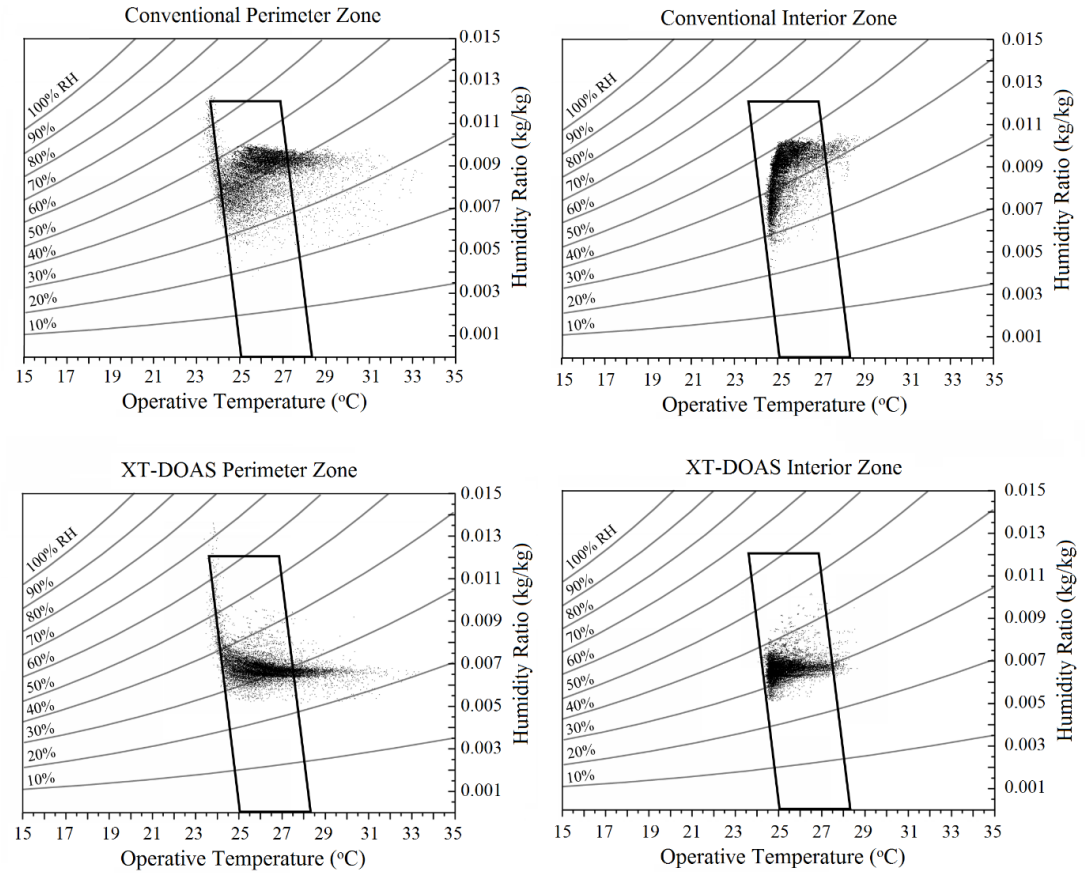

Figure 5.9 Resultant air conditions

Table 5.7 Annual average resultant space air conditions

System	Zone	Operative Temperature (°C)	Humidity Ratio (kg/kg)	SHR
XT-DOAS	Perimeter	26.39	0.00718	0.8992
	Interior	25.90	0.00727	0.8764
Conventional	Perimeter	25.99	0.00869	0.9159
	Interior	25.42	0.00873	0.8899

5.4.4 Condensation Risk

Though a cooling device is not needed in the XT-DOAS as well as the conventional systems, there still are moisture-related problems due to condensation on the SA terminal devices.

The annualised cumulative condensation hour ($ConH_{total}$), for the two systems were calculated. It was found that $ConH_{total}$ is none for XT-DOAS and that of the conventional system is 284.

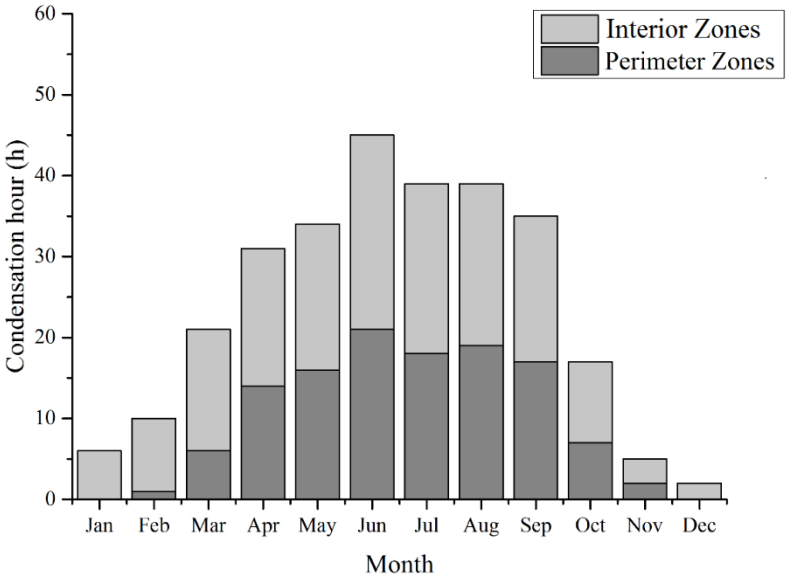

Figure 5.10 Monthly cumulative condensation hour for the conventional system

Figure 5.10 shows the monthly cumulative condensation hours for the conventional system by zones. It can be seen that in summer months (June, July and August), condensation hours are higher than in other months. To explain, the average RH in summer months and other months are compared in Table 5.8, illustrating that the

average RH is higher in summer months, which increases the condensation risk. Similarly, it is noted that the interior zones, with higher space RH (Table 5.8), always face condensation risk higher than the perimeter zones.

Table 5.8 Monthly average space RHs for the conventional system

Month	Perimeter zones	Interior zones	All zones
Jan.	39.49%	43.89%	41.69%
Feb.	41.07%	45.27%	43.17%
Mar.	43.43%	46.96%	45.20%
Apr.	46.61%	46.72%	46.66%
May	47.91%	48.14%	48.02%
Jun.	50.04%	50.20%	50.12%
Jul.	48.95%	49.64%	49.29%
Aug.	49.14%	49.62%	49.38%
Sep.	48.59%	48.88%	48.73%
Oct.	44.88%	45.13%	45.01%
Nov.	41.34%	41.42%	41.38%
Dec.	38.57%	40.55%	39.56%

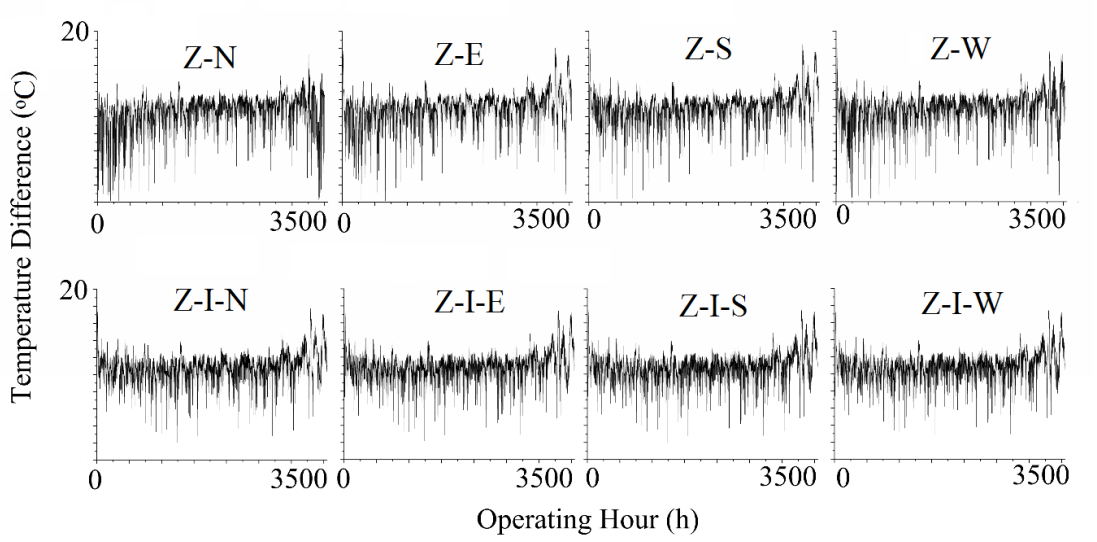

Figure 5.11 Temperature difference between SA and DP for XT-DOAS

To explain the zero condensation risk in the case of XT-DOAS, Figure 5.11 presents the temperature difference between the SA and DP for the 8 conditioned zones. It can be seen that they are all higher than zero and thus no condensation occurs on the SA terminal devices.

5.5 Summary

In this chapter, whether the proposed XT-DOAS can better achieve the desired air conditions and energy efficiency objectives than the conventional system was investigated. To facilitate the investigations, a field measurement from a pilot installation was conducted to ascertain the performance characteristics of the extra-low temperature DX coils. Based on the measurement results, performance models for *EnergyPlus* simulation were developed. In the simulation, the actual equipment performance models and the realistic building and system characteristics were used. Based on the simulation results, analyses on the energy use, resultant relative humidities, thermal comfort level, and the condensation risk were performed. It was found that XT-DOAS, as compared to conventional system, was superior for achieving the desired relative humidities; could better achieve the desired thermal comfort conditions; saved 22.6% annual energy use for AC; reduced the annual cumulative number of non-comfortable hours by 31%; and could completely eliminate the condensation risk at the terminal device.

CHAPTER 6

EXERGY ANALYSES AND OPTIMIZATION FOR XT-DOAS WITH A REALISTIC COIL PERFORMANCE MODEL

This chapter presents the determination of the optimum number of cooling stages and treated OA temperature to enhance the performance of XT-DOAS. In the process, a DX coil performance model that takes into account the extra-high entering air temperature (XHT) and extra-low entering air temperature (XLT) at the first and the last cooling stages was developed based on factory test data and field measurement data. Based on the developed model, energy and exergy analyses were conducted to evaluate use of XT-DOAS for space cooling of a typical office building in Hong Kong. The optimum configuration for XT-DOAS was determined based on better energy efficiency and performance for air-conditioning of office buildings in subtropical region.

6.1 Introduction

The effective usage of XT-DOAS as compared to the conventional system has been reported in Chapter 5. However, in the comparative study, the better performance of DX coil in handling OA with XHT has not been taken into account (Bao *et al.*, 2017). This is acceptable for performance comparison with conventional system. But for optimizing the system configuration to achieve the desired air conditions and better energy efficiency, it is not desirable because XT-DOAS receives hot and humid OA

at the first cooling stage and handles extra-low temperature air at the last cooling stage to introduce substantial influence on the DX coil's performance (EnergyPlus, 2015). Unfortunately, a performance curve that takes into account the XHT range is lacking in the public literature.

As for energy performance evaluation, exergy analysis based on the second law of thermodynamics, is a powerful evaluation method (Fan *et al.*, 2014). It can identify localized inefficiencies and thus is commonly used for the design, and performance evaluation of energy systems (Zmeureanu and Wu, 2007). For the proposed XT-DOAS using series-connected multi-stage DX unit, the moist air entering and leaving individual cooling stages is of different states to affect the available energy and thus the exergy efficiency (Chengqin *et al.*, 2002). Therefore, exergy analysis is essential for the optimum design of multi-stage DX unit.

It is evident from the above that in optimizing the system configuration of XT-DOAS to achieve the desired air conditions and better energy efficiency, a realistic coil performance model needs to be developed and energy and exergy analyses are essential in the optimization process.

The realistic coil performance model would take into account the XHT and XLT at the first and the last cooling stages. Based on the developed model, energy and exergy analyses were conducted to take into account the combined influence of the thermodynamic states of moist air entering and leaving individual cooling stages and the corresponding part load conditions on the overall performance of XT-DOAS. The multi-stage characteristics of the DX coil unit was considered in the exergy analysis.

6.2 System Configuration Optimization

Based on the system description in Chapter 3, it is noted that the energy performance of XT-DOAS is dominated by the consumption of the multi-stage DX unit and VAV fans. Thus to optimize the system configuration to achieve the desired air conditions and better energy efficiency, the focus is to determine the treated OA temperature (T_2, the leaving air temperature at the multi-stage DX unit, State 2) and the number of cooling stages (N) (see Figure 3.1 and 3.2), which correspondingly affect the thermodynamic states of moist air entering and leaving individual cooling stages and the associated part load conditions.

Energy simulations and exergy analysis were performed for the use of XT-DOAS in the case study building (Section 4.1) based upon a realistic coil performance model developed to account for the XHT and XLT (Section 6.3).

In deciding the range of values for the two studied parameters, reference was made to cold system design (Kirkpatrick and Elleson, 1996) and previous studies (Li, Han *et al.*, 2015; Li *et al.*, 2016; Bao *et al.*, 2017) T_2 was set at 4 °C to 10 °C (1 °C interval) and the number of cooling stage (N) was set as 2 to 4. Single cooling stage has been excluded to avoid operating at unfavourably high temperature differential (Kirkpatrick and Elleson, 1996) and to benefit from multi-stage characteristics.

6.3 Coil Model Development and Exergy Analyses

A realistic coil performance model accounting for the XHT and XLT were developed based on factory test data and field measurement data. Exergy analyses were introduced. In the analyses, moist air exergy, exergy flow and exergy efficiency were considered.

6.3.1 Coil Performance Model Development

Owing to the high entering air temperature and extra-low leaving air temperature to affect the coil performance for XT-DOAS (EnergyPlus, 2015), two default performance curves in *EnergyPlus* (*CAP-FT* and *EIR-FT*) for total cooling capacity (*CAP*) and the energy input ratio (*EIR*), as a function of temperature (*FT*), which are mentioned in Section 4,2,1, need to be developed.

The two performance curves that need to be developed are again shown below (EnergyPlus, 2015):

$$\begin{aligned} CAP\text{-}FT &= CAP/CAP_{rated} \\ &= a_1 + a_2 \cdot WB_{ei} + a_3 \cdot WB_{ei}^2 + a_4 \cdot DB_{ci} + a_5 \cdot DB_{ci}^2 + a_6 \cdot WB_{ei} \cdot DB_{ci} \end{aligned} \tag{6.1}$$

$$\begin{aligned} EIR\text{-}FT &= EIR/EIR_{rated} \\ &= b_1 + b_2 \cdot WB_{ei} + b_3 \cdot WB_{ei}^2 + b_4 \cdot DB_{ci} + b_5 \cdot DB_{ci}^2 + b_6 \cdot WB_{ei} \cdot DB_{ci} \end{aligned} \tag{6.2}$$

Regression analysis (Chatterjee and Hadi, 2015) was used to determine the empirical coefficients a_i and b_i in *CAP-FT* and *EIR-FT* curves based on real data.

To formulate the performance curves that cover a much higher temperature range than that of a conventional system, performance data for DX unit operating at XHT and

XLT range needs to be collected. The process for collecting the XLT side data from a field measurement has been introduced in Chapter 5. To avoid duplications, this chapter only gives the details of data collection for the XHT side.

DX units that can handle high temperature OA are rare in the market. With enormous effort made to contact different manufacturers, factory test data of a series of brand new DX units dedicated for OA conditioning were collected (Daikin, 2016). The test data covers performance characteristics of DX units treating OA at a maximum of 35 °C DB and 32 °C WB to a discharge temperature of 18 °C DB. It includes the total cooling capacity and input power at various outdoor air conditions. The total cooling capacity is a gross value. The total input power includes the consumption of compressor, condenser fan and auxiliary equipment (e.g., control panel power) but excludes the supply air fan.

By normalizing the field measurement (Section 5.3.2) data (XLT side) and factory test data (XHT side) into consistent format as summarized in Table 6.1, regression analysis using SPSS (Hayes and Matthes, 2009) was conducted to develop a standardized set of performance curves that covers the entire operation range of XT-DOAS. In Table 6.1, a normalized performance coefficient of 1 refers to the performance at AHRI standard rated test condition (AHRI, 2008).

Table 6.1 The normalized data sets

Range of WB_{ei}	6–32 °C
Range of DB_{ci}	6–35 °C
Range of normalized performance coefficient	*CAP-FT* (0.4–27) *EIR-FT* (0.5–3.876)
Total number of data sets	104

The resultant models for (Equations (6.1) and (6.2)) are shown below:

$$CAP\text{-}FT = 0.79107 - 0.11682 \times WB_{ei} + 0.00662 \times WB_{ei}^2 + 0.01253 \times DB_{ci} \\ -0.00014 \times DB_{ci}^2 - 0.00039 \times WB_{ei} \times DB_{ci}, \ (R_a^2 = 0.985) \tag{6.3}$$

$$EIR\text{-}FT = 6.91628 - 0.41839 \times WB_{ei} + 0.00588 \times WB_{ei}^2 - 0.03192 \times DB_{ci} \\ -0.00071 \times DB_{ci}^2 + 0.00293 \times WB_{ei} \times DB_{ci}, \ (R_a^2 = 0.981) \tag{6.4}$$

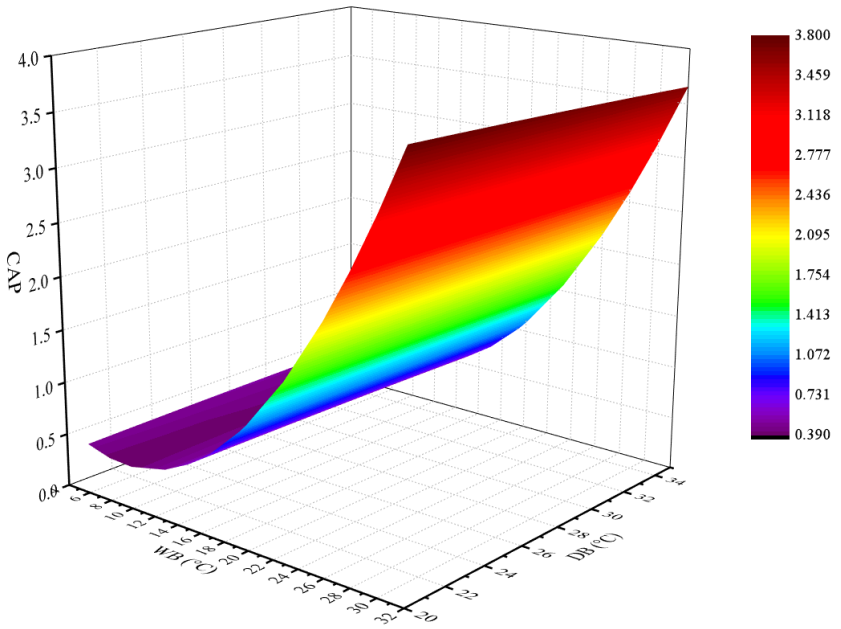

Figure 6.1 *CAP-FT* performance curve

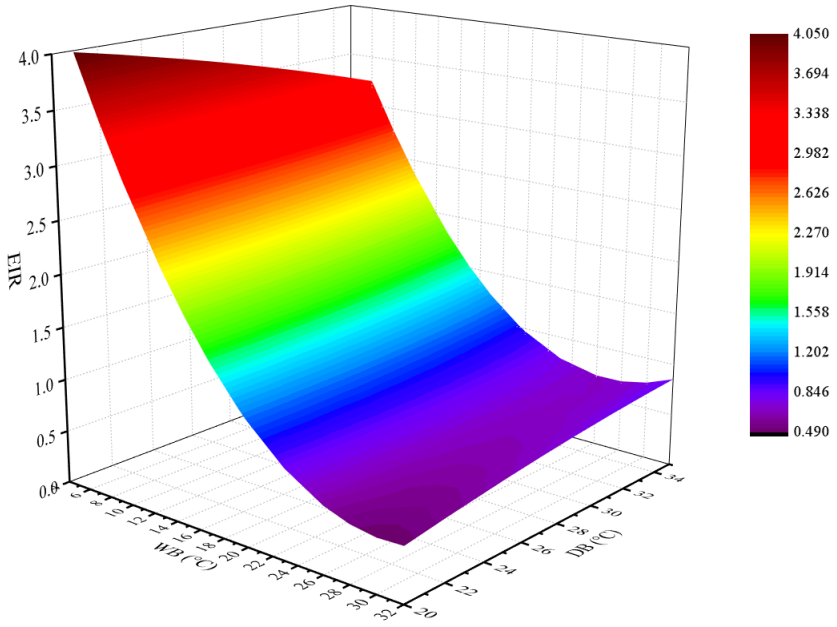

Figure 6.2 *EIR-FT* performance curve

Verification of the regression models is summarized in Appendix B. Figures 6.1 and 6.2 are visual representation of the *CAP-FT* and *EIR-FT* performance curves. The *CAP-FT* curve shows that the DX coil's cooling capacity *CAP* increases with entering air *WB* temperature WB_{ei} but varies very little with the condenser entering air *DB* temperature DB_{ci}. The *EIR-FT* curve shows that the *CAP* increases primarily with WB_{ei} but the power input *W* decreases with both WB_{ei} and DB_{ci}. In other words, a lower WB_{ei} results in a higher *EIR* and thus lower *COP*.

6.3.2 Energy Analysis

Based on the developed coil performance model, *EnergyPlus* simulations were performed. The inputs to *EnergyPlus* include the hourly meteorological conditions in Hong Kong, the internal heat sources (occupant, lighting and appliances), the studied

building's architectural and construction details (see Section 4.1), the AC system adopted (XT-DOAS in this case), the system and equipment characteristics and the range of studied parameters. The result generated after the simulation run is extensive. It allows users to extract the desired data, which include temperatures, moisture contents, mass flow rates, coils' cooling outputs, space sensible and latent loads and energy usage of the equipments. Based on the resultant space air conditions, the ability of the XT-DOAS operating under the pre-defined range of studied parameters to maintain the desired air conditions was evaluated. The corresponding energy usage was also extracted for exergy analysis.

6.3.3 Exergy Analysis

Based on energy simulation results from *EnergyPlus*, exergy analysis was performed based on the laws of thermodynamics. Exergy analysis has been used to examine the optimum air states entering and leaving the multi-stage coil associated with the changes in T_2 and N, which includes the calculation of moist air exergy and exergy efficiency of different system configurations.

6.3.3.1 Moist Air Exergy

AC systems handle moist air. The exergy level of moist air is therefore important. Moist air exergy is the maximum useful power when moist air is converted reversibly to the environment. Most exergy research regards the reference environment state as the dead state and assumes zero exergy to calculate the exergy change (Wark, 1995). While considering the unsaturated moist air still has energy available, the dead state is

suggested as the saturated moist air at the same temperature and pressure as the reference environment state (Ren *et al.*, 2001b). However, given the reference environment state varies with outdoor conditions, in this study, the hourly energy and exergy analysis based on year-round outdoor conditions were considered. By treating the moist air encountered in an AC system as an ideal gas, the moist air exergy transferred from the basic forms of relevant exergy can be represented by Equation (6.5) which is (Ren *et al.*, 2001a):

$$\begin{aligned} ex = {} & \left(C_{da} + \omega \cdot C_{wv}\right) \cdot \left[T' - T_0' - T_0' \cdot \ln\left(T'/T_0'\right)\right] \\ & + \left(1 + 1.608\omega\right) \cdot R_{da} \cdot T_0' \cdot \ln\left(p/p_0\right) \\ & + R_{da} \cdot T_0' \cdot \begin{Bmatrix} \left(1 + 1.608\omega\right) \cdot \ln\left[\left(1 + 1.608\omega_{0s}\right)/\left(1 + 1.608\omega\right)\right] \\ + 1.608\omega \cdot \ln\left(\omega/\omega_{0s}\right) \end{Bmatrix} \end{aligned} \tag{6.5}$$

where *ex* is the exergy of moist air per unit mass dry air, kJ/kg dry air; C_{da} is the specific heat of dry air, kJ/kg·K; C_{wv} is the specific heat of water vapour, kJ/kg·K; ω is the humidity ratio of moist air, kg/kg dry air; ω_{0s} is the humidity ratio of dead state, kg/kg dry air; T' is the temperature of moist air, K; T_0' is the reference environmental temperature, K; R_{da} is the ideal gas constant of dry air, kJ/kg·K; p is the pressure of moist air, kPa; p_0 is the reference environmental barometric pressure (atmospheric pressure), kPa.

The total exergy of moist air (*ex*) can also be represented as the sum of thermal exergy (ex_{th}), mechanical exergy (ex_{me}) and chemical exergy (ex_{ch}). Thermal exergy is the maximum useful work when moist air is transformed from the initial temperature state to the dead temperature state. Mechanical exergy is equal to the mechanical work itself. Chemical exergy represents the maximum useful work associated with the

transition of moisture content of moist air from the initial state to the dead state. They are represented by Equations (6.6) to (6.8), which are derived from Equation (6.5):

$$ex_{th} = \left(C_{da} + \omega \cdot C_{wv}\right) \cdot \left[T - T_0 - T_0 \cdot \ln\left(T/T_0\right)\right] \tag{6.6}$$

$$ex_{me} = \left(1 + 1.608\omega\right) \cdot R_{da} \cdot T_0 \cdot \ln\left(p/p_0\right) \tag{6.7}$$

$$ex_{ch} = R_{da} \cdot T_0 \cdot \begin{Bmatrix} \left(1 + 1.608\omega\right) \cdot \ln\left[\left(1 + 1.608\omega_{0s}\right)/\left(1 + 1.608\omega\right)\right] \\ +1.608\omega \cdot \ln\left(\omega/\omega_{0s}\right) \end{Bmatrix} \tag{6.8}$$

Since ω_{0s} in Equations (6.5) and (6.8) cannot be output directly from *EnergyPlus*, it has to be calculated by the ideal gas law from the reference environmental barometric pressure (p_0) and the saturation pressure of water vapour (p_{ws}), as described in Equation (6.9):

$$\omega_{0s} = 0.622\, p_{ws} / \left(p_0 - p_{ws}\right) \tag{6.9}$$

The saturation pressure of water vapour can be determined by Equation (6.10), which is of sufficient accuracy between 273.15K (0 °C) and 646.15 K (373 °C) (Wagner and Pruß, 2002).

$$\begin{aligned} &\ln\left(p_{ws}/p_c\right) = \left(T_c^{'}/T^{'}\right) \begin{pmatrix} -7.860\vartheta + 1.844\vartheta^{1.5} - 11.787\vartheta^3 \\ +22.681\vartheta^{3.5} - 15.962\vartheta^4 + 1.801\vartheta^{7.5} \end{pmatrix}, \\ &\vartheta = 1 - T_c^{'}/T^{'} \end{aligned} \tag{6.10}$$

where $T_c^{'}$ is the critical temperature, 647.096 K; p_c is the critical pressure, 22,064 kPa.

6.3.3.2 Exergy Flow

For calculation of the exergy efficiency of the multi-stage DX unit, the exergy flow and the exergy balance have to be defined. The exergy flow in a typical DX system is shown in Figure 6.3, and the exergy balance is represented in Equation (6.11). To address the multi-stage characteristics of DX system, the exergy flow and exergy balance have to be further defined as shown in Figure 6.4 and Equation (6.12) correspondingly:

$$Ex,ep,in + Ex,cd,in + W = Ex,ep,out + Ex,cd,out + Ex,loss \tag{6.11}$$

$$Ex,ep,in_1 + \sum_{j=1}^{N} Ex,cd,in_j + \sum_{j=1}^{N} W_j + W_{Fan} = Ex,ep,out_N + \sum_{j=1}^{N} Ex,cd,out_j + Ex,tot,loss \tag{6.12}$$

where j is the j-th stage DX coil; Ex,ep,in_1 is the exergy of moist air entering in the evaporator of first cooling stage, MWh; Ex,ep,out_N is the exergy of moist air out of the evaporator of last cooling stage, MWh; $\sum_{j=1}^{N} Ex,cd,in_j$ is the sum of moist air exergy entering in the all condensers, MWh; $\sum_{j=1}^{N} Ex,cd,out_j$ is the sum of moist air exergy out of all condensers, MWh; $\sum_{j=1}^{N} W_j$ is the sum of input power to the whole system, MWh; W_{Fan} is the power input of supply fan, MWh; $Ex,tot,loss$ is the total exergy loss of multi-stage DX system, MWh.

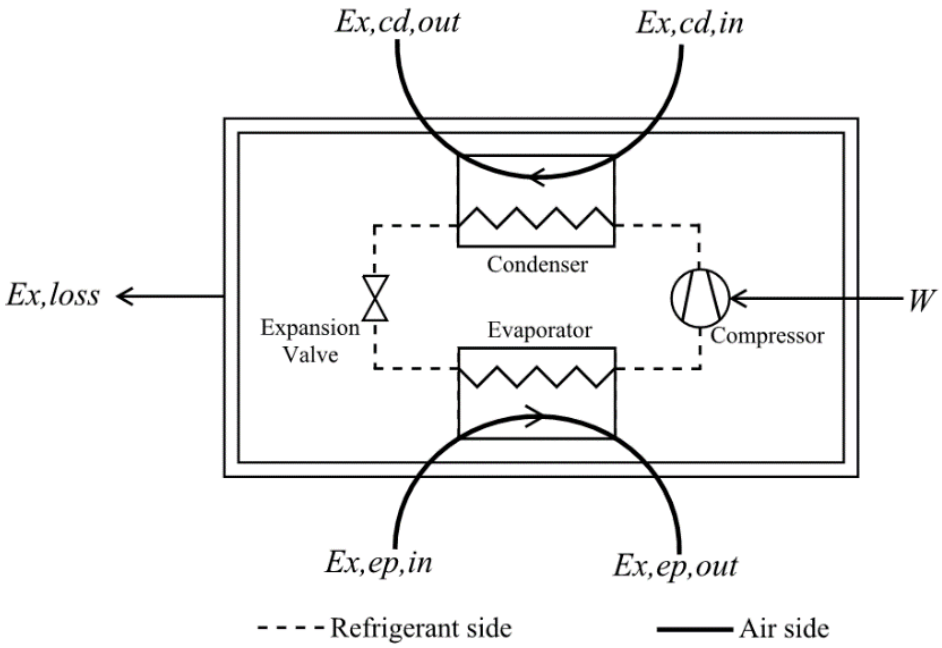

Ex,ep,in—exergy of moist air entering in the evaporator;

Ex,ep,out—exergy of moist air out of the evaporator;

Ex,cd,in—exergy of moist air entering in the condenser;

Ex,cd,out—exergy of moist air out of the condenser;

W—Input power for DX unit;

Ex,loss—exergy loss of DX unit.

Figure 6.3 Exergy flow of a typical DX unit

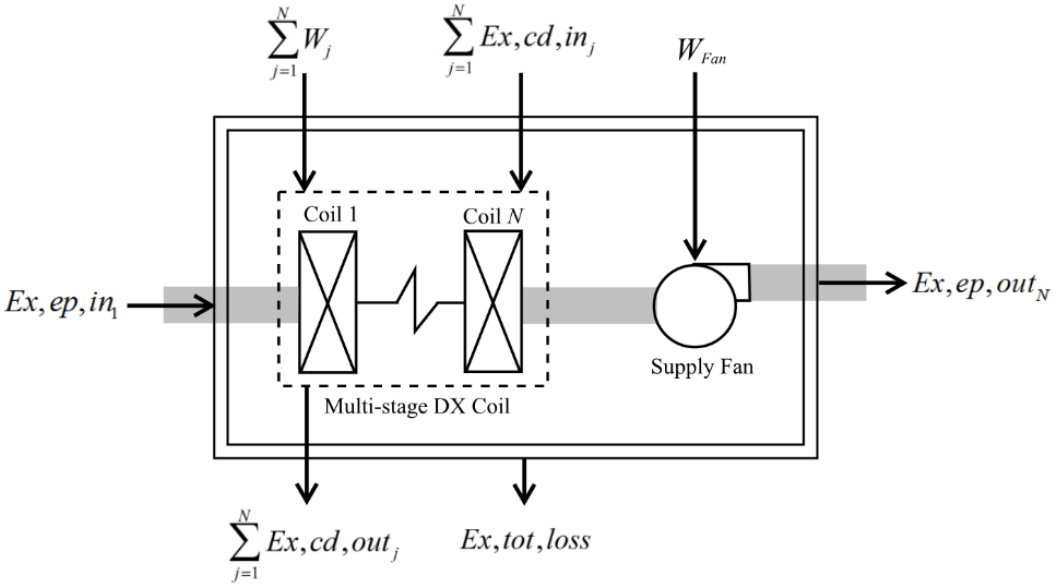

Ex,ep,in_1—exergy of moist air entering in the evaporator of first cooling stage;

Ex,ep,out_N—exergy of moist air out of the evaporator of last cooling stage;

$\sum_{j=1}^{N} Ex,cd,in_j$ —the sum of moist air exergy entering in the all condensers;

$\sum_{j=1}^{N} Ex,cd,out_j$ — the sum of moist air exergy out of all condensers;

$\sum_{j=1}^{N} W_j$ —the sum of input power to whole system;

W_{Fan}—the power input of supply fan;

$Ex,tot,loss$ —the total exergy loss of multi-stage DX system

Figure 6.4 Exergy flow of a multi-stage DX system

6.3.3.3 Exergy Efficiency

Exergy efficiency η_{Ex} for a system is defined as the ratio of the exergy desired *Ex,desired* and the exergy needed for the desired effect *Ex,needed* (Wark, 1995). A higher exergy efficiency means a more ideal system.

Based on the calculation results from Equations (6.5) to (6.12), for a multi-stage DX system where the exergy of moist air leaving the condenser is not recovered, the exergy efficiency can be determined by Equation (6.13).

$$\eta_{Ex} = \frac{Ex,desired}{Ex,needed} = \frac{Ex,ep,out_N}{\left(Ex,ep,in_1 + \sum_{j=1}^{N} W_j + \sum_{j=1}^{N} Ex,cd,in_j + W_{Fan} \right)} \tag{6.13}$$

6.4 Results and Discussion

To optimize the system configuration of XT-DOAS for maximum performance, based on the range of T_2 and N explained in Section 6.2 and assuming only one parameter was varied, 21 cases (seven T_2, and three N) were generated for hour-by-hour *EnergyPlus* simulations and exergy analysis. The design conditions of the 21 cases, based on common practice to allow equal sharing of load amongst cooling stages (Yu and Chan, 2007), are summarized in Table 6.2. The cooling capacity at each cooling stage was automatically adjusted according to T_2, N and OA mass flow rate m.

Based on the results of *EnergyPlus* simulations and the subsequent calculations, the year-round energy use and exergy efficiency of the 21 cases for different N and T_2 are presented in Figure 6.5, illustrating that in general, energy use (*En*) decreases with T_2 and increases with N, while exergy efficiency (η_{Ex}) peaks with T_2 at 7 °C and decreases with N. N equals 2 and thus always results in a lower energy use and higher exergy efficiency.

Table 6.2 Design conditions of 21 cases

N	Leaving Air Temperature (°C)				OA Mass Flow Rate *m* (kg/s)
	Stage 1	Stage 2	Stage 3	Stage 4	
2	18.5	4	-	-	3.10
	19	5	-	-	3.25
	19.5	6	-	-	3.43
	20	7	-	-	3.62
	20.5	8	-	-	3.84
	21	9	-	-	4.09
	21.5	10	-	-	4.37
3	23	13	4	-	3.10
	23	14	5	-	3.25
	24	15	6	-	3.43
	24.5	16	7	-	3.62
	24.5	16.5	8	-	3.84
	25	17	9	-	4.09
	25.5	18	10	-	4.37
4	25	18	11	4	3.10
	26	19	12	5	3.25
	26	19	12	6	3.43
	26.5	20	13.5	7	3.62
	26	20	14	8	3.84
	27	21	15	9	4.09
	27	21	15	10	4.37

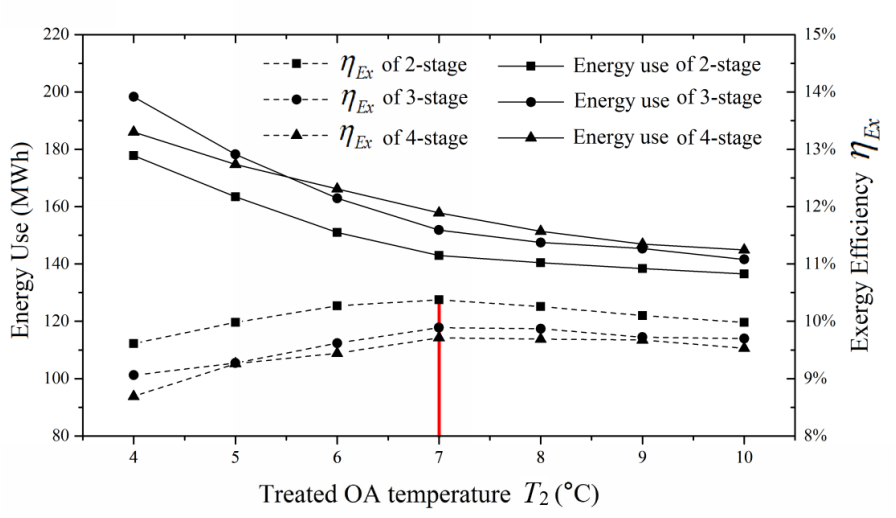

Figure 6.5 Energy use and exergy efficiency of multi-stage DX system for different N and T_2

As far as T_2 is concerned, considering exergy efficiency (η_{Ex}) is a more meaningful indicator of efficiency that accounts for quantity and quality aspects of energy flows when compared to energy (Dincer and Rosen, 2004), the optimum T_2 for a 2-stage XT-DOAS is 7 °C for having the highest exergy efficiency (=10.37%).

Since T_2 affects also the achievement of the desired air conditions, the achievable indoor conditions for different T_2 were also investigated. Given the indoor temperature can be controlled, the investigations are focused on the resultant indoor RH. Its achievement is one specific characteristic of XT-DOAS (Bao *et al.*, 2017). The RMSE value was again used to quantify the deviation between the hourly resultant space RH and the desired value (35%) for different T_2. RMSE can be calculated by Equation (6.14). A smaller $RMSE_{RH}$ means better humidity control:

$$RMSE_{RH} = \sqrt{\frac{1}{n} \cdot \sum_{i=1}^{n} \left(RH_{spx} - RH_{design} \right)^2} \tag{6.14}$$

where $RMSE_{RH}$ is the RMSE of the space RH; RH_{spx} is the resultant space RH; RH_{design} is the desired space RH, 35%; n is the annual operating hour.

Table 6.3 The resultant indoor air conditions for different T_2

Design T_2 (°C)	Resultant Indoor Air RH (%)	
	Mean	$RMSE_{RH}$
4	30.67	5.52
5	32.24	4.56
6	33.91	3.64
7	35.70	3.38
8	37.57	4.10
9	39.53	5.52
10	41.62	7.35

Table 6.3 presents the resultant space RH and calculated $RMSE_{RH}$ for different T_2. It indicates that the smallest $RMSE_{RH}$ occurs when T_2 is 7 °C (=3.38), which is accordant with the exergy analysis results.

To explain the influence of N and T_2 on the energy use, exergy efficiency and achievable space RH and thus the concluded optimum N and T_2, further energy and exergy analysis, as well space humidity condition evaluations were conducted.

6.4.1 Energy Result

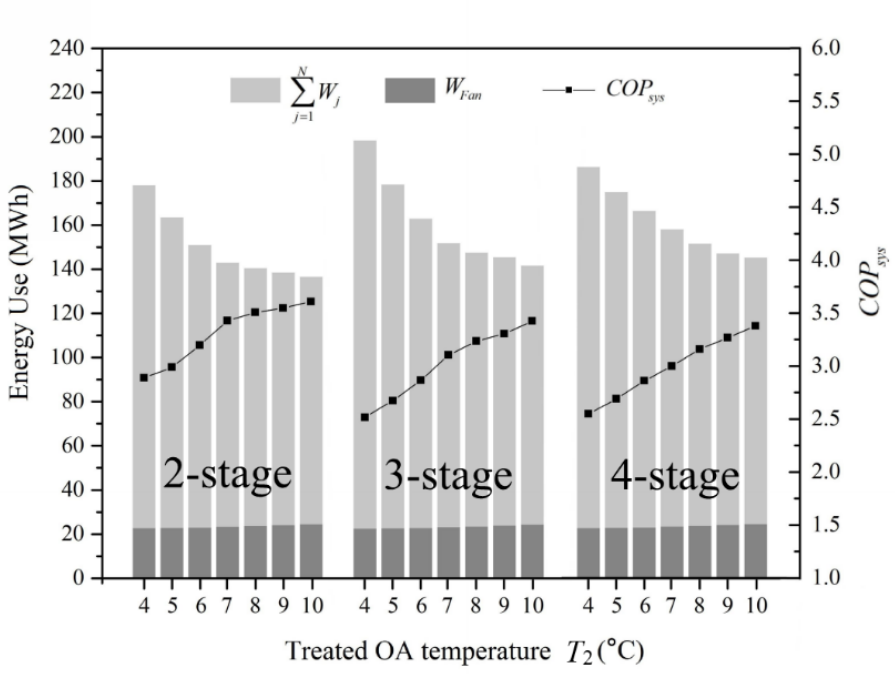

Figure 6.6 Energy use of multi-stage DX system for different N and T_2

Figure 6.6 shows the annual energy use and COP_{sys} for different N and T_2 which are basically determined by $\sum_{j=1}^{N} W_j$ and W_{Fan}.

In Figure 6.6, regardless of N, W_{Fan} increases with T_2 but the rate of increase, as compared to the rate of drop in $\sum_{j=1}^{N} W_j$ with T_2, is far less significant. Thus COP_{sys} also increases with T_2. However, as for the influence of N on $\sum_{j=1}^{N} W_j$ and thus COP_{sys}, an analysis on the influential factors is needed. For a DX coil with defined performance curves (Section 6.3.1), the parameters affecting its *COP*, by reference to *EnergyPlus*, are summarized in Equations (6.15) through (6.22):

$$COP = \frac{CAP}{W} \tag{6.15}$$

$$CAP = C_{da} \cdot m \cdot \Delta T \tag{6.16}$$

$$W = CAP \cdot RTF \cdot EIR \tag{6.17}$$

$$RTF = \frac{PLR}{PLF} = \frac{PLR}{\left(0.85 + 0.15 \times PLR\right)} \tag{6.18}$$

$$PLR = \frac{CAP}{CAP_{rated}} \tag{6.19}$$

$$EIR = EIR_{rated} \cdot (EIR\text{-}FT) \cdot (EIR\text{-}FF) \tag{6.20}$$

$$EIR\text{-}FF = c_1 + c_2 \cdot \left(m/m_{rated}\right) + c_3 \cdot \left(m/m_{rated}\right)^2 + c_4 \cdot \left(m/m_{rated}\right)^3 \tag{6.21}$$

$$COP = \frac{0.85 \times \dfrac{CAP_{rated}}{CAP} + 0.15}{\left(EIR_{rated} \cdot (EIR\text{-}FT) \cdot (EIR\text{-}FF)\right)} = f\left(m, \Delta T, WB_{ei}, DB_{ci}\right) \tag{6.22}$$

where ΔT is the entering and leaving air temperature difference across a DX coil, °C; *RTF* is the run time fraction; *EIR-FF* is a *EIR* modifier curve as a function of air flow fraction; m is the actual air mass flow rate, kg/s; m_{rated} is the rated air mass flow rate, kg/s; c_i are empirical coefficients.

In Equation (6.22), the CAP_{rated} and EIR_{rated} of each cooling stage are constant terms; *EIR-FT* is a function of WB_{ei} and DB_{ci}; *EIR-FF* is a function of air flow fraction which is the ratio of *m* entering the DX coil to a constant term m_{rated}; *CAP* is a function of *m* and ΔT. DB_{ci} is affected by the outdoor air condition which is the same for all system configuration and therefore is not necessary to consider. *m* is determined by T_2 so it is not an independent variable. Thus, *COP* can be described as a function of ΔT and WB_{ei} as shown in Equation (6.23):

$$COP \approx f(\Delta T, WB_{ei}) \tag{6.23}$$

Equation (6.23) can then be postulated as (Aiken *et al.*, 1991):

$$COP = d_1 + d_2 \cdot WB_{ei} + d_3 \cdot \Delta T + d_4 \cdot WB_{ei} \cdot \Delta T \tag{6.24}$$

where d_1, d_2, d_3, and d_4 are constants.

Based on *EnergyPlus* simulation results, regression analysis was performed using the statistical package SPSS (Hayes and Matthes, 2009) to determine the coefficients for Equation (6.24). The resultant model is shown below:

$$COP = -1.609 + 0.363 \times WB_{ei} - 0.442 \times \Delta T + 0.017 \times WB_{ei} \cdot \Delta T, \ (R^2 = 0.920) \tag{6.25}$$

The value of c_2 and c_3 indicate that WB_{ei} has a positive effect on *COP* while ΔT has a negative effect. The resultant model (Equation (6.25)) provides a convenient way to

quantify the influences of WB_{ei} and ΔT on the *COP* of a DX coil. This can be done by taking partial derivative of *COP* with respect to WB_{ei} and ΔT as follows:

$$\left(\frac{\partial COP}{\partial WB_{ei}}\right)\cdot\left(\frac{WB_{ei}}{COP}\right) \tag{6.26}$$

and:

$$\left(\frac{\partial COP}{\partial \Delta T}\right)\cdot\left(\frac{\Delta T}{COP}\right) \tag{6.27}$$

Based on Equations (6.26) through (6.27), and also the average values for WB_{ei}, ΔT and *COP*, the sensitivities of WB_{ei} and ΔT were estimated to be 2.035 and 0.179 to show that WB_{ei} introduces much higher influence on a DX coil's *COP*. The result is consistent with the visual representation in Section 6.3.1, Figures 6.1 and 6.2.

To confirm the need of the developed model that takes into account the XHT, the energy consumptions predicted based on the developed model and a conventional model (Bao *et al.*, 2017), were compared. It was found that for different WB_{ei}, the difference was high ranging from 7.23% to 12.67%.

In addition, for XT-DOAS with different *N*, the system *COP* (COP_{sys}) is related to individual cooling stage's *COP* and thus is also related to WB_{ei} and ΔT. Therefore, a higher COP_{sys} can be regarded as a function of the average ΔT ($\overline{\Delta T}$) and WB_{ei} ($\overline{WB}_{ei}$) of all cooling stages as expressed in Equation (6.28). A lower $\overline{\Delta T}$ and a higher $\overline{WB}_{ei}$ result in a higher COP_{sys}:

$$COP_{sys} = \frac{\sum_{j=1}^{N} CAP_j}{\sum_{j=1}^{N} W} = f(COP_1,\ COP_2 \cdots COP_N) \approx f(\overline{\Delta T}, \overline{WB}_{ei}) \tag{6.28}$$

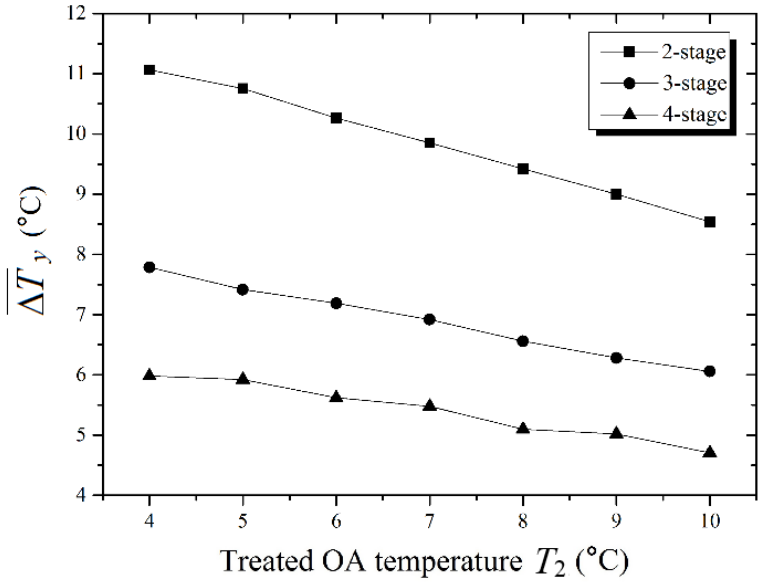

Figure 6.7 $\overline{\Delta T}_y$ for different N and T_2

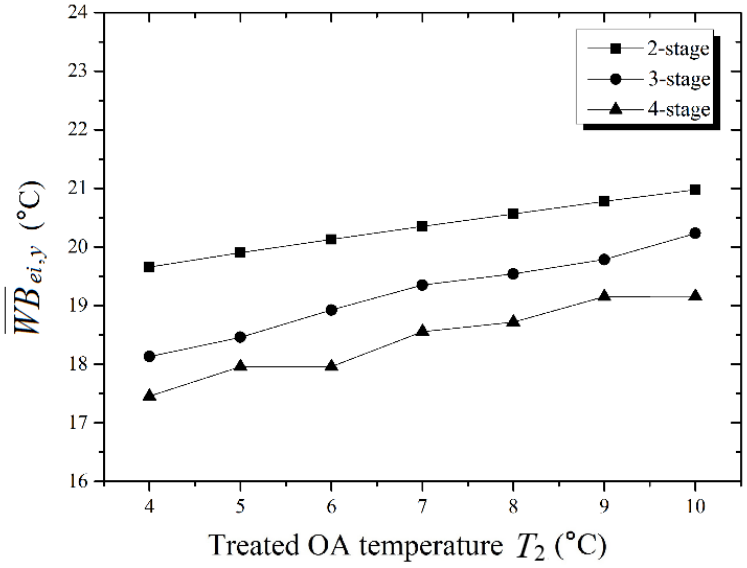

Figure 6.8 $\overline{WB}_{ei,y}$ for different N and T_2

Figures 6.7 and 6.8 show the variations of $\overline{\Delta T}$ and $\overline{WB}_{ei}$ for different N and T_2, illustrating that $\overline{\Delta T}$ decreases with T_2 and N, and $\overline{WB}_{ei}$ increases with T_2 and N. With the higher influence of $\overline{WB}_{ei}$ than $\overline{\Delta T}$ on COP_{sys}, the results explain the preference for a smaller N (2-stage over 4-stage) and a higher T_2 for better COP_{sys} and thus smaller $\sum_{j=1}^{N} W_j$.

The observations in Figures 6.7 and 6.8 accord with the energy use in Figure 6.6 to confirm the influence of N and T_2 on the energy use.

6.4.2 Exergy Result

Tables 6.4 and 6.5 summarize the exergy flow for the 21 cases calculated based on Equations (6.11) through Equation (6.13). $\sum_{j=1}^{N} W_j$ and W_{Fan} are included because according to Equation (6.12), they also contribute to the exergy balance.

In Table 6.4, under the same T_2 but different N, Ex,ep,in_1, Ex,ep,out_N and W_{Fan} are identical because they have the same entering and leaving air states (State 0 and State 2). While for $\sum_{j=1}^{N} Ex,cd,in_j$, as it is determined by the refrigerant pressures at the condenser, it decreases with N. However, its influence on η_{Ex} (−2.39% to −5.90%), as compared to $\sum_{j=1}^{N} W_j$ (4.61% to 15.10%), is far less significant. Given $\sum_{j=1}^{N} W_j$ increases with N as confirmed earlier (Section 6.4.1), this can explain the percentage change in

η_{Ex} relative to N at 2 are always negative (−2.47% to −9.58%), and the highest occurs when N is 2.

In Table 6.5, under the same N but different T_2, Ex,ep,in_1 and W_{Fan} increase with T_2 due to the corresponding increase in m of OA. On the contrary, Ex,ep,out_N decreases with T_2 due to the higher DB and higher humidity ratio of the treated OA (State 2). $\sum_{j=1}^{N} Ex,cd,in_j$ and $\sum_{j=1}^{N} W_j$ also decrease with T_2 as explained earlier (Section 6.4.1). With the counter-effect of two positive and three negative variables on η_{Ex}, the percentage change in η_{Ex} relative to T_2 at 7 °C are always negative (−0.20 % to −10.52%), and the highest occurs when T_2 is 7 °C.

It is evident from the above that the energy and exergy analyses results are well explained and consistent to confirm that the optimum N is 2 and T_2 is 7 °C.

The results highlight the significant influence of the entering air conditions on the overall performance of the multi-stage DX unit and the need of exergy analysis to determine the number of cooling N and the treated OA temperature T_2.

Table 6.4 Annual exergy results for the same T_2 but different N (% changed in bracket) *

T_2 (°C)	Cases with N	Exergy Flow (MWh)							η_{Ex} (%)
		Ex,ep,in_1	$\sum_{j=1}^{N} Ex,cd,in_j$	$\sum_{j=1}^{N} W_j$	W_{Fan}	Ex,ep,out_N	$\sum_{j=1}^{N} Ex,cd,out_j$	$Ex,tot,loss$	
4	2	1.04	24.00	140.03	22.66	18.05	27.09	142.59	9.61
	3		23.05 (−3.94%)	152.41 (8.84%)			26.65	154.47	9.06 (−5.74%)
	4		22.75 (−5.19%)	161.17 (15.10%)			25.97	163.61	8.69 (−9.58%)
	Average	1.04	23.27	151.20	22.66	18.05	26.57	153.55	9.12
5	2	1.09	23.60	129.52	22.79	17.67	26.52	132.82	9.98
	3		23.04 (−2.39%)	143.64 (10.90%)			26.24	146.65	9.27 (−7.11%)
	4		22.31 (−5.48%)	144.57 (11.62%)			25.28	147.82	9.26 (−7.21%)
	Average	1.09	22.98	139.24	22.79	17.67	26.01	142.43	9.50
6	2	1.15	23.39	120.75	23.07	17.29	26.26	124.80	10.27
	3		22.75 (−2.74%)	132.78 (9.96%)			25.90	136.55	9.62 (−6.34%)
	4		22.01 (−5.90%)	136.91 (13.39%)			25.20	140.64	9.44 (−8.07%)
	Average	1.15	22.71	130.15	23.07	17.29	25.79	134.00	9.78
7	2	1.21	23.14	115.15	23.39	16.90	26.03	119.96	10.37
	3		22.40 (−3.18%)	123.87 (7.57%)			25.57	128.40	9.89 (−4.67%)
	4		21.97 (−5.03%)	127.41 (10.64%)			24.93	132.15	9.71 (−6.37%)
	Average	1.21	22.50	122.14	23.39	16.90	25.51	126.84	9.99
8	2	1.28	22.94	112.87	23.74	16.50	25.89	118.44	10.26
	3		22.29 (−2.83%)	119.81 (6.14%)			25.45	125.17	9.87 (−3.76%)
	4		21.79 (−5.01%)	123.42 (9.35%)			24.84	128.89	9.69 (−5.52%)
	Average	1.28	22.34	118.70	23.74	16.50	25.39	124.17	9.94
9	2	1.36	22.64	111.14	24.14	16.09	25.66	117.53	10.10
	3		21.93 (−3.14%)	118.04 (6.21%)			25.19	124.19	9.72 (−3.74%)
	4		21.35 (−5.70%)	119.44 (7.47%)			24.44	125.76	9.67 (−4.22%)
	Average	1.36	21.97	116.21	24.14	16.09	25.10	122.49	9.83
10	2	1.45	22.38	109.40	24.59	15.69	25.50	116.64	9.94
	3		21.34 (−4.64%)	114.44 (4.61%)			24.74	121.39	9.70 (−2.47%)
	4		21.08 (−5.80%)	117.57 (7.47%)			24.42	124.59	9.53 (−4.17%)
	Average	1.45	21.60	113.80	24.59	15.69	24.88	120.87	9.72

Note: * % changed is based on N = 2.

Table 6.5 Annual exergy results for the same N but different T_2 (% changed in bracket) [#]

N	T_2 (°C)	Exergy Flow (MWh)							η_{Ex} (%)
		Ex,ep,in_1	$\sum_{j=1}^{N} Ex,cd,in_j$	$\sum_{j=1}^{N} W_j$	W_{Fan}	Ex,ep,out_N	$\sum_{j=1}^{N} Ex,cd,out_j$	$Ex,tot,loss$	
2	4	1.04 (−14.33%)	24.00 (3.72%)	140.03 (21.60%)	22.66 (−3.09%)	18.05 (6.79%)	27.09	142.59	9.61 (−7.34%)
	5	1.09 (−10.07%)	23.60 (2.01%)	129.52 (12.48%)	22.79 (−2.53%)	17.67 (4.54%)	26.52	132.82	9.98 (−3.80%)
	6	1.15 (−5.27%)	23.39 (1.08%)	120.75 (4.86%)	23.07 (−1.36%)	17.29 (2.32%)	26.26	124.80	10.27 (−1.00%)
	7	1.21	23.14	115.15	23.39	16.90	26.03	119.96	10.37
	8	1.28 (5.92%)	22.94 (−0.86%)	112.87 (−1.98%)	23.74 (1.50%)	16.50 (−2.39%)	25.89	118.44	10.26 (−1.14%)
	9	1.36 (12.58%)	22.64 (−2.15%)	111.14 (−3.48%)	24.14 (3.22%)	16.09 (−4.80%)	25.66	117.53	10.10 (−2.65%)
	10	1.45 (20.18%)	22.38 (−3.26%)	109.40 (−5.00%)	24.59 (5.15%)	15.69 (−7.13%)	25.50	116.64	9.94 (−4.15%)
	Average	1.23	23.16	119.84	23.48	16.88	26.13	124.68	10.08
3	4	1.04 (−14.33%)	23.05 (2.90%)	152.41 (23.04%)	22.66 (−3.09%)	18.05 (6.79%)	26.65	154.47	9.06 (−8.38%)
	5	1.09 (−10.07%)	23.04 (2.84%)	143.64 (15.95%)	22.79 (−2.53%)	17.67 (4.54%)	26.24	146.65	9.27 (−6.26%)
	6	1.15 (−5.27%)	22.75 (1.55%)	132.78 (7.19%)	23.07 (−1.36%)	17.29 (2.32%)	25.90	136.55	9.62 (−2.73%)
	7	1.21	22.40	123.87	23.39	16.90	25.57	128.40	9.89
	8	1.28 (5.92%)	22.29 (−0.49%)	119.81 (−3.28%)	23.74 (1.50%)	16.50 (−2.39%)	25.45	125.17	9.87 (−0.20%)
	9	1.36 (12.58%)	21.93 (−2.11%)	118.04 (−4.71%)	24.14 (3.22%)	16.09 (−4.80%)	25.19	124.19	9.72 (−1.69%)
	10	1.45 (20.18%)	21.34 (−4.72%)	114.44 (−7.62%)	24.59 (5.15%)	15.69 (−7.13%)	24.74	121.39	9.70 (−1.94%)
	Average	1.23	22.40	129.28	23.48	16.88	25.68	133.83	9.59
4	4	1.04 (−14.33%)	22.75 (3.54%)	161.17 (26.50%)	22.66 (−3.09%)	18.05 (6.79%)	25.97	163.61	8.69 (−10.52%)
	5	1.09 (−10.07%)	22.31 (1.53%)	144.57 (13.47%)	22.79 (−2.53%)	17.67 (4.54%)	25.28	147.82	9.26 (−4.66%)
	6	1.15 (−5.27%)	22.01 (0.15%)	136.91 (7.46%)	23.07 (−1.36%)	17.29 (2.32%)	25.20	140.64	9.44 (−2.80%)
	7	1.21	21.97 (0.00%)	127.41	23.39	16.90	24.93	132.15	9.71
	8	1.28 (5.92%)	21.79 (−0.84%)	123.42 (−3.13%)	23.74 (1.50%)	16.50 (−2.39%)	24.84	128.89	9.69 (−0.24%)
	9	1.36 (12.58%)	21.35 (−2.84%)	119.44 (−6.25%)	24.14 (3.22%)	16.09 (−4.80%)	24.44	125.76	9.67 (−0.40%)
	10	1.45 (20.18%)	21.08 (−4.05%)	117.57 (−7.72%)	24.59 (5.15%)	15.69 (−7.13%)	24.42	124.59	9.53 (−1.90%)
	Average	1.23	21.90	132.93	23.48	16.88	25.01	137.64	9.43

Note: [#] % change based on T_2 = 7 °C.

6.4.3 Space Relative Humidity Control

To explain better humidity control as identified earlier for T_2 at 7 °C, the space SHR and the designed equipment SHR were reviewed. Given the space RH is achieved by matching the equipment sensible heat ratio (SHR_{sys}) and the space SHR (SHR_{spx}) (Li *et al.*, 2006), to explain the better humidity control for T_2 at 7 °C, the divergence between SHR_{sys} and SHR_{spx} were reviewed. The hourly SHR_{spx} are outputs of *EnergyPlus*. Two indices have been employed to review the divergence between SHR_{sys} and SHR_{spx} for different T_2, they are the index of agreement (*IA*) and *RMSE*. *IA* is a dimensionless indicator that enables consistency comparison between models (Willmott *et al.*, 2012). A higher *IA* (from 0 to 1) means a more consistent tendency of change (Li *et al.*, 2017).

RMSE, as explained earlier, is used to quantify the deviation between SHR_{sys} and SHR_{spx}. IA_{SHR} and $RMSE_{SHR}$ are expressed in Equations (6.29) and (6.30).

$$IA_{SHR} = 1 - \frac{\sum_{i=1}^{n}\left(SHR_{sys} - SHR_{spx}\right)^2}{\sum_{i=1}^{n}\left(\left|SHR_{sys} - \overline{SHR}_{spx}\right| + \left|SHR_{spx} - \overline{SHR}_{spx}\right|\right)^2} \tag{6.29}$$

$$RMSE_{SHR} = \sqrt{\frac{1}{n}\cdot\sum_{i=1}^{n}\left(SHR_{sys} - SHR_{spx}\right)^2} \tag{6.30}$$

where $\overline{SHR}_{spx}$ is the annual average *SHR* of all zones.

Calculation results for different T_2 are summarized in Table 6.6, illustrating that the highest IA_{SHR} (=0.6705) and the smallest $RMSE_{SHR}$ (=0.0532) occurs when T_2 is at 7 °C.

Table 6.6 Divergence results for different T_2

T_2 (°C)	IA_{SHR}	$RMSE_{SHR}$
4	0.6602	0.0545
5	0.6659	0.0538
6	0.6682	0.0535
7	0.6705	0.0532
8	0.6697	0.0534
9	0.6641	0.0541
10	0.6619	0.0543

6.5 Summary

In this Chapter, a realistic DX coil performance model that covers an exceptionally large entering air temperature range (from 6 °C DB to 35 °C DB), which is absent in the current literature, was developed for energy simulations and analyses. The model was developed based on a set of factory test and field measurement data. Its validity was verified by different statistical analyses. Based on the developed performance model, hour-by-hour simulations under varying outdoor conditions, together with exergy analyses for moist air at different entering and leaving states associated with variations in system configurations, were conducted for the use of XT-DOAS in a typical office building. It was confirmed that the optimum configuration for XT-DOAS, taking into account the combined effect of the entering air states and part load conditions on the overall energy and exergy efficiency of the multi-stage DX system, is two cooling stage with a treated outdoor air temperature of 7 °C. The optimum treated OA temperature, through checking of divergence between equipment and space

SHRs, was confirmed able to achieve a better space humidity control. The results of this study enable optimizing the configuration of XT-DOAS for better energy efficiency and performance of office buildings in subtropical region. The developed model, which is validated, will contribute significantly for future study of atypical systems. The energy and exergy analyses described in this study would become a reference protocol to enhance future research in this area.

CHAPTER 7

PROBABILISTIC ASSESSMENT OF OVERCOOLING RISK FOR THE OPTIMIZED XT-DOAS

This chapter investigates the overcooling risk of XT-DOAS, which is a common problem for conventional VAV system due to the minimum air flow fraction requirement. In this assessment, a rigorous probabilistic mothed was conducted by using Monte Carlo simulation (MCS) with 10,000 iterations. Empirical data was used to develop the probability distribution functions of the studied operating parameters. A morphing method was employed to develop 10,000 weather files based upon the typical metrological year and 10 years' weather data of Hong Kong. The vast amount of probable operating characteristics were input to *EnergyPlus* for hour-by-hour simulations. The annual cooling load profile formulated by MCS was validated by in-situ measurements. The probabilistic assessment results include overcooling hours and long-term percentage of dissatisfied of XT-DOAS as compared to a conventional VAV system.

7.1 Introduction

VAV system has a better energy efficiency and humidity control, but the drawback is the risk of overcooling due to its specific operating principle. A typical VAV system varies the supply airflow rate at a constant temperature in response to the space cooling demand for maintaining the desired temperature. The minimum air flow fraction (MAFF) of SA should be set and can be as low as 30% of the peak flow to satisfy

ventilation requirement (ASHRAE, 2017). However, overcooling occurs when the space cooling demand drops further after reaching the minimum airflow setting (Arens *et al.*, 2012; Hoyt *et al.*, 2014)

To maintain space air temperature and to avoid overcooling, the common practice is to add a reheating coil at the VAV terminal box (Nassif *et al.*, 2005; Aynur *et al.*, 2009) but reheating wastes energy and should be eliminated (Aynur *et al.*, 2009). To eliminate or to reduce wasting of reheat energy, recent research suggests to adopt SAT reset in transition seasons (Nassif *et al.*, 2005; Murphy, 2011) or to reduce the MAFF to lower than 30% (Zhang *et al.*, 2014; Hurnik, 2015; Saber, 2017). However, resetting SAT unavoidably increases the supply air fan energy (Norford *et al.*, 1986) while lowering the MAFF value is more likely to cause IAQ problem (Saber, 2017). There are research results claiming that VAV systems can perform well without reheat provisions, but in reality, reheat coil is still provided because of uncertain fluctuations of cooling demand (Bannister, 2008; Feng *et al.*, 2015; Zhou *et al.*, 2016).

Fluctuations in cooling demand are due to the possible variations in weather conditions and use patterns of occupant, lighting systems and office appliances (Gang *et al.*, 2015a; Gang *et al.*, 2015b) Variations in weather conditions, especially in future, can be significant (Sun *et al.*, 2014), while use patterns can be highly variable and unpredictable (Gang *et al.*, 2015a).

Whether XT-DOAS can maintain the desired indoor temperature without reheat provisions under a highly variable and unpredictable cooling demand condition is a concern. To investigate the overcooling risk of a XT-DOAS as compared to

conventional VAV system (Con_VAV), a probabilistic approach was adopted to take into account the influence of future variations in yearly weather conditions, and the daily variations in use patterns, which significantly affect cooling demand. MCS technique was used to generate 10,000 weather files and 10,000 cases to cover all possible cooling demand fluctuations for *EnergyPlus* simulations. The validity of this approach is demonstrated through in-situ measurements at an office building in Hong Kong.

7.2 Systems Comparison

The schematic diagram and the psychrometric process of XT-DOAS used in this chapter are shown in Figures 7.1. The use of 2-stage DX coil and State 2 at 7 °C were determined based on the optimization results in Chapter 6 (Bao *et al.*, 2018).

For Con_VAV which is shown in Figure 7.2, to enable a fair comparison with XT-DOAS, the air handling unit (AHU) was also assumed to be using a DX coil. A variable amount of OA (State 0) is drawn to mix with the space RA (State 1) to become mixed air at State 2. The mixed air is then treated by the AHU to become SA (State 3) and is successively supplies to the space at variable volume to offset the instantaneous cooling demand and to maintain the desired indoor conditions (State 1). The SAT was set at 14 °C and desired indoor conditions were set at 24 °C DB and 50% RH which is within the thermal comfort zone for Hong Kong office environment (Macfarlane, 1978).

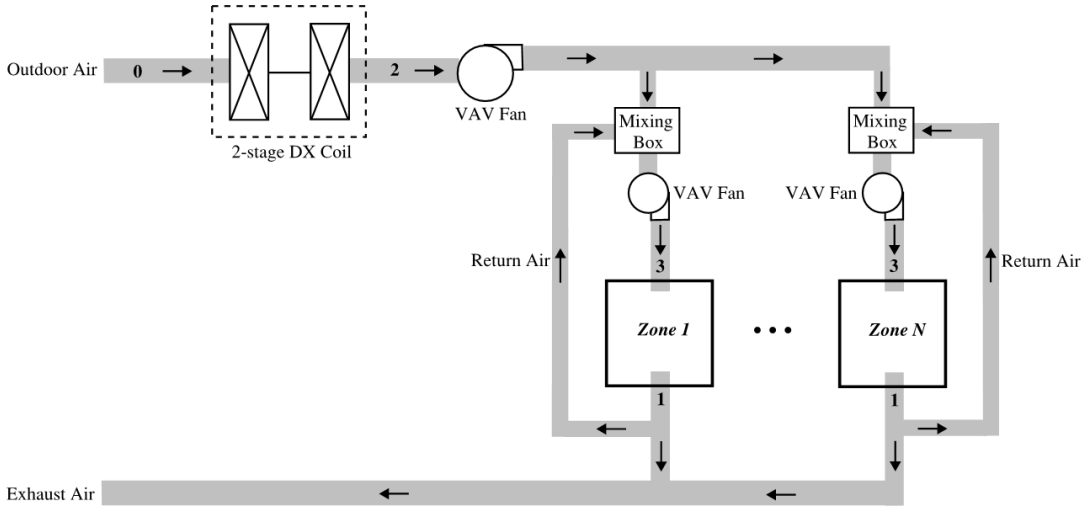

(a) Schematic diagram

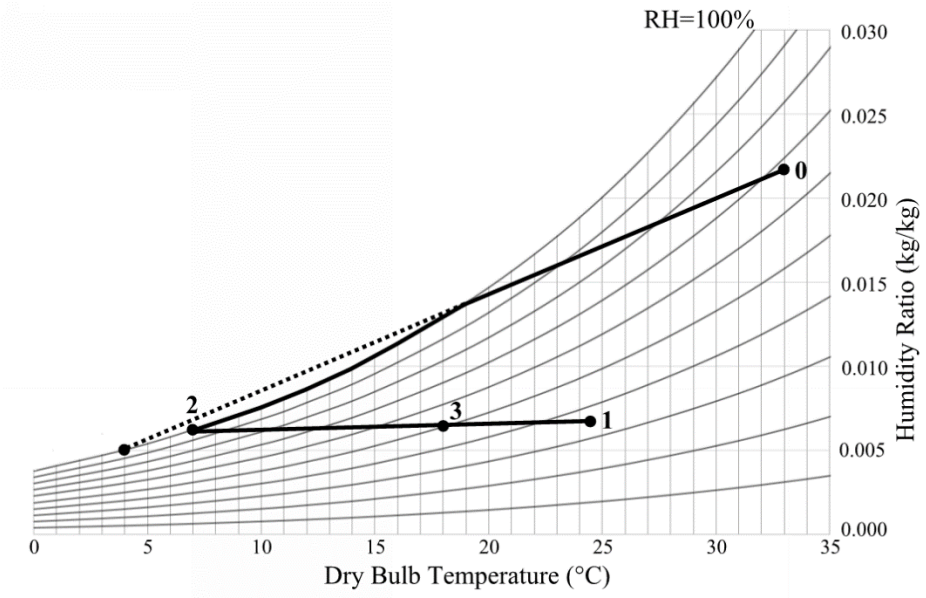

(b) Psychrometric process

Figure 7.1 XT-DOAS

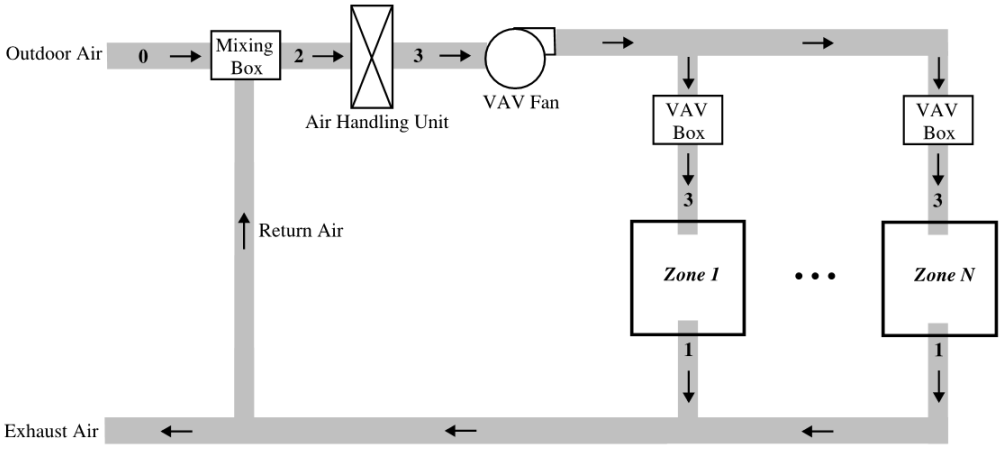

(a) Schematic diagram

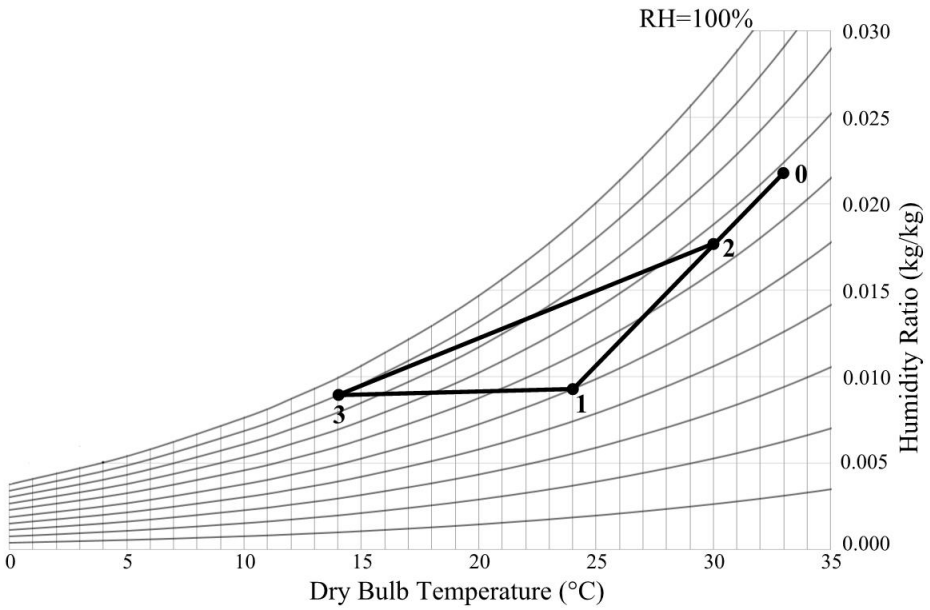

(b) Psychrometric process

Figure 7.2 Conventional VAV system (Con_VAV)

The MAFF of SA for both XT-DOAS and Con_VAV were set at 30% to satisfy the ventilation requirement (ASHRAE, 2017). The thermodynamic states in Figures 7.1 and 7.2 and the associated airflow rates were preliminarily determined by common design practice. Details are summarized in Table 7.1.

The typical office building in Hong Kong (see Section 4.1) was again adopted for the evaluation in this chapter. Tts building characteristics are shown in Table 4.1. To simplify the evaluation, the perimeter west zone (Z-W) with highly fluctuating cooling demand, was chosen as the worst scenario. The layout of the studied building and the studied zone are shown in Figure 4.1.

Table 7.1 Design conditions of XT-DOAS and Con_VAV

Parameters		**XT-DOAS**	**Con_VAV**
Space air temperature (°C)		24.5	24
Space relative humidity (%)		35	50
Sensible load (kW)		63.82	64.82
Latent load (kW)		6.13	5.83
State conditions (T°C[DB]/RH%)	0	33/68	33/68
	1	24.5/35	24/50
	2	7/100	30/67
	3	18/51	14/90
Mass flow rate (kg/s)	Supply air	9.77	6.85
	Outdoor air	3.62	1.55

7.3 Monte Carlo Simulation

To model the fluctuations in cooling demand, a sufficiently large volume of data sets covering all possible values of the studied parameters should be considered.

Monte Carlo Simulation (MCS) was adopted to generate the data sets. MCS is a probability approach where the output values are randomly generated based on the assumed distributions. With a sufficiently large number of iterations, all possible values for the studied parameters will be generated.

The distributions were assumed based on the uncertainty and operating range of the studied parameters. A higher number of iterations normally returns a better approximation. In this study, the studied parameters include the weather conditions and the use patterns including occupant, lighting and appliances. Previous studies have suggested that 10,000 iterations is considered sufficiently large (Barreto and Howland, 2005; Yi and Chan, 2013)

The procedures for MCS are shown in Figure 7.3 and outlined as follows (Note: those in italics are name of the software):

1) Develop 10,000 weather data files based on the typical meteorological year (TMY) and 10 years' weather data of Hong Kong using a morphing method. The development is programmed to be automatically generated by *Excel VBA*.

2) Develop the probability distribution function (PDF) for the use pattern-related operating parameters using *@RISK* which adopts curve-fitting techniques to develop PDF.

3) Create 10,000 *EnergyPlus* jobs using Latin Hypercube Sampling (LHS) approach, which stochastically selects internal load PDF to combine with the 10,000 weather data files.

4) Run 10,000 *EnergyPlus* simulations using a co-simulation tool-*jEPlus*.

5) Get hourly results from the outputs of *EnergyPlus*.

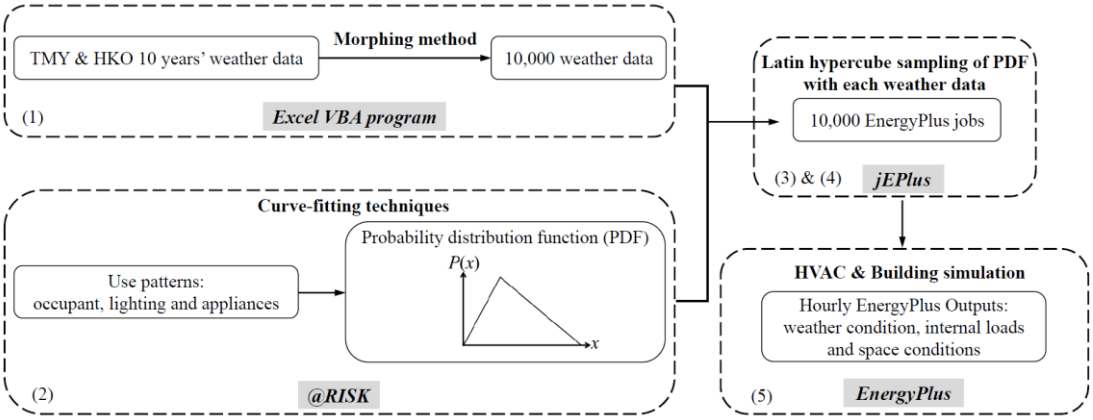

Figure 7.3 Flowchart of Monte Carlo simulation

Details of the above procedures are discussed in the following sections.

7.3.1 Morphing of Weather File

In *EnergyPlus*, TMY's hourly weather data is normally used to run year-round hour-by-hour simulation, 1995 is the year for Hong Kong (Chan *et al.*, 2006b). However, when assessing the impact of climate change on the overcooling risk of XT-DOAS, future weather data, which can affect the solar heat gain, incoming ventilation air temperature, and conductive and convective heat exchange through the building envelope, etc. needs to be developed. With these considerations, probabilistic simulation was applied to generate a large number of weather data files for *EnergyPlus* simulations. This was achieved using a "morphing method", which has been widely used by other research studies (Belcher *et al.*, 2005; Chan, 2011; Lee *et al.*, 2016).

The morphing method involves three generic operations: 1) a shift; 2) a linear stretch (scaling factor); and 3) a shift and a stretch, as listed in Equations (7.1) to (7.3) below respectively.

$$x = x_o + \Delta x_m \tag{7.1}$$

$$x = \alpha_m x_o \tag{7.2}$$

$$x = x_o + \Delta x_m + \alpha_m \left(x_o - \langle x_o \rangle_m \right) \tag{7.3}$$

where x is the new hourly weather variable; x_o is the hourly baseline weather variable; Δx_m is the absolute change in the monthly mean value of the variable for the month 'm'; α_m is the fractional change in the monthly mean value of the variable for the month 'm'; $\langle x_o \rangle_m$ is the monthly mean value of the weather variable x_o for the month 'm'.

A shift (Equation (7.1)) is used when the climate change scenario lists an absolute change of the mean, for instance adjusting atmospheric pressure. A linear stretch (Equation (7.2)) is used when there is a change of either the mean or the variance quoted as a percentage or fractional change rather than an absolute increment, or when the variable can be switched off altogether. A shift and a stretch (Equation (7.3)) is used when both the mean and the variance need to be changed.

Based on the morphing method and MCS, 10,000 new weather files consisting of hourly weather variables were programmed to generate automatically by *Excel VBA* (Halvorson, 2013). In the morphing exercise, hourly weather data of Hong Kong's TMY (Chan *et al.*, 2006b) and the Hong Kong Observatory's (HKO) data of the past ten years (2004-2013) were considered. Despite TMY and HKO containing hourly weather data including solar radiation, cloud cover, wind direction and wind speed, dry bulb temperature, wet bulb temperature, dew point temperature, relative humidity, rainfall amount, etc., only global solar radiation, dry bulb temperature and dew point

temperature were considered in this study as they are influential factors affecting cooling demand (Gang *et al.*, 2015a). Equations (7.4) to (7.9) explain how the influential factors were morphed to generate other possible weather data for *EnergyPlus* simulations.

3.2.1.1 Global Solar Radiation

For global solar radiation, which is zero at night, the linear stretch algorithm is appropriate for calculating its future value. The new hourly global solar radiation *gsr* was calculated based on the monthly scaling factor αgsr_m and existing hourly global solar radiation of the TMY weather data. The procedures are mathematically shown in Equations (7.4) and (7.5):

$$\alpha gsr_m = 1 + \frac{\Delta DSWF_m}{\langle gsr_o \rangle_m} \tag{7.4}$$

$$gsr = \alpha gsr_m \cdot gsr_o \tag{7.5}$$

where $\Delta DSWF_m$ is the absolute change in the monthly mean global solar radiation for the month '*m*' of HKO weather, Wh/m^2; $\langle gsr_o \rangle_m$ is the existing monthly mean global solar radiation for the month '*m*' of TMY weather, Wh/m^2; gsr_o is existing hourly global solar radiation of TMY weather, Wh/m^2.

3.2.1.2 Dry Bulb Temperature

For dry bulb temperature, its new hourly value *dbt* reflects changes in both the mean and the maximum and minimum temperatures and thus the combination of a shift and a stretch was adopted as shown in Equations (7.6) and (7.7):

$$\alpha dbt_m = \frac{\Delta TMAX_m - \Delta TMIN_m}{\langle dbt_{o\max}\rangle_m - \langle dbt_{o\min}\rangle_m} \tag{7.6}$$

$$dbt = dbt_o + \Delta TEMP_m + \alpha dbt_m \cdot \left(dbt_o - \langle dbt_o\rangle_m\right) \tag{7.7}$$

where $\langle dbt_{o\max}\rangle_m$, $\langle dbt_o\rangle_m$ and $\langle dbt_{o\min}\rangle_m$ are the monthly maximum, mean and minimum dry bulb temperatures respectively for the month '*m*' of TMY weather, °C; $\Delta TMAX_m$, $\Delta TEMP_m$ and $\Delta TMIN_m$ denote the monthly absolute change in the maximum, mean and minimum dry bulb temperature respectively for the month '*m*' of HKO weather, °C; αdbt_m is the monthly fractional change of the dry bulb temperature between HKO and TMY weather; dbt_o is the existing hourly dry bulb temperature of TMY weather, °C.

3.2.1.3 Dew Point Temperature

Dew point temperature reflects the saturation of water vapor in humid air, and the value is based on the dry bulb temperature and saturation of the humid air. Dew point temperature thus cannot be morphed directly and must be done based on the specific humidity *s* and dry bulb temperature determined by the psychrometric formulae (ASHRAE, 2009). The new hourly specific humidity *s* needs to be scaled from the

relative monthly mean change of the weather data and therefore the linear stretch was also adopted in Equations (7.8) and (7.9):

$$\alpha s_m = 1 + \frac{SPHU_m}{100} \tag{7.8}$$

$$s = \alpha s_m \cdot s_o \tag{7.9}$$

where $SPHU_m$ is the monthly percentage changes of specific humidity and temperature between HKO and TMY weather; αs_m is the scaling factor for the month 'm'; s_o is the existing hourly specific humidity of TMY weather, g/kg.

7.3.2 Probability Distribution Function for the Internal Load

Use patterns of occupant, lightings and appliances cause fluctuations in internal load and thus cooling demand. To quantify these fluctuations, probability distribution functions (PDF) of these three influential parameters need to be developed. PDF is used to describe the probability of a random variable falling within a given range of values. In this study, the PDFs were determined by curve-fitting techniques based upon goodness-of-fit. Three testing methods, namely Chi-Square (Chi-S), Anderson-Darling (A-D) and Kolmogorov-Smirnov (K-S), were used to rank the fitted curves. The lower the statistical value, the closer the theoretical distribution appears to fit the available data set. The curve with the best goodness-of-fit was used to determine the PDFs (Vose, 2000).

Table 7.2 Daily patterns of air-conditioning supply, occupant, lighting and appliances

a) Weekdays

Hour		Air-conditioning	Occupant	Lighting		Appliances
From	To			Perimeter	Interior	
0	6	Off	0.00	0.05	0.05	0.10
6	7	Off	0.00	0.05	0.05	0.10
7	8	Off	0.05	0.10	0.10	0.15
8	9	On	0.40	0.50	0.50	0.50
9	10	On	0.95	0.90	1.00	1.00
10	11	On	0.95	0.90	1.00	1.00
11	12	On	0.95	0.90	1.00	1.00
12	13	On	0.95	0.90	1.00	1.00
13	14	On	0.45	0.80	0.90	0.80
14	15	On	0.95	0.90	1.00	1.00
15	16	On	0.95	0.90	1.00	1.00
16	17	On	0.95	0.90	1.00	1.00
17	18	On	0.50	0.80	0.80	0.60
18	19	On	0.25	0.50	0.50	0.40
19	20	Off	0.10	0.30	0.30	0.20
20	21	Off	0.05	0.20	0.20	0.15
22	23	Off	0.00	0.05	0.05	0.10
23	24	Off	0.00	0.05	0.05	0.10

b) Saturdays

Hour		Air- conditioning	Occupant	Lighting		Appliances
From	To			Perimeter	Interior	
0	7	Off	0.00	0.05	0.05	0.05
7	8	Off	0.05	0.10	0.10	1.00
8	9	On	0.30	0.50	0.50	1.00
9	13	On	0.60	0.75	0.80	1.00
13	17	Off	0.10	0.20	0.20	0.20
17	18	Off	0.05	0.10	0.10	0.10
18	24	Off	0.00	0.05	0.05	0.05

c) Sundays

Hour		Air-conditioning	Occupant	Lighting		Appliances
From	To			Perimeter	Interior	
0	9	Off	0.00	0.05	0.05	0.05
9	17	Off	0.05	0.10	0.10	0.10
17	24	Off	0.00	0.05	0.05	0.05

Table 7.3 Probabilistic distribution function of internal load parameters

Parameters	**Peak value**	**PDF of parameters fraction**					
		Distribution	5% level	Mean	Mode	95% level	Standard Deviation
Occupant density	$9m^2$/person	Triangular continuous	0.2179	0.6500	0.950	0.9500	0.2300
Perimeter lighting power density	$25W/m^2$	Triangular continuous	0.4438	0.7554	0.8831	0.9657	0.1625
Interior lighting power density	$25W/m^2$	Triangular continuous	0.2236	0.6667	1.000	0.9747	0.2357
Appliances power density	$25W/m^2$	Triangular continuous	0.2236	0.6667	1.000	0.9747	0.2357

BEAM Plus' daily patterns for occupant, lighting and appliances (Table 7.2) for office buildings in Hong Kong (Lee, 2012) were used to develop the PDF. The patterns were developed based on findings of a series of extensive surveys (Lee *et al.*, 2012). The patterns are in fractions of their respective peak values. Thus, the range is between zero and one. *@RISK*, a widely adopted software for conducting similar analysis, was employed to conduct curve-fittings based upon the three testing methods described above (Palisade, 2017). The peak value of the internal load parameters and the best-fitted PDFs are shown in Table 7.3.

7.3.3 Co-simulation

As there were 10,000 simulations, *jEPlus* was adopted as a co-simulation tool to accelerate the *EnergyPlus* simulations. *jEplus* allows users to load user-defined weather data and input parameters in a graphical interface to automatically create and carry out *EnergyPlus* simulation jobs (Zhang and Korolija, 2010). Latin hypercube sampling (LHS) was used to generate 10,000 input combinations with input parameter values picked stochastically from the best-fitted PDFs. LHS is commonly used in MCS as it requires a smaller sample size to reflect the actual shape of a defined distribution (Yi and Braham, 2015; Lee *et al.*, 2016; Sun *et al.*, 2016). Based on the 10,000 weather data files and the randomly picked input parameters, *jEPlus* can automatically create and run 10,000 *EnergyPlus* jobs. The outputs from *EnergyPlu*s were then used for overcooling and thermal comfort analyses.

7.4 Results and Discussion

The output of MCS is usually described as a probability distribution that indicates the probability associated with each possible outcome (Elyamany and Abdelrahman, 2010). However, as the output of *EnergyPlus* is on hourly basis, thus for each studied parameter, there were 10,000 data sets per hour. To analyse the hourly probability distribution for a whole year (8760 hours), the most probable value for each hour out of the 10,000 data sets (also as the expected value of the distribution) need to be determined to draw the annual profile (Walpole *et al.*, 2012). *@RISK* was again employed for this process (Palisade, 2017). Figure 7.4 illustrates the hour-by-hour determination of the most probable value of a studied parameter constituting to an annual profile. In other words, the annual profile represents the hourly probability value of the 10,000 MCS outputs. Representation validation of the annual cooling load profile formulated based on MCS and overcooling analyses are discussed in the following sections.

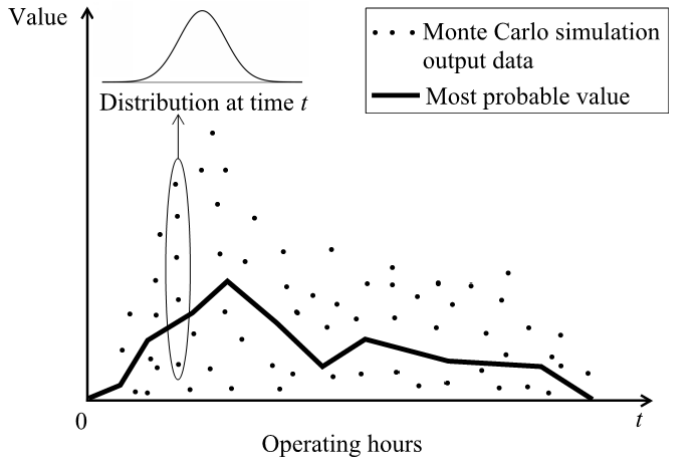

Figure 7.4 Most probable value identification process

7.4.1 Validation

In-situ measurements were conducted at an office building in Hong Kong to ascertain the annual cooling profile to validate the profile drawn by MCS. The studied building is a Grade A[1] commercial building that consists of three parts: the basement carpark, the retail floors and the office floors. The focus of this study is on the office floors, which are from 4/F to 33/F. The floor layout is shown in Figure 7.5. The building was selected for in-situ measurements because its air-conditioned area per floor (1051.4 m^2) and the AC operating schedule (from 8:00 to 22:00 on weekdays and from 8:00 to 13:00 on Saturdays) are comparable to the case study building described in Section 4.1.

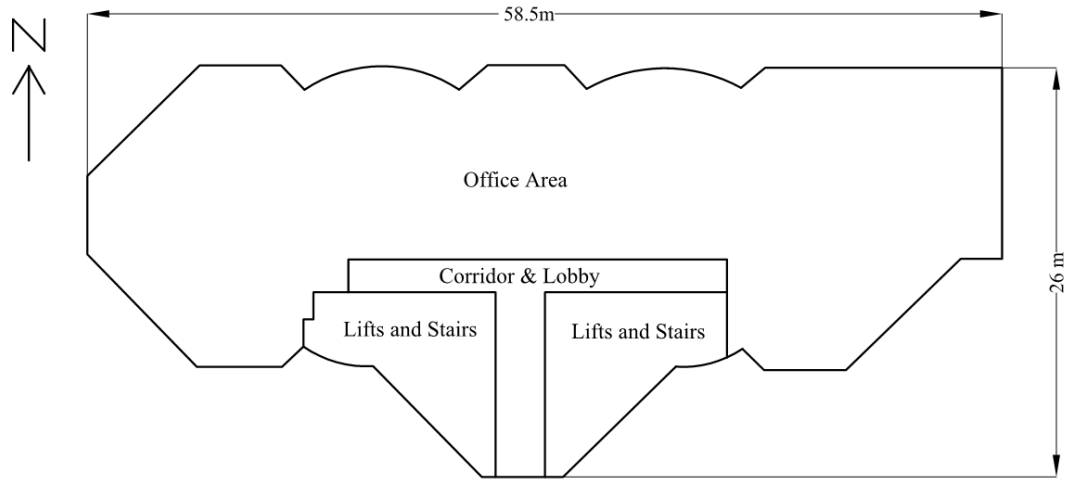

Figure 7.5 Floor layout of the studied building

[1] Modern buildings with high quality finishes; flexible layout and large floor area; well decorated lobbies and circulation areas; effective central services installations; professional management; and parking facilities.

For the AC system of the office floors of the building, there is no building management system or control system to record the operating conditions of the major equipments. The building owner could only provide the last three years' monthly electricity consumption figures (kWh) and the logged AC operating hours (*t*). Thus, the metered consumption was the only source of information for determination of the annual cooling profile.

Based on the metered consumptions, the annual cooling profile can be determined based on Equations (7.10) to (7.13).

$$E_m = W_t \cdot t_m \tag{7.10}$$

$$PLR = \frac{Q}{Q_{rated}} = \frac{C_{pw} \cdot \rho_w \cdot V_w \cdot \left(T_{rw} - T_{sw}\right)}{Q_{rated}} \tag{7.11}$$

$$COP = \frac{Q}{W_t} \tag{7.12}$$

$$COP = a \cdot PLR^2 + b \cdot PLR + c \tag{7.13}$$

$$Q = \frac{\left(\frac{1}{W_t} - \frac{b}{Q_{rated}}\right) \pm \sqrt{\left(\frac{b}{Q_{rated}} - \frac{1}{W_t}\right)^2 - \frac{4ac}{Q_{rated}^2}}}{\frac{2a}{Q_{rated}}} \quad (Q > 0) \tag{7.14}$$

where E_m is the monthly electricity consumptions for the month '*m*', kWh; W_t is the calculated chiller power input, kW; t_m is the sum of AC operation hours for the month '*m*', h; *PLR* is the part load ratio; *Q* is chiller cooling output, kW; Q_{rated} is the rated chiller cooling output, kW, which can be obtained from manufacturer data; C_{pw} is the specific heat capacity of water, J/(kg·°C); ρ_w is the density of water, kg/m^3; V_w is the

chilled water volume flow rate through the chiller, m^3/s; T_{rw} is the return chilled water temperature, °C; T_{sw} is the supply chilled water temperature, °C; *COP* is the coefficient of performance of the chiller; *a*, *b*, *c* are empirical coefficients.

In order to determine the empirical coefficients in Equation (7.13) and thus *Q* at different W_t, in-situ measurements were conducted.

In in-situ measurements, plant operating conditions were logged by data loggers, and the instruments used are summarized in Table 7.4. The chilled water flow (V_w) was measured by the ultrasonic flow meter. The supply and returned chilled water temperatures (T_{sw} and T_{rw}) were measured by the temperature transducers. The instantaneous power input (*W*) for different part load conditions was measured by the power quality analyser.

All measurements were recorded at 10-second intervals for a period of ten days, and the 10-minute average data calculated from the records, which amounted to about 1000 sets of data, which were used for analysis of performance of the chillers.

The 1000 data sets, covering a full range of part load operating conditions, were used to develop the chiller performance model (Equation 7.13) by regression method. The resultant model is shown in Equation (7.15) and the coefficient of determination (R^2) of the model is 0.835.

$$COP = -8.0384 \times PLR^2 + 11.964 \times PLR + 0.797 \quad (R^2 = 0.835) \tag{7.15}$$

Table 7.4 Instruments used for in-situ measurement (plant operation conditions)

Description	Parameters	Instrument	Brand	Model	Accuracy
AC plant operation conditions	Chilled water flow (V_w)	Ultrasonic Flow Meter	SiteLab	SL1188P	±1% of measured value
	Supply chilled water temperatures (T_{sw})	Temperature Transducer	Jumo	90/00359141ER	±0.15°C
	Returned chilled water temperatures (T_{rw})				
	Instantaneous power input (W)	Power Quality Analyser	Chauvin Arnoux (1ϕ phase power monitor)	CA8230	DC V: ± (0.5 %+2 counts) (6 VRMS to 600 VRMS) AC V: ± (0.5 %+2 counts) (1A to 1700 A) DC A: ± (1 %+1 counts) (6 VRMS to 600 VRMS) AC A: ± (0.5 %+1 counts) (6 VRMS to 600 VRMS)
Indoor thermal conditions	Indoor temperature	Temperature and Humidity Logger	HOBO	U12 Temp/RH	Temperature: ±0.35 °C from 0 to 50 °C Relative humidity: 3.5%
	Indoor humidity				

The indoor temperature and humidity were also measured and recorded at 1-minute interval for a week in summer by using stick-on integrated sensors and data loggers (see Table 7.4) at six randomly selected locations in the office floors. A summary of the ranges of hourly temperature and relative humidity data measured by the 6 loggers during AC operating hours (08:00-22:00) of the office floors is given in (see Table 7.5).

Table 7.5 The range of hourly indoor temperature and humidity

Data logger	**Dry bulb air temperature (°C)**	**Relative Humidity (%)**
1	23.2 – 26.4	59.2 – 87.5
2	23.0 – 26.2	58.8 – 85.7
3	23.2 – 26.3	59.3 – 82.0
4	23.5 – 26.5	57.7 – 77.3
5	23.2 – 28.5	48.2 – 83.0
6	22.6 – 26.8	61.2 – 79.0
Average indoor conditions	24.5 – 25.5	59.0 – 65.5

It is noted that indoor temperatures (24.5 °C to 25.5 °C) are within the recommended value in EMSD's energy efficiency code and close to the assumed conditions of the case study building (Table 7.1) to indicate that there is no obvious overcooling or overheating. Thus, the cooling output of chillers for offices can be assumed to be equal to the cooling demand for determining the annual cooling profiles.

Three annual cooling profiles were determined for the studied building. Their monthly average values were normalized for unit floor area (m^2) and were compared with the most probable values derived from the 10,000 data sets generated from MCS. Results are shown in Figure 7.6.

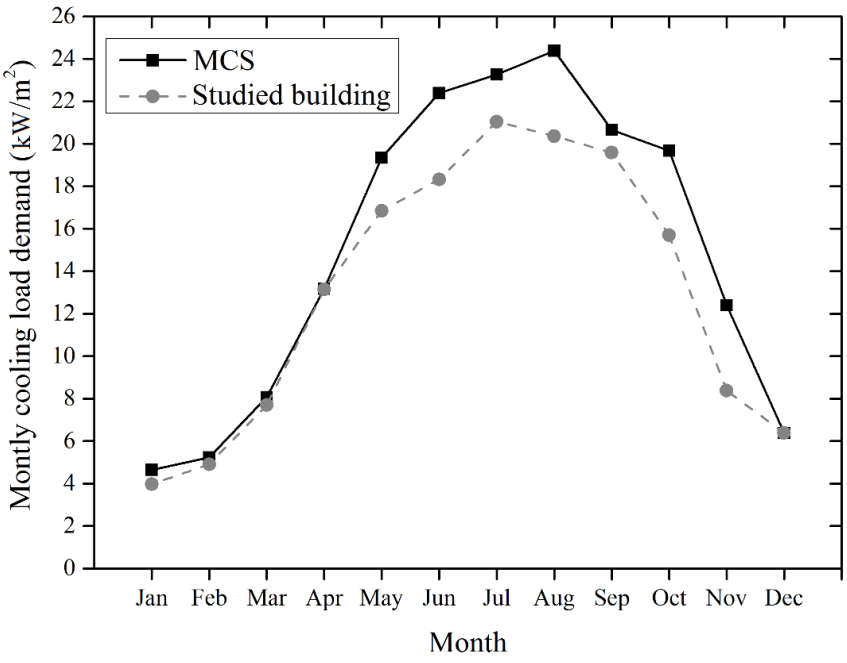

Figure 7.6 Annual cooling profiles of the studied building and the MCS

Figure 7.6 shows the studied building's annual cooling profile and the MCS profile. It can be seen that the trends match well. However, to check similarity and consistency, several assessment metrics were adopted. They include the mean absolute error (*MAE*), mean absolute percentage error (*MAPE*), root-mean-squared error (*RMSE*) and index of agreement (*IA*). *MAE* is used to quantify the average of the absolute error between two data sets. *MAPE* is used to measure the relative error between the two data sets. *RMSE* is used to quantify the deviation of one data set from the other. *IA* (Willmott *et al.*, 2012) is a dimensionless indicator that enables consistency comparison between two data sets and its range is from 0 to 1. Their mathematical definitions are given in Equation (7.16) to (7.19) and the calculation results are shown in Table 7.6.

$$MAE = \frac{1}{m} \cdot \sum_{i=1}^{m} \left| O_i - P_i \right| \tag{7.16}$$

$$MAPE = \frac{1}{m} \cdot \sum_{i=1}^{m} \left(\frac{\left| O_i - P_i \right|}{\left| O_i \right|} \right) \times 100\% \tag{7.17}$$

$$RMSE = \sqrt{\frac{1}{m} \cdot \sum_{i=1}^{m} \left(O_i - P_i \right)^2} \tag{7.18}$$

$$IA = 1 - \frac{\sum_{i=1}^{m} \left(P_i - O_i \right)^2}{\sum_{i=1}^{m} \left(\left| P_i - \overline{O} \right| + \left| O_i - \overline{O} \right| \right)^2} \tag{7.19}$$

where O_i represents values calculated from the studied building; P_i represents the most probable values from MCS; $\overline{O}$ is the three years' mean values. m is the month.

Table 7.6 The validation metrics between the studied building and MCS

Metric	**Values**
MAE	1.94
MAPE	14.55%
RMSE	2.54
IA	0.964

To demonstrate a good match between two data sets, *MAE*, *MAPE* and *RMSE* should be close to zero and the *IA* should be close to 1. In Table 7.6, *IA* is close to 1 (Li *et al.*, 2017) and other metric values are within a reasonable range for cooling load prediction (Liu *et al.*, 2017). Thus, the validity of using MCS to develop the possible values of the studied parameters is confirmed.

7.4.2 Overcooling hours

Overcooling hours is defined as the accumulated hours when the space air temperature (T_1) drops below the desired temperature (ΔT_1) to a level lower than the threshold. According to studies, the threshold *is* 21 °C for office environments (Chow and Lam, 1992; Lam and Hui, 1996; Shi *et al.*, 2015), and thus below that is considered overcooling.

The most probable hourly T_1 for the 10,000 simulation cases, for XT-DOAS and Con_VAV were extracted for a detailed analysis and results are shown in Figures 7.7 and 7.8, respectively.

Figures 7.7 and 7.8 show the relative frequency and cumulative distribution function of T_1 to illustrate the probability distribution of T_1 under uncertainties of weather conditions and use patterns.

Based on the range of T_1, it is noted that for 90% probability, T_1 of XT-DOAS lies between 23.66 °C and 24.84 °C, and that of Con_VAV lies between 20.10 °C and 24.33 °C. While for 100% probability, T_1 of XT-DOAS is from 18.53 °C to 27.66 °C (mean temperature is 24.42 °C, standard deviation is 0.5864 °C) and that of Con_VAV is from 16.76 °C to 26.31 °C (mean temperature is 23.24 °C, standard deviation is 1.4156 °C). The results indicate that XT-DOAS is more robust than Con_VAV in controlling the space air temperature for being able to maintain a smaller temperature range.

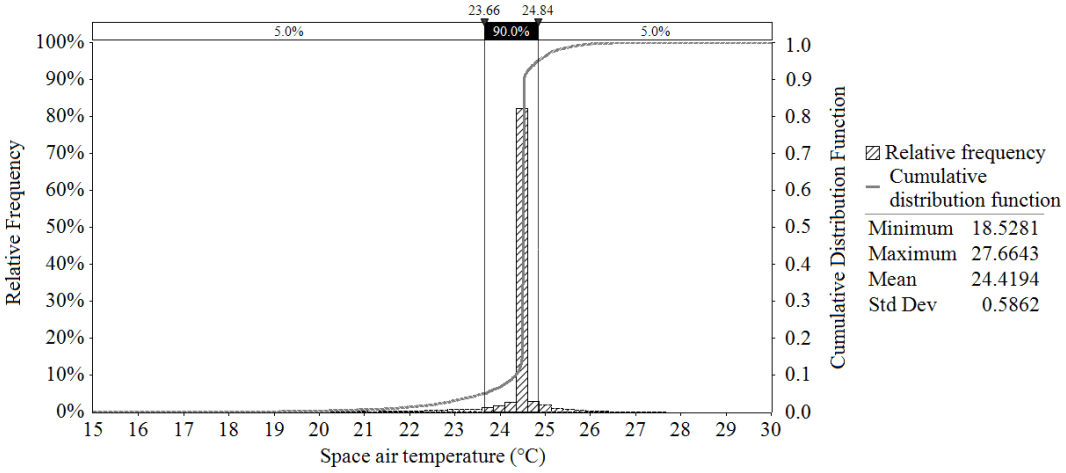

Figure 7.7 Hourly space air temperature distribution (T_1) of XT-DOAS

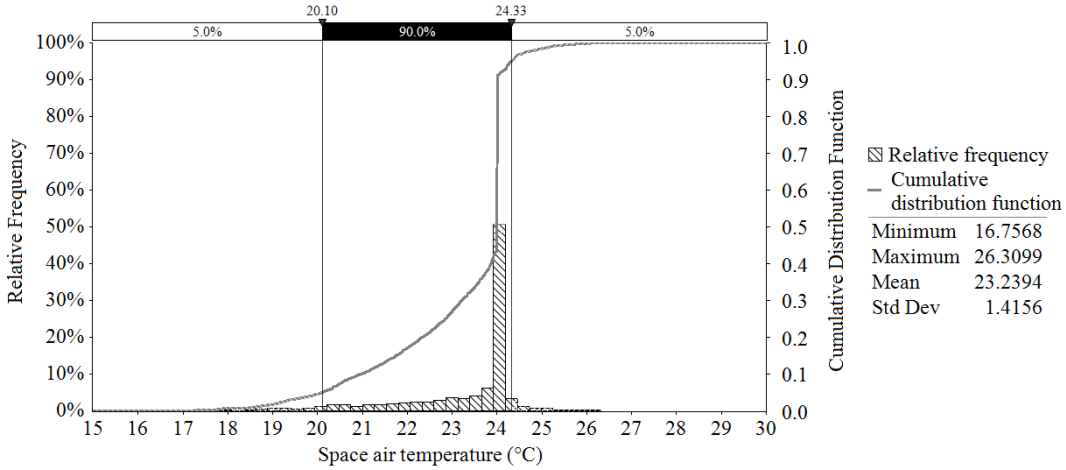

Figure 7.8 Hourly space air temperature distribution (T_1) of Con_VAV

The range of T_1 achieved by XT-DOAS for 100% probability in fact falls within the indoor temperature range achieved by majority of the office buildings in Hong Kong using VAV with a reheating system (18.2 °C and 26.6 °C and mean value is 23.1 °C) (HKEPD, 2003).

Using T_1 equals 21 °C as the threshold, cumulative overcooling hours for XT-DOAS and Con_VAV over a year were determined. Results are shown in Table 7.7, illustrating that the annual cumulative overcooling hours for XT-DOAS is 29 and that of Con_VAV is 426. For XT-DOAS, overcooling occurred from January to February, and it occurred from December to March for Con_VAV. This is judged to be reasonable because as revealed in Figure 7.6, the cooling demand in these four months is less than 36% of the peak in July (3.97kW/m^2 to 7.70kW/m^2 Vs 21.04kW/m^2).

Table 7.7 The overcooling hours of XT-DOAS and Con_VAV

Month	**XT-DOAS**	**Con_VAV**
January	24	140
February	5	115
March	0	97
December	0	74

To explain the smaller number of overcooling hours for XT-DOAS, Table 7.8 compares the percentage of SAT undershooting (ΔT_3) hours of the two systems from December to March. It can be seen that the extent of SAT undershooting for Con_VAV is higher than XT-DOAS, especially for March (2.50% Vs 0%) and December (1.91% Vs 0%).

Table 7.8 The extent of undershooting in SAT for XT-DOAS and Con_VAV

Month	**Extent of SAT undershooting**	
	XT-DOAS	Con_VAV
January	0.62%	3.61%
February	0.13%	2.96%
March	0%	2.50%
December	0%	1.91%

For XT-DOAS, a smaller extent of SAT undershooting implies a smaller overcooling risk that can be explained by Equations (7.20) to (7.24).

When VAV system reaches MAFF (=30%), a further drop in space load (Q_{spx}) results in a surplus cooling output (ΔQ). Recall that:

$$Q_{sen} = m_3 \cdot C_{pa} \cdot (T_1 - T_3) \tag{7.20}$$

$$\Delta Q_{sen} = m_3 \cdot C_{pa} \cdot (\Delta T_1 - \Delta T_3) \tag{7.21}$$

where m_3 is the supply air mass flow rate, kg/s; C_{pa} is the specific heat of moist air, kJ/kg·°C; Q_{sen} is the sensible cooling output, kW.

Thus ΔT_1 is also determined by ΔT_3.

Considering that (Q_{lat} is the latent cooling output, kW):

$$\Delta Q = \Delta Q_{sen} + \Delta Q_{lat} \tag{7.22}$$

ΔQ_{sen} is the same for XT-DOAS and Con_VAV, but ΔQ_{lat} for XT-DOAS tends to zero. Hence, Con_VAV has a higher ΔQ.

On the refrigeration side, since:

$$\Delta Q = U \cdot A \cdot \Delta LMTD \tag{7.23}$$

where U is the overall heat transfer coefficient between air and evaporator surface, W/(m^2·°C); A is the heat transfer area for airside, m^2.

For Con_VAV, the higher ΔQ results in a correspondingly higher $\Delta LMTD$.

Since:

$$LMTD = \frac{T_2 - T_3}{\ln\left(\frac{T_2 - T_e}{T_3 - T_e}\right)} \tag{7.24}$$

where T_e is the evaporating temperature, °C.

When $\Delta LMTD$ is higher, implying ΔT_e and ΔT_3 are higher to increase ΔT_1.

The above explains the higher overcooling risk of Con_VAV compared to XT-DOAS.

7.4.3 Long-term Percentage of Dissatisfied

The above discussions indicate that the use of XT-DOAS without reheating provision can achieve the desired indoor temperature under a highly variable and unpredictable cooling demand condition. The number of overcooling hours is much less than that of Con_VAV, which is 29 hours as compared to 426 hours.

To investigate the thermal discomfort caused by overcooling, the long-term percentage of dissatisfied (*LPD*), which is a comfort-model based index, was introduced (Carlucci, 2013; Carlucci *et al.*, 2015) *LPD* is appropriate to quantify predicted thermal discomfort over a specific period in consideration of the variations in occupancy level.

For a mechanically cooled single office room, *LPD* of overcooling (LPD_{oc}) based on ASHRAE's adaptive comfort model can be defined as:

$$LPD_{oc}\big|_{T_{op,in}<T_{comf,ASHRAE}} = \frac{\sum_{t=1}^{k}\left(OCC_t \cdot ALD_t \cdot HR_t\right)}{\sum_{t=1}^{k} OCC_t \cdot HR_t} \tag{7.25}$$

where t is the counter for the time step of the calculation period; k is the last progressive time step of the calculation period; OCC_t is the zone occupation rate at time t; HR_t is the duration of a calculation time step (by default one hour); *ALD* is the ASHRAE likelihood of dissatisfied to estimate the severity of the deviations from a theoretical thermal comfort objective, given certain outdoor and indoor conditions at a specified time and a space location. *ALD* is a continuous function obtained by using statistical analysis of the comfort surveys in the ASHRAE RP-884 database (de Dear, 1998) and can be calculated by Equations (7.26) and (7.27).

$$ALD \equiv \frac{e^{0.008\Delta T_{op}^2 + 0.406\Delta T_{op} - 3.050}}{1 + e^{0.008\Delta T_{op}^2 + 0.406\Delta T_{op} - 3.050}} \in [0.05, 1.00). \tag{7.26}$$

$$\Delta T_{op} = \left|T_{comf,ASHRAE} - T_{op,in}\right| \tag{7.27}$$

where $T_{op,in}$ is the indoor operative temperature, °C; $T_{comf,ASHRAE}$ is the comfortable operative temperature according to the ASHRAE adaptive model, °C (ASHRAE, 2013).

Based on Equations (7.25), (7.26) and (7.27), LPD_{oc} for XT-DOAS and Con_VAV were calculated. It was found that LPD_{oc} for Con_VAV was five times that of XT-DOAS; these were 1.69 % and 0.31% respectively. Given that the zone occupation rate (OCC_t) has been taken into account to discount the calculated LPD_{oc}, 1.69% of LPD_{oc} for Con_VAV is already a significant value.

7.5 Summary

This chapter adopted a probabilistic approach to assess the overcooling risk of XT-DOAS operating under uncertainties of weather conditions and use patterns of occupant, lighting and appliances. To address the uncertainties, Monte Carlo simulations were employed to generate 10,000 weather data files and 10,000 cases to cover all possible values of the studied parameters for *EnergyPlus* simulations. The possible values generated were validated by the 3-year operating characteristics of a commercial building in Hong Kong to confirm the viability of using the proposed probabilistic approach for addressing uncertainties. It was found that the potential annual overcooling hours using XT-DOAS in office buildings in Hong Kong were 29 hours, which is equivalent to 0.31% long-term percentage of dissatisfied (LPD). These results, as compared to 426 overcooling hours and 1.69% LPD achieved by the conventional VAV system, confirm the excellent performance of XT-DOAS. The proposed probabilistic approach would be useful for uncertainty and risk analyses.

CHAPTER 8

CONCLUSIONS AND RECOMMENDATIONS FOR FUTURE RESEARCH

Hong Kong is of subtropical climate where summers are hot and humid. The energy efficiency and environmental health associated with use of air conditioning, especially for office environments where air-conditioning is used almost year-round, is receiving greater attention nowadays. Recent research advocates the use of dedicated outdoor air system (DOAS) to avoid moisture-related and cross contamination problems for better environmental health and energy efficiency. A conventional DOAS often comprises two systems: an outdoor air (OA) system dedicated to produce high quantities of OA that handles the entire latent loads and part of the space sensible loads; and a terminal system to handle the remaining space sensible loads. The OA system often uses active-desiccant technology; whilst the terminal system can be chilled beams/ceilings. Energy savings can be derived from reheating and dehumidification energy reductions with such a system configuration. However, the space intensive characteristics for active-desiccant technology and the condensation problem associated with chilled beams/ceilings hinder their popular use in Hong Kong.

A novel DOAS for better energy efficiency and environmental health objectives is proposed in this study. The proposed DOAS system is a cold air distribution system that consists of a DOAS central system to produce extra-low temperature (XT) OA to handle the entire space cooling load and a mixing chamber as the terminal system to mix XT OA and return air (RA) to become supply air (SA). The SA of variable air

volume (VAV) control successively delivers to the space to offset the instantaneous cooling demand. With this configuration, no cooling is required at the conditioned space to avoid moisture-related problems and there is no re-circulation of RA across conditioned spaces to introduce cross-contamination problems. Energy savings can be derived from reheating, pumping and fan energy reductions. For generating XT OA, a multi-stage variable speed direct expansion (DX) air-conditioner is proposed because of higher equipment efficiency associated with working under higher evaporating temperature (first-stage) and smaller temperature lifts (between evaporator and condenser). Moreover, because the XT OA is dry and cold, the conditioned spaces can be maintained at lower humidity and higher space DB temperature conditions to derive further energy savings.

To successfully facilitate the application of the proposed system (XT-DOAS), this study investigated its humidity control, energy performance and overcooling risk when applied in the office building in subtropical region like Hong Kong. The major findings from this study and the recommendations for future research are detailed below.

8.1 Conclusions

8.1.1 Performance Evaluation

To investigate the performance of the novel XT-DOAS as compared to a conventional system for achieving better energy efficiency and environmental health objectives, a comparative study was conducted. *EnergyPlus* simulations were employed for the comparative study. They were conducted based on actual equipment performance

models and realistic building and system characteristics to compare the resultant space relative humidities, thermal comfort level, energy performance and the condensation risk achieved by the two systems. The key findings are detailed as follows:

1) XT-DOAS saves 22.6% annual energy use for air-conditioning as compared to the conventional system.

2) *RMSE* and *SD* analyses indicate that XT-DOAS is superior for achieving the desired relative humidities.

3) XT-DOAS can better achieve the desired thermal comfort conditions. The annual cumulative number of non-comfortable hours for XT-DOAS is 641.2 hours, while that for the conventional system is 929.2 hours, a reduction of 31%.

4) XT-DOAS completely eliminates the condensation risk at the terminal device, while the conventional system faces condensation risk for 284 hours.

8.1.2 A Realistic Coil Performance Model

As XT-DOAS receives hot and humid high temperature OA at the first cooling stage and handles extra-low temperature air at the last cooling stage, which affect the DX coil performance, a realistic coil performance model, which covers a wide range of entering and leaving air conditions, was developed for energy simulations and analyses. Factory test data and field measurement data were collected to develop and

validate the coil performance model defined by the *CAP-FT* and *EIR-FT* performance curves. The key findings are detailed as follows:

1) A realistic DX coil performance model that covers an exceptionally large entering air temperature range (from 6 °C DB to 35 °C DB), which is absent in the current literature, was successfully developed.

2) The *CAP-FT* is the total cooling capacity (*CAP*) modifier curve represented as a function of temperature. The developed curve shows that the DX coil's *CAP* increases with entering air WB temperature at the DX coil (WB_{ei}) but varies very little with the entering air DB temperature at the condenser (DB_{ci}).

3) The *EIR-FT* is the energy input ratio (*EIR*) modifier curve represented as a function of temperature. The developed curve shows that the *CAP* increases primarily with WB_{ei} but the power input *W* decreases with both WB_{ei} and DB_{ci}. In other words, a lower WB_{ei} results in a higher *EIR* and thus lower coefficient of performance (*COP*).

8.1.3 Optimum Configuration

The configuration of XT-DOAS was optimized for the number of cooling stages and the treated OA temperature. The optimization was based on the developed realistic coil performance model. The moist air entering and leaving individual cooling stages is of different states to affect the performance of XT-DOAS for achieving the desired air conditions and better energy efficiency, thus energy and exergy analyses were

conducted to optimize the configuration of XT-DOAS. The key findings are detailed as follows:

1) The optimum configuration for XT-DOAS was determined as two cooling stage with a treated outdoor air temperature of 7 °C when considering the combined effect of the entering air states and part load conditions on the overall energy and exergy efficiency of the multi-stage DX unit.

2) The optimum treated OA temperature was also confirmed able to achieve a better space humidity control through checking of divergence between equipment and space SHRs.

3) The need for the use exergy analysis for system optimization was confirmed. The energy and exergy analyses adopted in this study can be a reference protocol to enhance future research in this area.

8.1.4 Overcooling Risk

Probabilistic assessment of the overcooling risk of the optimized XT-DOAS and the conventional system with VAV control (Con_VAV), both without reheating provisions, was conducted. This is in consideration of the minimum air flow fraction (MAFF) characteristics of VAV system and the variations in indoor and outdoor conditions (weather conditions and use patterns of occupant, lighting and appliances). The assessment was done based on Monte Carlo simulations (MCS) with 10,000 iterations. *EnergyPlus* simulations were performed based on the 10,000 iteration cases

and 10,000 weather files which covered all possible cooling demand fluctuations. The results were used to analyze the overcooling risk of XT-DOAS and Con_VAV. The key findings are detailed as follows:

1) The potential annual overcooling hours using XT-DOAS in office building in Hong Kong were 29 hours, which is as far less than 426 overcooling hours of the typical conventional VAV system (Con_VAV).

2) Due to the overcooling, the long-term percentage of dissatisfied (LPD) of XT-DOAS is 0.31%, is also less than 1.69% LPD achieved by Con_VAV.

8.2 Limitations

However, there are several limitations with the above findings:

1) The strong dehumidifying ability of XT-DOAS may not be advantageous for use in countries/regions having significantly different climatic and living conditions from that of Hong Kong, and in situations where space must be maintained at a higher relative humidity level.

2) The optimum treated OA temperature for XT-DOAS, determined by exergy analyses, is applicable only to Hong Kong climate conditions, because exergy efficiency is affected mostly by the OA conditions.

3) The better indoor thermal comfort achieved by XT-DOAS was confirmed based on an ideal indoor air distribution. The influence on air distribution due to changes in SA conditions during part load conditions were not considered.

4) Fast mixing of XT OA and RA was assumed at the mixing box to by-pass the two-phase region to avoid condensation.

5) The better overall performance of XT-DOAS was confirmed based on simulation study which assumed the desired SAT could always be achieved by the multi-stage DX unit.

8.3 Recommendations for Future Research

Based on the above limitations, further research works on the use of XT-DOAS include:

1) Its feasible application in countries/regions with significantly different climatic and living conditions from that of Hong Kong.

2) An investigation of the influence of SA conditions on the indoor air distribution and thus thermal comfort. Computation fluid dynamics (CFD) can be employed as the main simulation tool for further evaluations. Monte Carlo simulations can again be used to predict the possible fluctuations in SA conditions.

3) Experimental works can be done to identify the optimum air mixing speed at the mixing box whereby condensation can be avoided to achieve environmental health objective.

4) Experimental verifications on whether the desired SAT can be achieved by the multi-stage DX unit is recommended.

APPENDIX A

Equivalent thermal comfort is calculated as follows:

According to an experimental study by Berglund (1991), factors affecting thermal comfort can be related by the following regression equation:

$$TS = 0.217DB + 0.020DP + 0.61M - 17.49 \quad (R = 0.96) \tag{A.1}$$

where *TS* is the average response of people on ASHRAE's seven-point thermal sensation scale (ASHRAE, 2013); *M* is the activity level in Met; *R* is the square root of the correlation coefficient.

Equation (A.1) indicates that *TS* remains almost constant for a 0.5 °C increase in DB temperature, together with a 5.8 °C decrease in DP temperature.

For a constant space DB temperature, a lower RH results in a lower DP. They can be related as shown in Equation (A.2) below (Lawrence, 2005):

$$DP = \frac{237.7 \times \left[\ln\left(RH\right) + \frac{17.27 \times DB}{237.7 + DB} \right]}{17.27 - \ln\left(RH\right) - \frac{17.27 \times DB}{237.7 + DB}} \tag{A.2}$$

where *DP* is the dew point temperature, °C, $DP \in [0, 60]$; *DB* is the dry bulb temperature, °C, $DB \in [0, 50]$; RH is the relative humidity, $RH \in [1\%, 100\%]$.

Thus by combining Equations (A.1) and (A.2), Equation (A3) can be formulated, which can be used to determine the equivalent comfort condition for a design condition of 24 °C /50%:

$$\ln\left(RH\right) = \frac{972.904DB - 22442.467}{0.217DB^2 - 2429.532 + 41.36DB} \quad \text{(A.3)}$$

Based on Equation (A.3), when *RH* is set as 35%, the corresponding *DB* temperature is 24.5 °C, which is the equivalent design space condition for XT-DOAS as shown in Section Case study building.

APPENDIX B

The acceptability of the regression models presented in Section 6.3.1 was verified by checking both goodness of fit and linearity as follows:

The goodness-of-fit indices, R^2 and the adjusted R^2 (R_a^2) were used to determine how well the regression models fit the observations and predictions. R_a^2 is more suitable for multiple regression in this study as it can adjust the goodness-of-fit for the additional variables. They are mathematically shown in Equations (B.1) and (B.2) (Chatterjee and Hadi, 2015):

$$R^2 = 1 - \frac{\sum_{i=1}^{n} \left(y_i - \hat{y}_i \right)^2}{\sum_{i=1}^{n} \left(y_i - \bar{y} \right)^2} \tag{B.1}$$

$$R_a^2 = 1 - \frac{\left(1 - R^2\right) \cdot \left(n - 1\right)}{\left(n - p - 1\right)} \tag{B.2}$$

where y_i is the i-th actual value of CAP/CAP_{rated} and EIR/EIR_{rated} based on different WB_{ei} and DB_{ci} in Equations (4.2) and (4.3) for Section 6.3.1; $\bar{y}$ is the mean of actual values; $\hat{y}_i$ is the i-th fitted value which can be calculated from the different WB_{ei}, DB_{ci} and regressed coefficients; n is total number of data pairs; p is the number of independent variables.

The results show that the R^2 and R_a^2 are 0.986 and 0.985 for the *CAP-FT* model and 0.982 and 0.981 for the *EIR-FT* model which are close to 1 to confirm their accuracy (Chatterjee and Hadi, 2015).

In addition to checking of goodness-of-fit, the linearity validation has been considered. In general, the validity of linear assumption can be confirmed by examining the scatter plot of the data pairs, but considering the large number of variables for the *CAP-FT* and *EIR-FT* models, the scatter plots of the standardized residuals and fitted values have been used instead. The *i*-th standardized residual ZRE_i has been introduced to standardize the ordinary least squares residual e_i as shown in Equations (B.3) to (B.4), and the result of the scatter plots with a random distribution (in Figure B.1 and B.2) confirmed the validity of linear assumption (Baty *et al.*, 2015).

$$e_i = y_i - \hat{y}_i \tag{B.3}$$

$$ZRE_i = \frac{e_i}{\sqrt{\frac{1}{(n-p-1)} \cdot \sum_{i=1}^{n} e_i^2}} \tag{B.4}$$

Figures B.3 and B.4 correspondingly show the deviation between the actual values y_i and the fitted values $\hat{y}_i$ for *CAP-FT* and *EIR-FT*. They reflect the distribution of the corresponding ordinary least squares residual e_i and no obvious deviation is noted.

Consistent result from the goodness of fit and linearity checks confirmed the acceptability of the developed coil model.

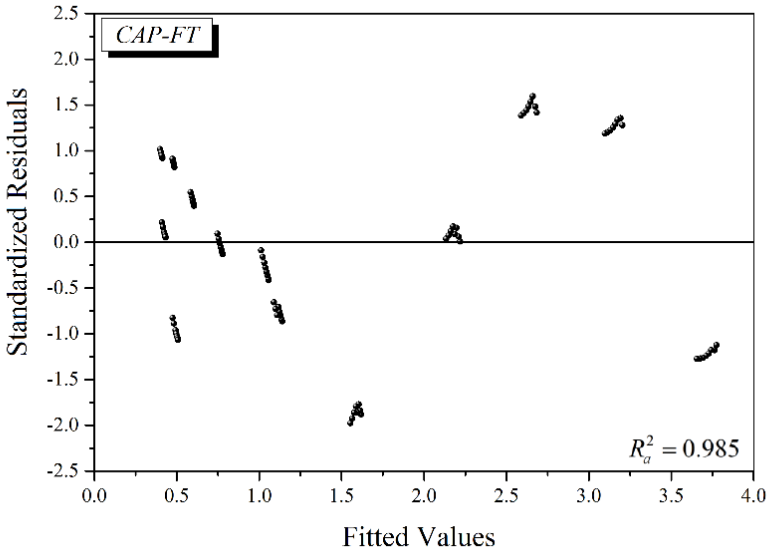

Figure B.1 *CAP-FT* standardized residuals plot

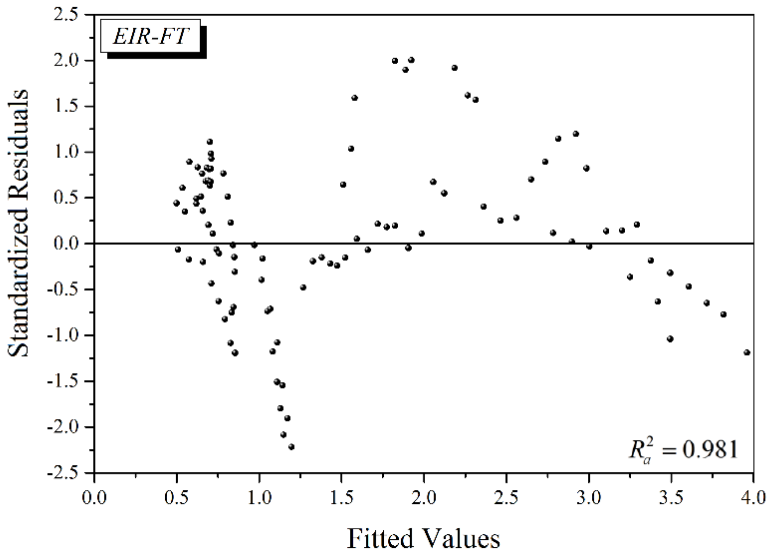

Figure B.2 *EIR-FT* standardized residuals plot

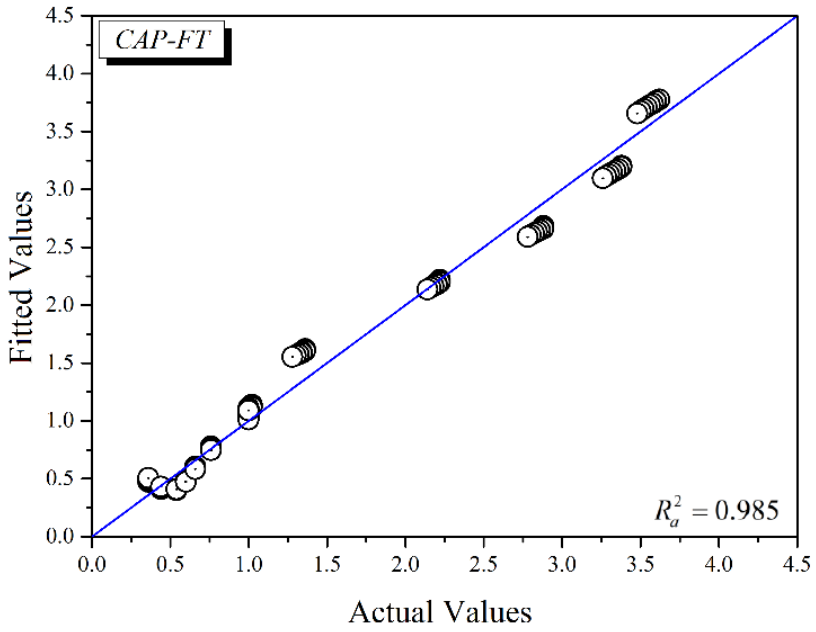

Figure B.3 *CAP-FT* actual values Vs fitted values

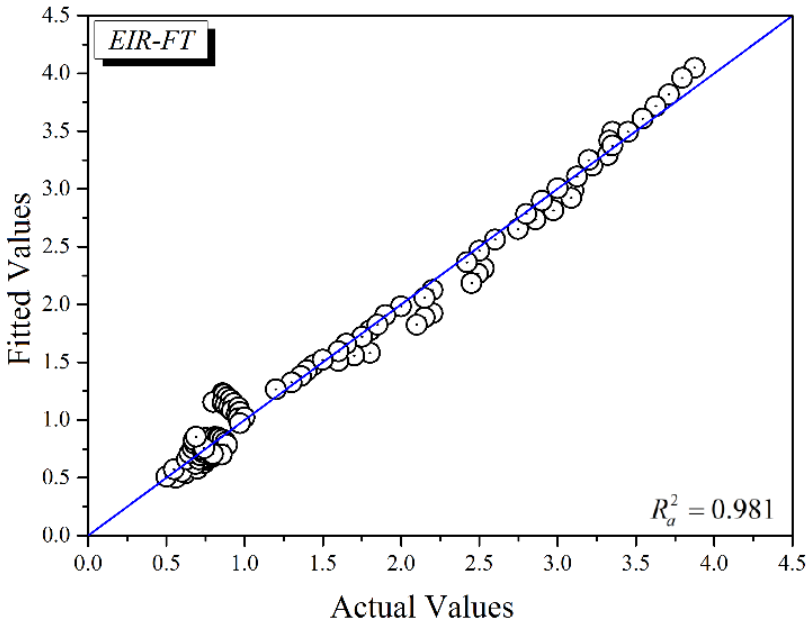

Figure B.4 *EIR-FT* actual values Vs fitted values

REFERENCES

1. AHRI (2001) *Standard 410-2001: Forced Circulation Air-Cooling and Air-Heating Coils*. Air-Conditioning, Heating, and Refrigeration Institute.

2. AHRI (2008) *Standard 210/240-2008. Performance Rating of Unitary Air Conditioning and Air-Source Heat Pump Equipment*. Air-Conditioning, Heating, and Refrigeration Institute.

3. Aiken, L. S., West, S. G. and Reno, R. R. (1991) *Multiple regression: Testin and interpreting interactions*. Sage.

4. Andrade, M. A. and Bullard, C. W. (2002) Modulating blower and compressor capacities for efficient comfort control, *ASHRAE Transactions*, 108: 631–637.

5. Arens, E., Zhang, H., Hoyt, T., Kaam, S. and Goins, J. (2012) *ASHRAE RP-1515:Thermal and Air Quality Acceptability in Buildings that Reduce Energy by Reducing Minimum Airflow from Overhead Diffusers*.

6. ASHRAE (2009) *ASHRAE Handbook Fundamentals*. Atlanta, GA, USA.

7. ASHRAE (2011) *ASHRAE Handbook - HVAC Applications*. Atlanta, GA, USA.

8. ASHRAE (2013) *ASHRAE Standard 55-2013 Thermal Environmental Conditions for Human Occupancy*. Atlanta, GA, USA.

9. ASHRAE (2016) *ASHRAE Standard 62.1-2016, Ventilation for Acceptable Indoor Air Quality*. Atlanta, GA, USA.

10. ASHRAE (2017) *ASHRAE Handbook Fundamentals*. Atlanta, GA, USA.

11. Aynur, T. N., Hwang, Y. and Radermacher, R. (2009) Simulation comparison of VAV and VRF air conditioning systems in an existing building for the cooling season, *Energy and Buildings*, 41(11): 1143–1150.

12. Bannister, P. (2008) Energy Efficiency and the Control and Simulation of VAV Systems, in *2008 ACEEE Summer Study on Energy Efficiency in Buildings*.

13. Bao, Y., Lee, W. L. and Jia, J. (2017) Applying a novel extra-low temperature dedicated outdoor air system for humidity control and energy efficiency, *Science and Technology for the Built Environment*, 23(1): 16–29.

14. Bao, Y., Lee, W. L. and Jia, J. (2018) Exergy analyses and modelling of a novel extra-Low temperature dedicated outdoor air system, *Energies*, 11: 1165.

15. Barreto, H. and Howland, F. (2005) *Introductory econometrics: using Monte Carlo simulation with Microsoft excel*. Cambridge University Press.

16. Baty, F., Ritz, C., Charles, S., Brutsche, M., Flandrois, J. P. and Delignette-Muller, M. L. (2015) A Toolbox for Nonlinear Regression in R : The Package nlstools, *Journal of Statistical Software*, 66(5): 1–21.

17. Bauman, F. S., Borgers, T., Laberge, P. and Gadgi1, A. J. (1992) *Cold Air Distribution in Office Buildings: Technology Assessment of California*, *Energy and Environment Division*. Berkeley, CA, US.

18. BEAM (2012) *BEAM Plus for New Buildings Version 1.2. Hong Kong GBC*

and BEAM Society Limited. Hong Kong.

19. Beghi, A., Cecchinato, L. and Rampazzo, M. (2011) A multi-phase genetic algorithm for the efficient management of multi-chiller systems, *Energy Conversion and Management*, 52(3): 1650–1661.

20. Belcher, S. E., Hacker, J. N. and Powell, D. S. (2005) Constructing design weather data for future climates, *Building Services Engineering Research and Technology*, 26(1): 49–61.

21. Berglund, L. G. (1991) Comfort benefits for summer air conditioning with ice storage, *ASHRAE Transactions*, 97(1): 843–847.

22. Berglund, L. G. (1994) *Thermal Comfort with Cold Air Distribution/Cold Thermal Storage.Advances in Cold AirDistribution Technology*. Fort Collins, CO: Electric Power Research Institute.

23. Bernal, W., Behl, M., Nghiem, T. and Mangharam, R. (2012) MLE+: A Tool for Integrated Design and Deployment of Energy Efficient Building Controls, in *The Fourth ACM Workshop on Embedded Sensing Systems for Energy-Efficiency in Buildings*. Toronto, Canada.

24. Camacho, E. F. and Bordons, C. (2007) *Model Predictive Control*. 2nd edn. London: Springer.

25. Carlucci, S. (2013) *Thermal comfort assessment of buildings*. London: Springer.

26. Carlucci, S., Cattarin, G., Causone, F. and Pagliano, L. (2015) Multi-objective optimization of a nearly zero-energy building based on thermal and visual

discomfort minimization using a non-dominated sorting genetic algorithm (NSGA-II), *Energy and Buildings*, 104(2015): 378–394.

27. Chan, A. L. S. (2011) Developing future hourly weather files for studying the impact of climate change on building energy performance in Hong Kong, *Energy and Buildings*, 43(10): 2860–2868.

28. Chan, A. L. S., Chow, T. T., Fong, S. K. F. and Lin, J. Z. (2006) Generation of a typical meteorological year for Hong Kong, *Energy Conversion and Management*, 47(1): 87–96.

29. Chan, A. L. S., Chow, T. T., Fong, S. K. F. and Lin, J. Z. (2006) Performance evaluation of district cooling plant with ice storage, *Energy*, 31: 2750–2762.

30. Chang, Y. C. and Chen, W. H. (2009) Optimal chilled water temperature calculation of multiple chiller systems using Hopfield neural network for saving energy, *Energy*, 34(4): 448–456.

31. Chang, Y. C., Lin, J. K. and Chuang, M. H. (2005) Optimal chiller loading by genetic algorithm for reducing energy consumption, *Energy and Buildings*, 37(2): 147–155.

32. Chatterjee, S. and Hadi, A. S. (2015) *Regression Analysis by Example*. John Wiley & Sons.

33. Chen, C., Cai, W., Giridharan, K. and Wang, Y. (2014) A hybrid dynamic modeling of active chilled beam terminal unit, *Applied Energy*, 128: 133–143.

34. Chen, C., Cai, W., Wang, Y., Lin, C. and Wang, L. (2015) Operating characteristics of an active chilled beam terminal unit under variable air

volume mode, *Applied Thermal Engineering*, 85: 71–79.

35. Chengqin, R., Nianping, L. and Guangfa, T. (2002) Principles of exergy analysis in HVAC and evaluation of evaporative cooling schemes, *Building and Environment*, 37(11): 1045–1055.

36. Chow, T. T. and Lam, J. C. (1992) Thermal Comfort and Energy Conservation in Commercial Buildings in Hong Kong, *Architectural Science Review*, 35(2): 67–72.

37. Coelho, L. dos S., Klein, C. E., Sabat, S. L. and Mariani, V. C. (2014) Optimal chiller loading for energy conservation using a new differential cuckoo search approach, *Energy*, 75: 237–243.

38. Crawley, D. B., Lawrie, L. K., Army, U. S., Champaign, C., Curtis, I., Pedersen, O. and Winkelmann, F. C. (2000) EnergyPlus: Energy Simulation Program, *ASHRAE Journal*, 42: 49–56.

39. Daikin (2016) Performance data of ED34-845A. Daikin Airconditioning (Hong Kong) Ltd., Hong Kong.

40. de Dear, R. J. (1998) Global database of thermal comfort field experiments, in *ASHRAE Transactions*, 1141–1152.

41. Dieckmann, J., Roth, K. W. and Brodrick, J. (2003) Dedicated outdoor air systems, *ASHRAE Journal*, 45(3): 58–59.

42. Dincer, I. and Rosen, M. (2002) *Thermal Energy Storage Systems and Applications*, *Wiley*. New York.

43. Dincer, I. and Rosen, M. A. (2004) Exergy as a Driver for Achieving Sustainability, *International Journal of Green Energy*, 1(1): 1–19.

44. Elyamany, A. and Abdelrahman, M. (2010) Contractor Performance Evaluation for the Best Value of Superpave Projects, *Journal of Construction Engineering and Management*, 136(5): 606–614.

45. EMSD (2012) *Code of practice for energy efficiency of building services installation. Electrical and Mechanical Services Department*. Hong Kong.

46. EnergyPlus (2015) EnergyPlus Energy Simulation Software Version 8.1: EnergyPlus Engineering Reference. U.S. Department of Energy.

47. Fan, B., Jin, X. and Du, Z. (2011a) Optimal control strategies for multi-chiller system based on probability density distribution of cooling load ratio, *Energy and Buildings*, 43(10): 2813–2821.

48. Fan, B., Jin, X. and Du, Z. (2011b) Optimal control strategies for multi-chiller system based on probability density distribution of cooling load ratio, *Energy and Buildings*, 43(10): 2813–2821.

49. Fan, B., Jin, X., Fang, X. and Du, Z. (2014) The method of evaluating operation performance of HVAC system based on exergy analysis, *Energy and Buildings*, 77: 332–342.

50. Feng, X., Yan, D. and Hong, T. (2015) Simulation of occupancy in buildings, *Energy and Buildings*, 87: 348–359.

51. Fong, K. F., Chow, T. T., Lee, C. K., Lin, Z. and Chan, L. S. (2011) Solar hybrid cooling system for high-tech offices in subtropical climate - Radiant

cooling by absorption refrigeration and desiccant dehumidification, *Energy Conversion and Management*, 52(8–9): 2883–2894.

52. Gang, W., Wang, S., Shan, K. and Gao, D. (2015) Impacts of cooling load calculation uncertainties on the design optimization of building cooling systems, *Energy and Buildings*, 94: 1–9.

53. Gang, W., Wang, S., Xiao, F. and Gao, D. (2015) Robust optimal design of building cooling systems considering cooling load uncertainty and equipment reliability, *Applied Energy*, 159: 265–275.

54. Ge, G., Xiao, F. and Niu, X. (2011) Control strategies for a liquid desiccant air-conditioning system, *Energy and Buildings*, 43(6): 1499–1507.

55. Halvorson, M. (2013) *Microsoft Visual Basic 2013 Step by Step*. Pearson Education.

56. Hayes, A. F. and Matthes, J. (2009) Computational procedures for probing interactions in OLS and logistic regression: SPSS and SAS implementations, *Behavior research methods*, 41(3): 924–936.

57. Hickey, D. (2001) Focus on humidity control, *ASHRAE Journal*, 43(10): 10–11.

58. HKEPD (2003) *Indoor air quality certification scheme for offices and public places*. Hong Kong.

59. Honeywell (1997) *Engineering manual of automatic control for commercial buildings : heating, ventilation, air conditioning*. Honeywell Inc.

60. Hoyt, T., Arens, E. and Zhang, H. (2014) Extending air temperature setpoints: Simulated energy savings and design considerations for new and retrofit buildings, *Building and Environment*, 88: 89–96.

61. Huang, G. and Li, Z. (2014) Stochastic chiller sequencing control for multiple-chiller plants, in *IEEE International Conference on Automation Science and Engineering*, 1085–1090.

62. Huang, S., Zuo, W. and Sohn, M. D. (2016) Amelioration of the cooling load based chiller sequencing control, *Applied Energy*, 168: 204–215.

63. Huh, J. H. and Brandemuehl, M. J. (2008) Optimization of air-conditioning system operating strategies for hot and humid climates, *Energy and Buildings*, 40(7): 1202–1213.

64. Hurnik, M. (2015) Experimental and numerical testing of an induction variable air volume (VAV) controller with two damper blades, *International Journal of Ventilation*, 14(1): 53–64.

65. IPCC (2014) *Fifth Assessment Report (AR5)*. Intergovernmental Panel on Climate Change (IPCC).

66. jeplus (2015) jEPlus. Available at: http://www.jeplus.org/wiki/doku.php.

67. Jia, J. and Lee, W. L. (2013) Condensation risk of DCDV system for hot and humid Hong Kong, *Indoor and Built Environment*, 23(6): 814–822.

68. Jia, J., Lee, W. L. and Chen, H. (2013) Experimental study of performance of a dry cooling and dedicated ventilation (DCDV) system under different space cooling load conditions, *Energy Conversion and Management*, 73: 158–166.

69. Kirkpatrick, A. T. and Elleson, J. S. (1996) *Cold Air Distribution System Design Guide*. Atlanta: American Society of Heating, Refrigerating and Air-Conditioning Engineers.

70. Kosonen, R. and Tan, F. (2005) A feasibility study of a ventilated beam system in the hot and humid climate: A case-study approach, *Building and Environment*, 40(9): 1164–1173.

71. Krakow, K. I., Lin, S. and Zeng, Z. S. (1995) Analytical determination of PID coefficients for temperature and humidity control during cooling and dehumidifying by compressor and evaporator fan speed variation, *ASHRAE Transactions*, (1): 343–354.

72. Krakow, K. I., Lin, S. and Zeng, Z. shu (1995) Temperature and humidity control during cooling and dehumidifying by compressor and evaporator fan speed variation, *ASHRAE*, 292–304.

73. Lam, J. C. and Hui, S. C. M. (1996) Sensitivity analysis of energy performance of office buildings, *Building and Environment*, 31(1): 27–39.

74. Lawrence, M. G. (2005) The relationship between relative humidity and the dewpoint temperature in moist air: A simple conversion and applications, *Bulletin of the American Meteorological Society*, 86(2): 225–233.

75. Lee, P., Lam, P. T. I., Lee, W. L. and Chan, E. H. W. (2016) Analysis of an air-cooled chiller replacement project using a probabilistic approach for energy performance contracts, *Applied Energy*, 171: 415–428.

76. Lee, S. H. and Lee, W. L. (2013) Site verification and modeling of desiccant-

based system as an alternative to conventional air-conditioning systems for wet markets, *Energy*, 55: 1076–1083.

77. Lee, W. L. (2010) *Evaluating the energy use of a store building. Consultancy Report submitted to Business Environment Council 2010*.

78. Lee, W. L. (2012) Benchmarking energy use of building environmental assessment schemes, *Energy and Buildings*, 45: 326–334.

79. Lee, W. L., Chen, H., Leung, Y. C. and Zhang, Y. (2012) Decoupling dehumidification and cooling for energy saving and desirable space air conditions in hot and humid Hong Kong, *Energy Conversion and Management*, 53(1): 230–239.

80. Levine, D. G. and Friedlander, S. K. (1960) The condensation of a vapour by mixing with a cool gas, *Chemical Engineering Science*, 13(2): 49–56.

81. Li, H., Lee, W. L. and Jia, J. (2016) Applying a novel extra-low temperature dedicated outdoor air system in office buildings for energy efficiency and thermal comfort, *Energy Conversion and Management*, 121: 162–173.

82. Li, H., Lee, W. L. and Ng, T. F. (2015) Developing a novel dedicated outdoor air system (DOAS) for energy efficiency and environmental health, in *Mainland–HongKong Joint Symposium 2015: Building Technologies – An Epoch of Enlightenment*. Harbin, China, 26–27.

83. Li, H., You, S., Zhang, H., Zheng, W., Zheng, X., Jia, J., Ye, T. and Zou, L. (2017) Modelling of AQI related to building space heating energy demand based on big data analytics, *Applied Energy*, 203: 57–71.

84. Li, Z., Chen, W., Deng, S. and Lin, Z. (2006) The characteristics of space cooling load and indoor humidity control for residences in the subtropics, *Building and Environment*, 41(9): 1137–1147.

85. Li, Z. and Deng, S. (2007a) A DDC-based capacity controller of a direct expansion (DX) air conditioning (A/C) unit for simultaneous indoor air temperature and humidity control - Part II: Further development of the controller to improve control sensitivity, *International Journal of Refrigeration*, 30: 124–133.

86. Li, Z. and Deng, S. (2007b) A DDC-based capacity controller of a direct expansion (DX) air conditioning (A/C) unit for simultaneous indoor air temperature and humidity control Part I: Control algorithms and preliminary controllability tests, *International Journal of Refrigeration*, 30: 113–123.

87. Li, Z. and Deng, S. (2007c) An experimental study on the inherent operational characteristics of a direct expansion (DX) air conditioning (A/C) unit, *Building and Environment*, 42(1): 1–10.

88. Li, Z., Xu, X., Deng, S. and Pan, D. (2015) A novel neural network aided fuzzy logic controller for a variable speed (VS) direct expansion (DX) air conditioning (A/C) system, *Applied Thermal Engineering*, 78: 9–23.

89. Li, Z., Xu, X., Deng, S. and Pan, D. (2015) A novel proportional-derivative (PD) law based fuzzy logic principles assisted controller for simultaneously controlling indoor temperature and humidity using a direct expansion (DX) air conditioning (A/C) system, *International Journal of Refrigeration*, 57: 239–256.

90. Liang, X., Chan, M. Y. and Deng, S. (2008) Development of a method for calculating steady-state equipment sensible heat ratio of direct expansion air conditioning units, *Applied Energy*, 85(12): 1198–1207.

91. Liu, K., Liu, T.-Z., Fang, P. and Li, Z.-P. (2017) Comprehensive approach to modeling and simulation of dynamic soft-sensing design for real-time building energy consumption, *International Journal of Distributed Sensor Networks*, 13(5).

92. Liu, W., Lian, Z., Radermacher, R. and Yao, Y. (2007) Energy consumption analysis on a dedicated outdoor air system with rotary desiccant wheel, *Energy*, 32(9): 1749–1760.

93. Luo, Y., Wang, M., Yang, H., Lu, L. and Peng, J. (2015) Experimental study of internally cooled liquid desiccant dehumidification: Application in Hong Kong and intensive analysis of influencing factors, *Building and Environment*, 93(2): 210–220.

94. Macfarlane, W. V. (1978) Thermal comfort studies since 1958, *Architectural Science Review*, 21(4): 86–92.

95. Meggers, F. and Leibundgut, H. (2011) The potential of wastewater heat and exergy: Decentralized high-temperature recovery with a heat pump, *Energy and Buildings*, 43(4): 879–886.

96. Meggers, F., Mast, M. and Leibundgut, H. (2010) The missing link for low exergy buildings: low temperature-lift, ultra-high COP heat pumps, in *Clima 2010: Sustainable Energy Use in Buildings*.

97. Mui, K. W. (2006) Energy policy for integrating the building environmental performance model of an air conditioned building in a subtropical climate, *Energy Conversion and Management*, 47(15–16): 2059–2069.

98. Mumma, S. A. (2001) Overview of integrating dedicated outdoor air systems with parallel terminal systems, *ASHRAE Transactions*, 107: 545–552.

99. Mumma, S. A. (2002) Chilled ceilings in parallel with dedicated outdoor air systems: Addressing the concerns of condensation, capacity, and cost, *ASHRAE Transactions*, 108: 220–231.

100. Murphy, J. (2010) Using VAV to limit humidity at part load, *ASHRAE Journal*, 52(10): 18–22.

101. Murphy, J. (2011) High-performance VAV systems, *ASHRAE Journal*, 53(10): 18–28.

102. Naboni, E., Zhang, Y., Maccarini, A., Hirsh, E. and Lezzi, D. (2013) Extending the use of parametric simulation in practice through a cloud based online service, in *First IBPSA-Italy conference BSA 2013*, 105–112.

103. Nassif, N., Kajl, S. and Sabourin, R. (2005) Simplified Model-based Optimal Control of VAV Air-conditioning System, in *Ninth International IBPSA Conference*. Montreal, Canada, 823–830.

104. Niu, J. L., Zhang, L. Z. and Zuo, H. G. (2002) Energy savings potential of chilled-ceiling combined with desiccant cooling in hot and humid climates, *Energy and Buildings*, 34(5): 487–495.

105. Norford, L. K., Rabl, A. and Socolow, R. H. (1986) Control of supply air

temperature and outdoor airflow and its effect on energy use in a variable air volume system, in *ASHRAE Transactions*, 30–45.

106. Nutprasert, N. and Chaiwiwatworakul, P. (2014) Radiant cooling with dehumidified air ventilation for thermal comfort in buildings in tropical climate, *Energy Procedia*, 52: 250–259.

107. Palisade (2017) @RISK 7.5, Industrial – student. Sydney.

108. Pérez-Lombard, L., Ortiz, J. and Pout, C. (2008) A review on buildings energy consumption information, *Energy and Buildings*, 40(3): 394–398.

109. Qi, Q. and Deng, S. (2008) Multivariable control-oriented modeling of a direct expansion (DX) air conditioning (A/C) system, *International Journal of Refrigeration*, 31(5): 841–849.

110. Qi, Q. and Deng, S. (2009) Multivariable control of indoor air temperature and humidity in a direct expansion (DX) air conditioning (A/C) system, *Building and Environment*, 44(8): 1659–1667.

111. Reddy, T. A. and Claridge, D. E. (2000) Uncertainty of "measured" energy savings from statistical baseline models, *ASHRAE Transactions*, 106.

112. Ren, C. Q., Tang, G. F., Li, N. P., Zhang, G. F. and Yang, J. (2001a) Analysis of Exergy of Moist Air and Energy Saving Potential in Hvac By Evaporative Cooling or Energy Recovery, *International Journal on Architectural Science*, 2(4): 113–117.

113. Ren, C. Q., Tang, G. F., Li, N. P., Zhang, G. F. and Yang, J. (2001b) Discussion on principles of exergy analysis applied to HVAC systems, in

International Conference on Energy Conversion and Application (ICECA'2001). Wuhan, China.

114. Rismanchi, B., Saidur, R., Masjuki, H. H. and Mahlia, T. M. I. (2012) Energetic, economic and environmental benefits of utilizing the ice thermal storage systems for office building applications, *Energy and Buildings*, 50: 347–354.

115. Saber, E. M. (2017) Performance evaluation of damper control settings for operation of multiple-zone variable air volume reheat system in different building applications and climate types, *Building Simulation*, 10(5): 687–696.

116. Sanaye, S. and Hekmatian, M. (2016) Ice thermal energy storage (ITES) for air-conditioning application in full and partial load operating modes, *International Journal of Refrigeration*, 66: 181–197.

117. Shi, Z., Abdelalim, A., Brien, W. O., Attar, R., Akiki, P., Graham, K., Waarden, B. Van, Fai, S., Tessier, A. and Khan, A. (2015) Digital Campus Innovation Project : Integration of Building Information Modelling with Building Performance Simulation and Building Diagnostics, in *The Symposium on Simulation for Architecture and Urban Design*, 25–32.

118. Song, X., Zhu, T., Liu, L. and Cao, Z. (2018) Study on optimal ice storage capacity of ice thermal storage system and its influence factors, *Energy Conversion and Management*, 164: 288–300.

119. Strand, R. K., Crawley, D. B., Pedersen, C. O., Liesen, R. J., Lawrie, L. K., Winkelmann, F. C., Buhl, W. F., Huang, Y. J. and Fisher, D. E. (2000) EnergyPlus : A New-Generation Energy Analysis and Load Calculation

Engine for Building Design, in *Association of Collegiate Schools of Architecture Technology Conference*.

120. Sun, S., Kensek, K., Noble, D. and Schiler, M. (2016) A method of probabilistic risk assessment for energy performance and cost using building energy simulation, *Energy and Buildings*, 110: 1–12.

121. Sun, Y., Gu, L., Wu, C. F. J. and Augenbroe, G. (2014) Exploring HVAC system sizing under uncertainty, *Energy and Buildings*, 81: 243–252.

122. Sun, Y., Wang, S. and Huang, G. (2010) Model-based optimal start control strategy for multi-chiller plants in commercial buildings, *Building Services Engineering Research and Technology*, 31(2): 113–129.

123. Thangavelu, S. R., Myat, A. and Khambadkone, A. (2017) Energy optimization methodology of multi-chiller plant in commercial buildings, *Energy*, 123: 64–76.

124. Trane (2012) *VAV systems one of the systems series TRG-TRC014-EN*.

125. TRANE (2000) Cold Air Makes Good $ ense, *Trane Engineers Newsletter*, 29(2): 1–6.

126. Tso, G. K. F. and Yau, K. K. W. (2003) A study of domestic energy usage patterns in Hong Kong, *Energy*, 28(15): 1671–1682.

127. Vetterli, J. and Benz, M. (2012) Cost-optimal design of an ice-storage cooling system using mixed-integer linear programming techniques under various electricity tariff schemes, *Energy and Buildings*, 49: 226–234.

128. Vose, D. (2000) *Quantitative Risk Analysis: A guide to Monte Carlo simulation modelling*. New York: John Wiley and Sons.

129. Wagner, W. and Pruß, A. (2002) The IAPWS formulation 1995 for the thermodynamic properties of ordinary water substance for general and scientific use, *Journal of Physical and Chemical Reference Data*, 31(2): 387–535.

130. Walpole, R. E., Myers, R. H., Myers, S. L. and Ye, K. (2012) *Probability and Statistics for Engineers and Scientists*, *Power*.

131. Wan, J. W., Zhang, J. L. and Zhang, W. M. (2007) The effect of heat-pipe air-handling coil on energy consumption in central air-conditioning system, *Energy and Buildings*, 39(9): 1035–1040.

132. Wark, K. (1995) *Advanced thermodynamics for engineers*. New York: McGraw-Hill.

133. Willmott, C. J., Robeson, S. M. and Matsuura, K. (2012) A refined index of model performance, *International Journal of Climatology*, 32(13): 2088–2094.

134. Wyssen, I., Gasser, L., Kleingries, M. and Wellig, B. (2011) High efficient heat pumps for small temperature lift applications, in *10th IEA Heat Pump Conference*, 1–12.

135. Wyssen, I., Gasser, L., Wellig, B. and Meier, M. (2010) Chiller with small temperature lift for efficient building cooling, in *Proceedings of Clima2010*. REHVA.

136. Xu, X., Xia, L., Chan, M. and Deng, S. (2010) Inherent correlation between

the total output cooling capacity and equipment sensible heat ratio of a direct expansion air conditioning system under variable-speed operation (XXG SMD SHR DX AC unit), *Applied Thermal Engineering*, 30(13): 1601–1607.

137. Yi, H. and Braham, W. W. (2015) Uncertainty characterization of building emergy analysis (BEmA), *Building and Environment*, 92(MAY): 538–558.

138. Yi, W. and Chan, A. P. C. (2013) Optimizing work-rest schedule for construction rebar workers in hot and humid environment, *Building and Environment*, 61(March): 104–113.

139. Yin, Y. L., Wang, R. Z., Zhai, X. Q. and Ishugah, T. F. (2014) Experimental investigation on the heat transfer performance and water condensation phenomenon of radiant cooling panels, *Building and Environment*, 71: 15–23.

140. Youssef, A. A., Mina, E. M., ElBaz, A. R. and AbdelMessih, R. N. (2017) Studying comfort in a room with cold air system using computational fluid dynamics, *Ain Shams Engineering Journal*. Ain Shams University.

141. Yu, B., Hu, Z., Liu, M., Yang, H., Kong, Q. and Liu, Y. (2009) Review of research on air-conditioning systems and indoor air quality control for human health, *International Journal of Refrigeration*, 32(1): 3–20.

142. Yu, F. W. and Chan, K. T. (2006) Low-energy design for air-cooled chiller plants in air-conditioned buildings, *Energy and Buildings*, 334–339.

143. Yu, F. W. and Chan, K. T. (2007) Optimum load sharing strategy for multiple-chiller systems serving air-conditioned buildings, *Building and Environment*, 42(4): 1581–1593.

144. Zhang, B., Li, Y., Lau, J. and Liu, M. (2014) Demand control ventilation: Influence of terminal box minimum airflow setting on system energy use, *Energy and Buildings*, 79: 173–183.

145. Zhang, Y. (2009) 'Parallel' EnergyPlus and the Development of a Parametric Analysis Tool, in *Eleventh International IBPSA Conference*, 1382–1388.

146. Zhang, Y. and Korolija, I. (2010) Performing complex parametric simulations with jEPlus, in *SET2010-9th International Conference on Sustainable Energy Technologies*.

147. Zhao, J., Lam, K. P. and Ydstie, B. E. (2013) EnergyPlus Model-Based Predictive Control (EPMPC) by Using Matlab / Simulink and MLE +, in *13th Conference of International Building Performance Simulation Association*. Chambéry, France, 26–28.

148. Zhou, X., Yan, D., Jiang, Y. and Shi, X. (2016) Influence of asynchronous demand behavior on overcooling in multiple zone AC systems, *Building and Environment*, 110: 65–75.

149. Zmeureanu, R. and Wu, X. Y. (2007) Energy and exergy performance of residential heating systems with separate mechanical ventilation, *Energy*, 32: 187–195.